CONFIDENTIAL

NASA TECHNICAL MEMORANDUM

NASA TM X-997

NASA TM X-997

N70-77673 (ACCESSION NUMBER)
23 (PAGES)
(NASA CR OR TMX OR AD NUMBER)
(THRU)
None (CODE)
(CATEGORY)
FACILITY FORM 602

Declassified by authority of NASA
Classification Change Notices No. 207
Dated **11-30-70

87359

PRESSURE DISTRIBUTIONS FOR THE M-2 LIFTING ENTRY VEHICLE AT MACH NUMBERS OF 0.23, 5.2, 7.4, AND 10.4

CLASSIFICATION CHANGED
UNCLASSIFIED
TO
By Authority of 10-70-43 Date 9-15-70

by John A. Axelson

Ames Research Center
Moffett Field, Calif.

NATIONAL AERONAUTICS AND SPACE ADMINISTRATION • WASHINGTON, D. C. • SEPTEMBER 1964

CONFIDENTIAL

CONFIDENTIAL

PRESSURE DISTRIBUTIONS FOR THE M-2 LIFTING ENTRY VEHICLE AT MACH NUMBERS OF 0.23, 5.2, 7.4, AND 10.4

By John A. Axelson

Ames Research Center
Moffett Field, Calif.

GROUP 4
Downgraded at 3 year intervals;
Declassified after 12 years

CLASSIFIED DOCUMENT—TITLE UNCLASSIFIED

This material contains information affecting the national defense of the United States within the meaning of the espionage laws, Title 18, U.S.C., Secs. 793 and 794, the transmission or revelation of which in any manner to an unauthorized person is prohibited by law.

NATIONAL AERONAUTICS AND SPACE ADMINISTRATION

CONFIDENTIAL

[redacted]

PRESSURE DISTRIBUTIONS FOR THE M-2 LIFTING ENTRY VEHICLE AT MACH NUMBERS OF 0.23, 5.2, 7.4, AND 10.4*

By John A. Axelson

Ames Research Center
Moffett Field, Calif.

SUMMARY

16367

Surface pressure distributions for a 1-foot model of the M-2 lifting entry configuration have been measured at test Mach numbers of 0.23, 5.2, 7.4, and 10.4 in support of structural and aerodynamic heating studies of this and closely related configurations. The subsonic measurements were made over a range of angles of attack from 0° to 35°, sideslip angles from -15° to +12°, and at a Reynolds number of 1.6 million. The hypersonic measurements were made for angles of attack from -5° to +55°, sideslip angles from -15° to +5°, and at Reynolds numbers varying from 0.8 million to 1.6 million.

The M-2 configuration is a modified 13° half-cone with a blunted nose and a boattailed afterbody fitted with a pair of vertical fins. The test results for both speed ranges indicated that the most severe loading conditions occurred over the nose and fins. Estimated hypersonic pressure coefficients from modified Newtonian impact theory agreed well with the measured forebody pressure coefficients. The pressure coefficients for the aft-mounted controls which were immersed in the body shock and boundary layers were not amenable to accurate prediction, but they followed the qualitative trends indicated by impact and oblique shock theories. Conf. Author.

INTRODUCTION

The present pressure-distribution study supports a general research program directed toward the development of a maneuverable entry configuration. Two basic requirements of the configuration are that it have a lateral range of approximately 1000 nautical miles, realized through the development of a hypersonic lift-to-drag ratio of 1.3, and also be capable of conventional landing. The evolution of the present, modified, 13° half-cone configuration, generally known as the M-2, is documented in references 1 through 6 which present the subsonic and supersonic aerodynamic performance and stability and control characteristics. The hypersonic pressure distributions herein presented are among the first to be published and should find use in structural design and aerodynamic heating studies in support of future flight programs of the M-2 and related configurations.

[redacted]

NOTATION

C_p	pressure coefficient, $\frac{p-p_\infty}{q_\infty}$
M	Mach number
p	local static pressure
p_∞	free-stream static pressure
q_∞	free-stream dynamic pressure
α	angle of attack
β	angle of sideslip
γ	isentropic exponent
δ	control deflection
θ	surface inclination to free stream
σ	cone semivertex angle
φ	azimuth angle (see fig. 4)

Subscripts

f	pitch flap
r	rudder
max	maximum
min	minimum
stag	stagnation

EXPERIMENT

Wind Tunnels

Hypersonic tests.- The high-speed pressure measurements were obtained in the Ames 3.5-foot hypersonic wind tunnel shown schematically in the sketch of figure 1. The facility is a blowdown-type tunnel in which pressurized air is heated during passage through a pebble-bed heater and accelerated in one

of the available, interchangeable nozzles leading to the 3.5-foot diameter test section. The facility incorporates the novel feature of using a helium film for cooling of the nozzle and test section wall.

The servo-controlled, hydraulically operated model support system is shown in the photograph of figure 2 and has an operating range of angle of attack from -5° to $+15^{\circ}$. For the present study, an internally air-cooled canister, housing the pressure transducers, was mounted downstream of the model at the forward end of the water-jacketed sting. The transducer outputs were programmed into a Beckman 210 system and recorded on magnetic tape.

Subsonic tests.- The subsonic pressure distributions were measured in the Ames 7- by 10-foot wind tunnel No. 1, a conventional, return-passage type. The model pressures were measured on a water-filled, multiple glass-tube manometer.

Tests

The nominal test conditions for the wind-tunnel investigations are summarized as follows:

Mach number	Total pressure, lb/sq in.	Total temperature, $^{\circ}$F	Reynolds number, millions per ft
0.23	14.7	60	1.6
5.2	100	1500	0.8
7.4	500	1400 - 1700	1.2 - 1.6
10.4	500	1700	0.5
10.4	1000	1700	1.0

Model

The model used for the pressure measurements is shown in figure 3 and the pertinent dimensions are given in figure 4. The locations of the pressure orifices (on the left side of the model) are listed in table I and indicated in the sketch at the top of figure 5. The model was machined from an Inconel casting. The controls and canopy were made from 347 stainless steel. Rudder deflections of 0°, 15°, 25°, and 35° were simulated by the addition of wedges to the outer surfaces of the fins. Pressure measurements were taken for pitch-flap deflections of 0°, 30°, and 45°, and for the model with and without the canopy. The elevons included in some of the earlier tests (refs. 1-6) were not included on the present model.

Through the use of three different model-sting adapters which alined the model at 0°, 20°, and 40° to the sting, a range of angles of attack from -5° to $+55^{\circ}$ was covered in the hypersonic tests. The angles of attack for the

subsonic investigation extended from -5° to +35°. Sideslip tests were conducted at Mach numbers of 0.23 and 10.4 with the model rolled 90° on the sting, the pitching motion of the model support providing yawing motion to the model.

Precision

The accuracies of the pressure distributions presented here are calculated to be within the following limits:

M	C_p, percent
0.23 ± 0.001	±1
5.20 ± 0.03	±2
7.40 ± 0.05	±3
10.40 ± 0.07	±3

The uncertainty in the pressure coefficients results primarily from the corresponding uncertainty in calculating the free-stream dynamic pressure. In the present program, dynamic pressure was calculated from the measured total pressures and the assumed average Mach number which was obtained from wind-tunnel calibration measurements. The small uncertainties in Mach number result in relatively larger uncertainties in dynamic pressure at hypersonic speeds.

For both the subsonic and hypersonic tests, the angles of attack and sideslip are accurate within ±0.2°, while the rudder and pitch flap deflections are accurate within ±0.3°.

RESULTS AND DISCUSSION

Presentation of Results

The subsonic pressure coefficients for the model are presented in figures 5, 6, and 7. Figures 5(a) through 5(e) show the experimental results for angles of attack of 0°, 6°, 15°, 20°, and 35°. Figures 6(a) through 6(d) present the pressure coefficients for the model in sideslip at angles of +6°, 0°, -6°, and -12°, all at a model angle of attack of 0°. Figures 7(a) and 7(b) show the pressure coefficients for the inner surface of the fin and for the model base over the test range of angles of attack and of sideslip.

The hypersonic pressure distributions for the model in pitch are presented in figures 8, 9, and 10 for Mach numbers of 5.2, 7.4, and 10.4, respectively. Results are shown for nominal angles of attack of -5°, 0°, +6°, +15°, +20°, +26°, +35°, +40°, +46°, and +55°. Figures 11, 12, and 13 present the pressure coefficients for the model in sideslip at Mach number 10.4 for angles of attack of 0°, 20°, and 40°, respectively.

A summary of the hypersonic pressure coefficients on the conical portion of the model at the three hypersonic test Mach numbers is presented in figure 14. A summary of pressure coefficients for the pitch flap and rudder is shown in figure 15. Figure 16 summarizes the pressure coefficients for the rudder during sideslip at Mach number 10.4.

Subsonic Pressure Distributions

There are no appropriate theories for estimating the subsonic pressure distributions for complex, nonaxisymmetric shapes at angle of attack. The following paragraphs discuss some of the more prominent features evident in the pressure distributions shown in figures 5, 6, and 7.

Peak negative pressure coefficients.- In subsonic flow, high local velocities occur around sharp corners and around edges having small, local radii. Accompanying the high local velocity is, of course, the reduction in local static pressure which appears in the pressure distributions as large negative values of the pressure coefficients. The other principal source for the occurrence of high local velocity and low local pressure is the formation of vortex flow which accompanies the production of lift on three-dimensional wings or bodies. Inspection of the figures reveals two areas in particular where large negative pressure coefficients resulted. The first was around the nose radius along the top center line. The peak value for the coefficient in this region started at approximately -0.7 at 0° angle of attack (fig. 5(a)) and reached -2.5 at 35° angle of attack (fig. 5(e)). The other localized region where large negative pressure coefficients occurred was on the outer surface of the fin. Relatively smaller peaks occurred on the canopy also, as may be seen in the figures.

The large, negative pressure coefficients for the nose are associated with the thickness effects and the small local radius of curvature. (It is interesting that the measured peak negative value was -2.5, whereas characteristic peak values in subsonic flow are -1.3 for a sphere and -3.0 for two-dimensional flow around a cylinder.) The peaks in the pressure coefficients measured by the orifice on the side of the fin, on the other hand, are believed to have been caused by the local passage of vortex flow emanating from the edge of the body.

Regions of low local static pressure, indicated by large negative pressure coefficients, must be followed by increases or recovery in pressure back to free-stream values. The adverse pressure gradient associated with this pressure recovery is the principal flow feature tending to promote flow separation. Interestingly enough, the present subsonic pressure distributions indicate generally good pressure recovery behind the peaks to coefficients near zero or slightly positive. This can possibly be attributed to the three-dimensional relief afforded the boundary layer by the basically conical shape of the M-2. Separation problems generally become more severe, however, at transonic speeds and must be investigated.

Comparison of windward and leeward pressures.- Another feature of the subsonic pressure distributions which bears noting is the effect of angle of attack on the distribution of loading on the windward and leeward surfaces. As the angle of attack was increased, the pressure coefficients for the lower center line became increasingly positive, while those for the upper center line became increasingly negative (fig. 5(e)). The coefficients for these two rows of orifices moved vertically apart but continued to straddle the zero pressure coefficient axis. It might be inferred, then, that the lift due to the overpressure of the lower surface relative to the free-stream pressure was about the same magnitude as the lift contributed by the underpressure of the upper surface relative to free-stream pressure.

There was almost no change in the pressure coefficients for the row of orifices along the 45° lower plane as the angle of attack was increased from 0° to 20°. A slight reduction in coefficient occurred as the angle was increased further to 35° (fig. 5(e)). The pressure coefficients for this same row of orifices underwent the expected increase as the orifices became more windward during the sideslip tests, the results of which are shown in figure 6.

The pressure coefficients for the inner surface of the port fin and for the base with and without the canopy on the model show that the canopy exerted a sizable influence on the leeward surface pressures (fig. 7). The reversal in trend of the variation of fin inner surface pressure with angle of attack above 20° (fig. 7(a)) suggests the possibility of the onset of flow separation between the fins, or of a forward shift of the loading on the body upper surface. The pressure coefficients for this same orifice demonstrate the expected reduction in local pressure at negative sideslip angles where this surface became leeward (fig. 7(b)).

Hypersonic Pressure Distributions

Several dominant features prevail throughout the hypersonic pressure distributions, and, in some instances, the contrasts between the trends in pressure coefficients for the subsonic and hypersonic regimes bear noting.

Stagnation pressure coefficient.- The pressure coefficient corresponding to the maximum local pressure in subsonic flow may be calculated from the isentropic compression relation:

$$C_{p_{max}} = \frac{2}{\gamma M^2}\left\{\left[1 + \left(\frac{\gamma-1}{2}\right)M^2\right]^{\frac{\gamma}{\gamma-1}} - 1\right\} \qquad (1)$$

The stagnation pressure coefficient varies from unity at a Mach number of 0 to 1.28 at a Mach number of unity. At Mach numbers above unity, where a detached bow shock forms in front of blunt shapes, the stagnation pressure coefficient can be evaluated from normal shock theory.

$$C_{p_{stag}} = \frac{2}{\gamma M^2}\left\{\left[\frac{(\gamma+1)M^2}{2}\right]^{\frac{\gamma}{\gamma-1}}\left[\frac{\gamma+1}{2\gamma M^2-(\gamma-1)}\right]^{\frac{1}{\gamma-1}}-1\right\} \qquad (2)$$

The stagnation pressure coefficients for the hypersonic test Mach numbers of the present investigation are very close to 1.83. Although it is possible for regions to develop higher pressures than that occurring at the forward stagnation point (such as for flared bodies and aft mounted flaps preceded upstream by a series of multiple weak shocks), the results for the M-2 indicate that the surface pressures were everywhere less than the nose stagnation pressure. The largest values of pressure coefficient occurred along the bottom center line at the highest angle of attack (figs. 8(j), 9(j), and 10(j)), on the pitch flap (fig. 10(d)), and on the fin leading edge during sidelsip (fig. 11(d)). These areas, then, would deserve special attention during possible future structural and heating studies.

Canopy.- A small increase in pressure occurred over the canopy at hypersonic speeds as evidenced by the increase in pressure coefficients relative to the canopy-off configuration (figs. 8-12). This is in contrast to the negative pressure coefficients for the canopy for subsonic speed. The canopy exerted little or no influence on the pressure measurements around the rest of the model at hypersonic speed, especially at the higher angles of attack (fig. 10(j)).

It might be pointed out that the absence of sizable negative pressure coefficients in the hypersonic pressure distributions does not mean that local pressures cannot be less than free-stream static pressure. On the contrary, the pressures can approach vacuum, but the corresponding pressure coefficients at hypersonic speeds remain very small negative numbers.

Minimum pressure coefficient.- The base pressure measurements for the present tests are not shown in the figures in coefficient form, because they were influenced by a portion of the internal cooling air, which bled out the base of the model. It can readily be shown, however, what the limiting pressure coefficients might have been with a vacuum on the model base, that is, $p = 0$ in the definition of pressure coefficient. The minimum pressure coefficient may then be written:

$$C_{p_{min}} = -\frac{p_\infty}{q_\infty} = -\frac{2}{\gamma M^2} \qquad (3)$$

$$= -0.074 \text{ at } M = 5.2$$

$$= -0.036 \text{ at } M = 7.4$$

$$= -0.018 \text{ at } M = 10.4$$

Effect of varying hypersonic Mach number.- Comparison of the results presented in figures 8, 9, and 10 indicates that there were relatively minor changes accompanying the variation of Mach number. The similarity between

the results for the three Mach numbers can be readily seen in the cross-plots of the pressure coefficients for the conical portion of the body in figure 14 and for the pitch flap and rudder in figure 15.

Comparison of Hypersonic Experimental Results and Theoretical Estimates

Conical surface.- The average pressure coefficients for the three rows of orifices along elements of the conical surface are compared with estimates from modified Newtonian impact theory and from the tangent-cone approximation in figure 14. The modified impact theory is based on the stagnation pressure coefficient (eq. (2)) as follows:

$$C_p = C_{p_{stag}} \sin^2 \theta \qquad (4)$$

$$= 1.83 \sin^2 \theta$$

The tangent-cone estimate is the inviscid sharp-cone solution evaluated for a cone having a semivertex angle such that the cone would be tangent to the local region of the model under consideration. The semivertex angle of the cone tangent to the lower center line may be taken as the sum of the angle of attack and the model 13° half-cone angle. The tangent cone for the horizontal center line may be assumed to have a 13° semivertex angle. For the row of orifices along the 45° lower plane, the semivertex angle of the tangent cone may be evaluated from

$$\sigma = \sin^{-1}(\sin \theta \cos \alpha - \cos \theta \sin \varphi \sin \alpha) \qquad (5)$$

$$= \sin^{-1}(\sin 13^\circ \cos \alpha - \sin 225^\circ \cos 13^\circ \sin \alpha)$$

The sharp-cone solutions were taken from the summary figure 6 of reference 7.

There was agreement between the measured pressure coefficients and those estimated from modified impact theory, except for the horizontal row at high angles of attack. The tangent-cone estimates were roughly 20 percent too large. Over the range of angles of attack covered, the pressures around the conical forebody followed an approximately $\sin^2 \varphi$ distribution.

Rudder.- The pressure coefficients summarized in figures 15(a) and 16 indicate that these controls possibly became engulfed in the vortical flow and in the entropy boundary layer of the body, especially around 5° angle of attack. The pressure coefficients for the 25° rudder deflection at -5° angle of attack were around 0.4 which was close to the impact theory estimate. With increasing angle of attack, however, there was a large reduction in pressure on the rudder, with minimums occurring around 5°. With further increase in angle of attack, the rudder pressures rose and agreed with impact theory again around 40° angle of attack. The rudder pressure coefficients shown in figure 16 for sideslip tests at a Mach number of 10.4 were

CONFIDENTIAL

significantly less than the estimates from modified impact theory and from oblique shock theory, but they did exhibit the expected trend of increasing as the measuring orifice became more windward.

Pitch flap.- The pressure coefficients for the pitch flap are cross-plotted in figure 15(b) for deflections of 0° and 45° at the three hypersonic test Mach numbers and for a deflection of 30° at Mach number 10.4. At low angles of attack, the flaps were partially shielded by the body and tended to become immersed in the entropy boundary layer. The pressure coefficients under these conditions were less than those estimated from impact and oblique shock theories. At higher angles of attack, the flaps tended to emerge from the entropy boundary layer, and the corresponding pressure coefficients exceeded the estimates from impact theory and approached the estimates from oblique shock theory. For the oblique shock estimates, the body bow shock was neglected and free-stream Mach number was assumed at the control.

CONCLUDING REMARKS

Wind-tunnel investigations of the surface pressure distributions for the M-2 lifting entry configuration indicated that the most severe loading conditions occurred over the nose and fins at both subsonic and hypersonic speeds.

The low pressures over the nose upper surface at subsonic speed resulted from the acceleration of the air flow in passing around the locally small radius of curvature. The low pressures on the fin resulted from the low pressures which existed on the adjacent body upper surface and from possible vortex flows induced by the body lift.

Varying the hypersonic Mach number from 5.2 to 10.4 had very little effect on pressure coefficients. The pressure coefficients measured for the conical forebody could be predicted with good accuracy by means of modified Newtonian impact theory. Only qualitative agreement was possible, however, between the measured pressure coefficients for the rudder and pitch flap and those estimated from impact and oblique shock theories.

Ames Research Center
National Aeronautics and Space Administration
Moffett Field, Calif., May 6, 1964

CONFIDENTIAL

REFERENCES

1. Rakich, John V.: Supersonic Aerodynamic Performance and Static Stability Characteristics of Two Blunt-Nosed, Modified 13° Half-Cone Configurations. NASA TM X-375, 1960.

2. Kenyon, George C., and Edwards, George G.: A Preliminary Investigation of Modified Blunt 13° Half-Cone Re-entry Configurations at Subsonic Speeds. NASA TM X-501, 1961.

3. Rakich, John V.: Aerodynamic Performance and Static-Stability Characteristics of a Blunt-Nosed, Boattailed, 13° Half-Cone at Mach Numbers From 0.6 to 5.0. NASA TM X-570, 1961.

4. Kenyon, George C., and Sutton, Fred B.: The Longitudinal Aerodynamic Characteristics of a Re-entry Configuration Based on a Blunt 13° Half-Cone at Mach Numbers to 0.92. NASA TM X-571, 1961.

5. Kenyon, George C.: The Lateral and Directional Aerodynamic Characteristics of a Re-entry Configuration Based on a Blunt 13° Half-Cone at Mach Numbers to 0.90. NASA TM X-583, 1961.

6. Hassell, James L., Jr., and Ware, George M.: Investigation of the Low-Subsonic Stability and Control Characteristics of a 0.34-Scale Free-Flying Model of a Modified Half-Cone Reentry Vehicle. NASA TM X-665, 1962.

7. Ames Research Staff: Equations, Tables, and Charts for Compressible Flow. NACA Rep. 1135, 1953.

TABLE I.- PRESSURE ORIFICE LOCATIONS

Orifice	Location	Longitudinal station	Percent length
1	Nose	0	0
2	Bottom	.134	1.12
3	Center line	.456	3.80
4	↓	1.200	10.00
5		3.200	26.67
6		5.200	43.33
7		7.212	60.10
8		9.120	76.00
9		10.704	89.20
10		11.700	97.50
11	Top	.134	1.12
12	Center line	.456	3.80
13	↓	1.200	10.00
14		3.200	26.67
15		5.200	43.33
16		7.212	60.10
17		9.120	76.00
18	Base	12.000	100.00
19	Horizontal	.456	3.80
20	Center line	1.200	10.00
21	↓	3.200	26.67
22		5.200	43.33
23		7.212	60.10
24	45° lower	.456	3.80
25	plane	1.200	10.00
26		3.200	26.67
27		5.200	43.33
28		7.212	60.10
29		9.120	76.00
30		10.704	89.20
31		11.500	95.80
32	Forward of pitch flap	10.200	85.00
33	Pitch flap	11.300	94.20
34	Fin leading edge	9.120	76.00
35	Fin outer surface	10.704	89.20
36	Fin outer surface	11.625	96.80
37	Fin inner surface	11.000	91.70

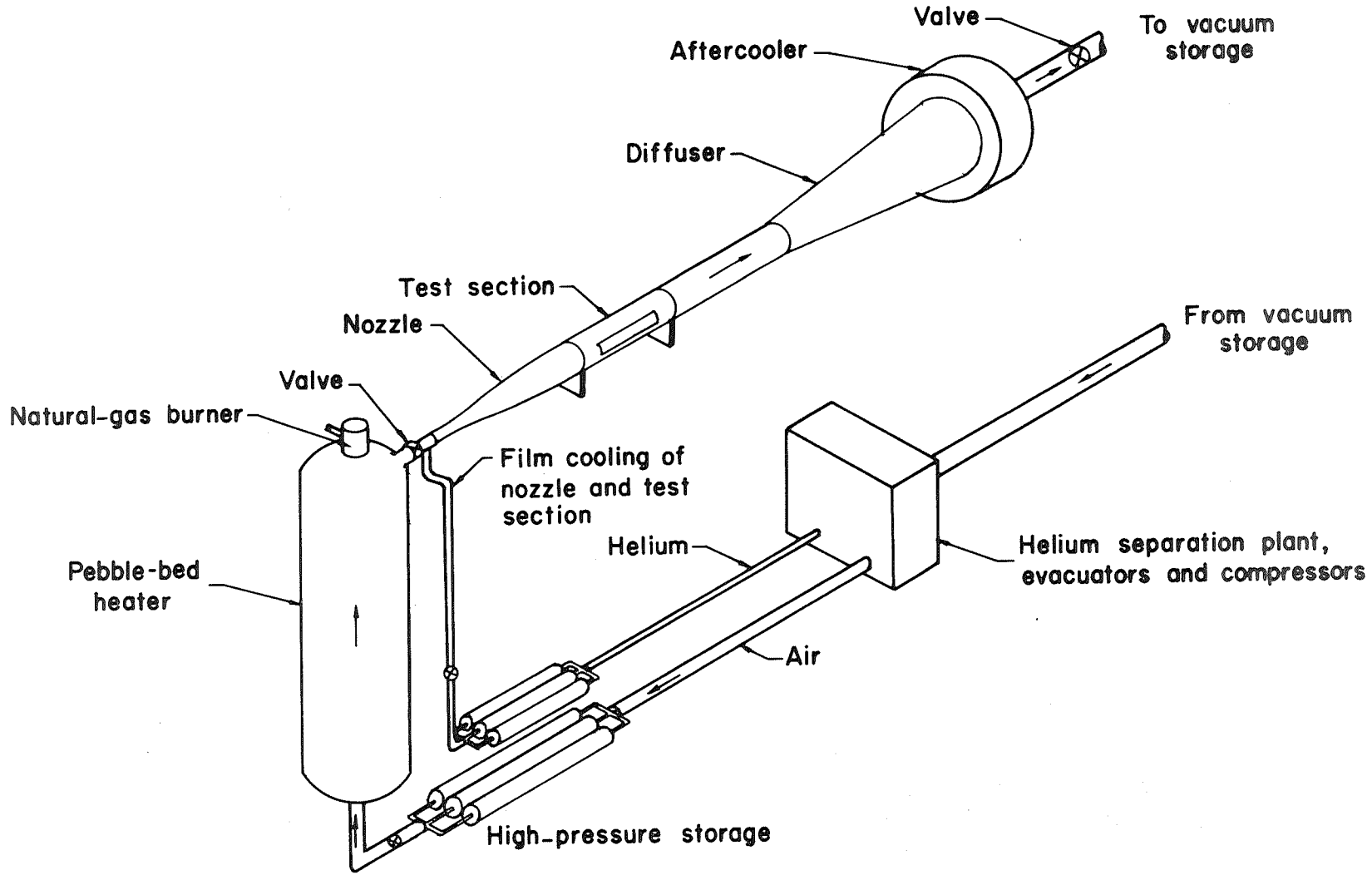

Figure 1.- Schematic sketch of the Ames 3.5-Foot Hypersonic Wind Tunnel.

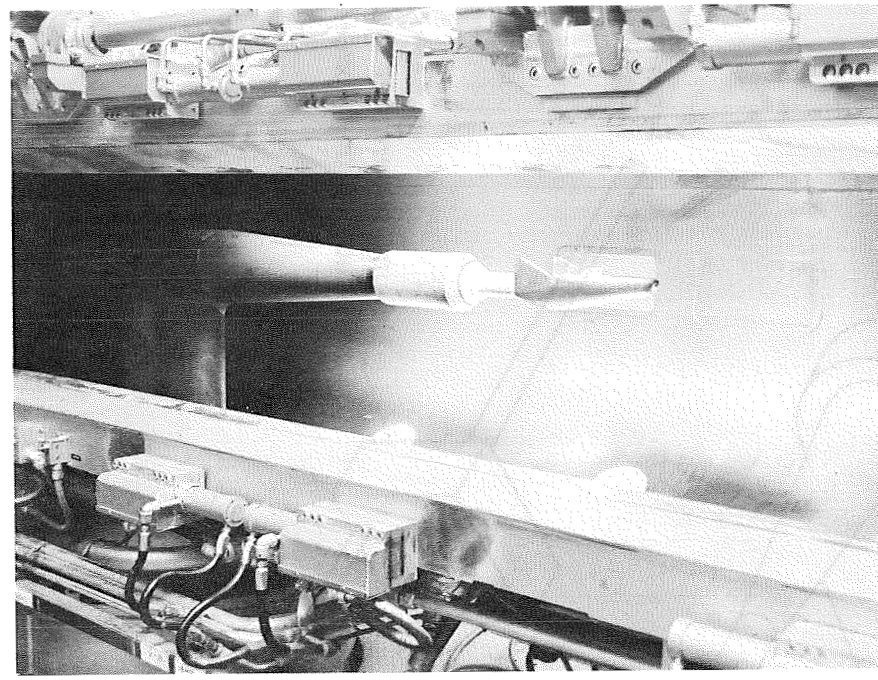

A-29737

Figure 2.- Photograph of the M-2 model mounted in the Ames 3.5-Foot Hypersonic Wind Tunnel.

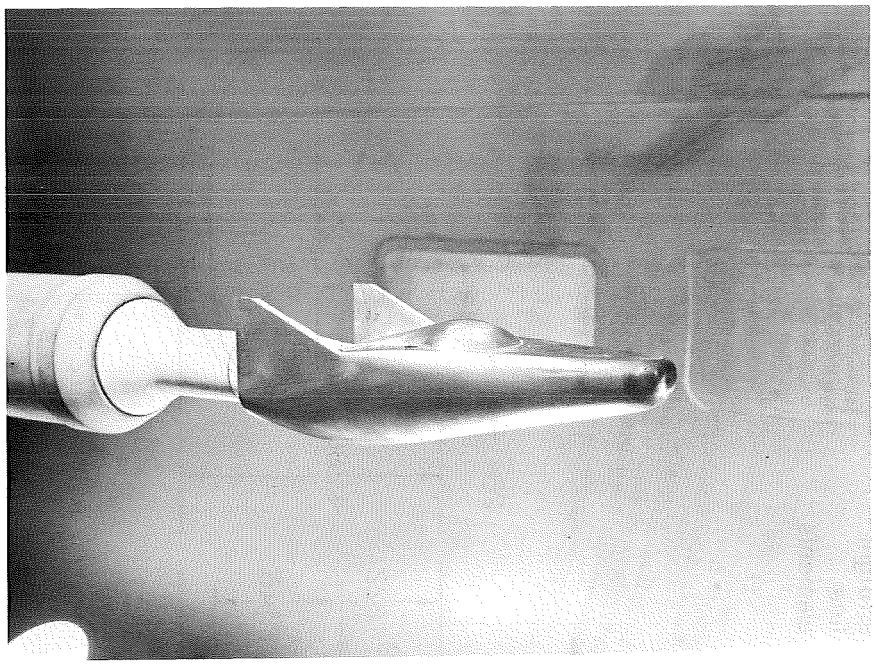

(a) 3/4 front view. A-29735

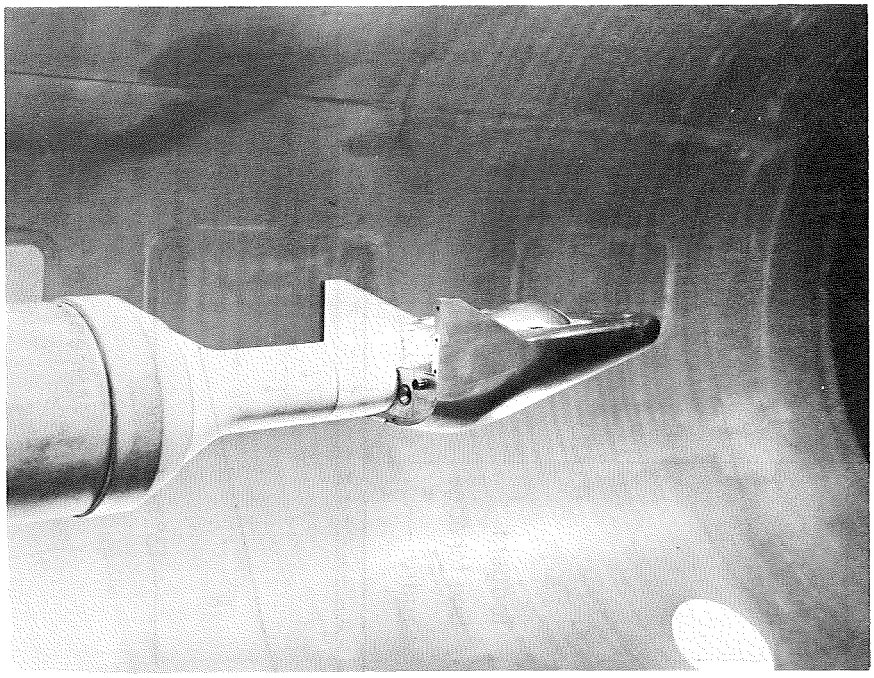

(b) 3/4 rear view. A-29736

Figure 3.- Photographs of the test model of the M-2 reentry configuration.

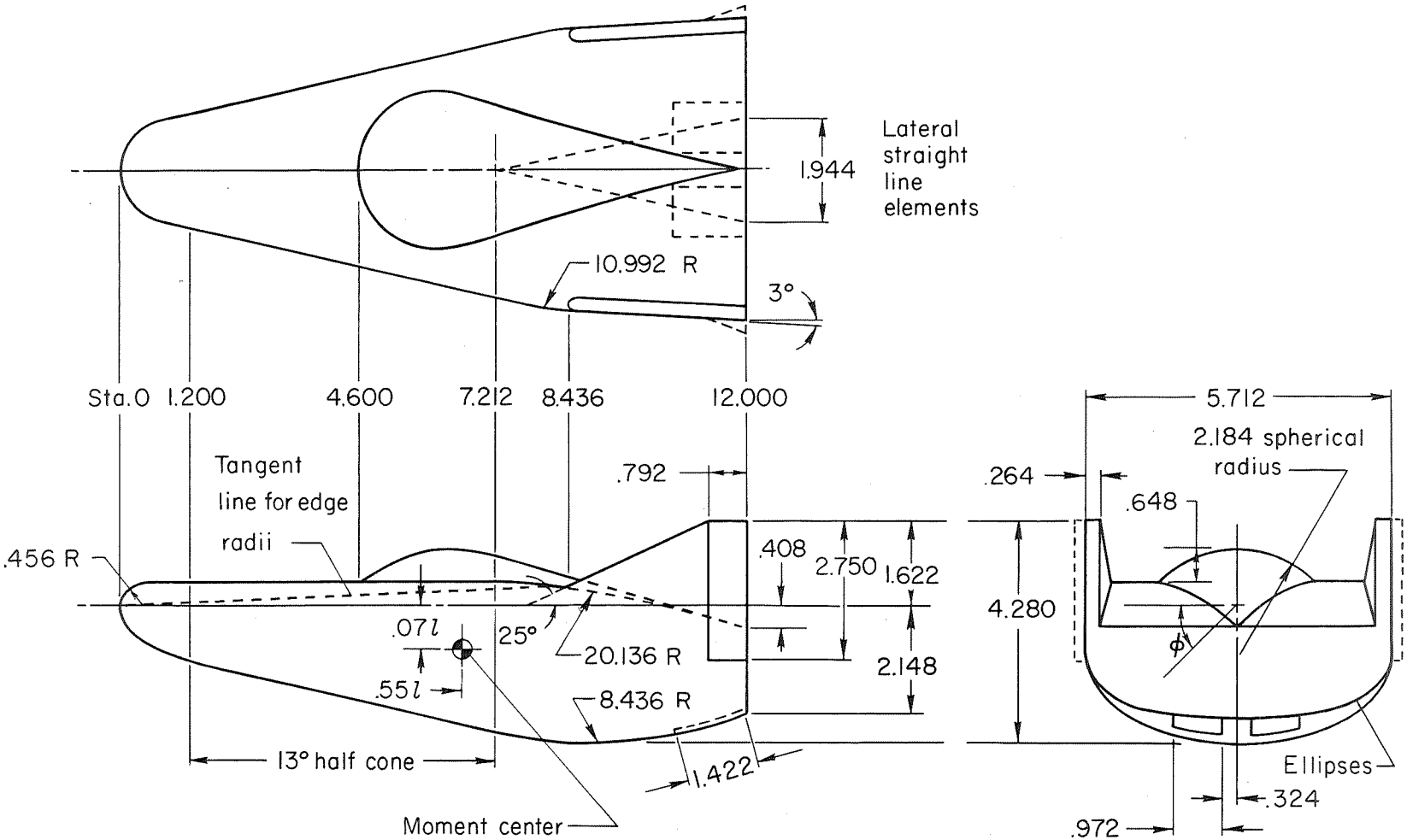

NOTE: All dimensions in inches

Figure 4.- Dimensional details of the M-2 model.

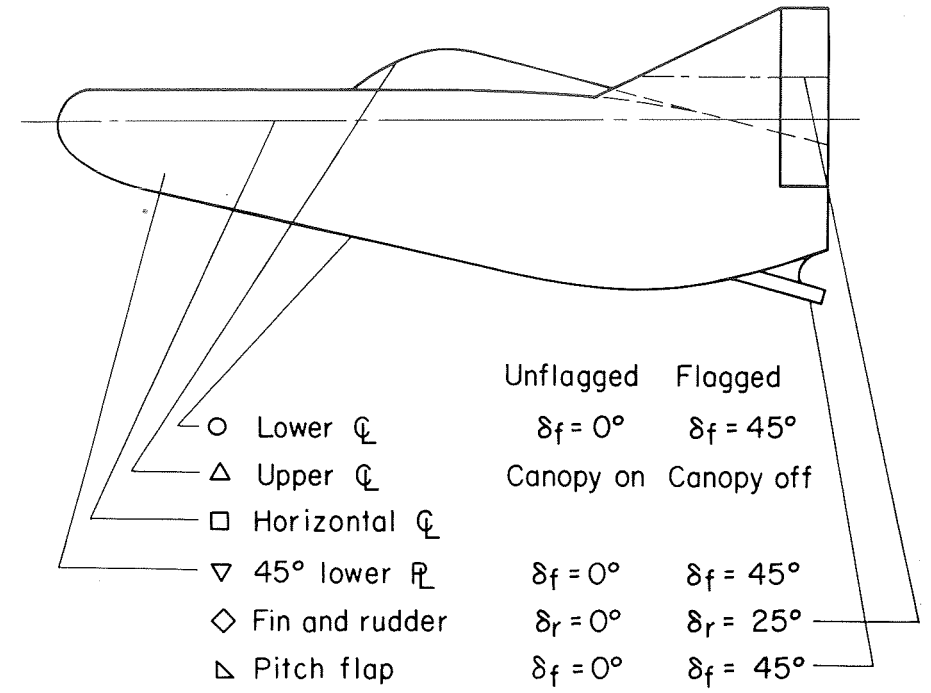

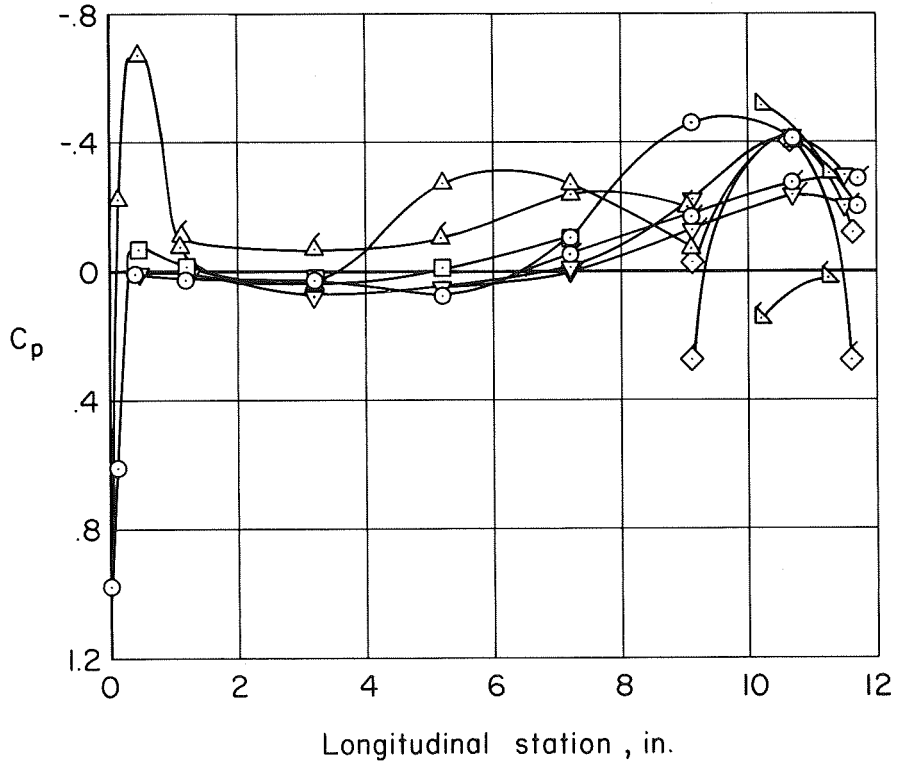

(a) $\alpha = 0^{\circ}$

Figure 5.- Subsonic pressure distributions for the model in pitch; M = 0.23.

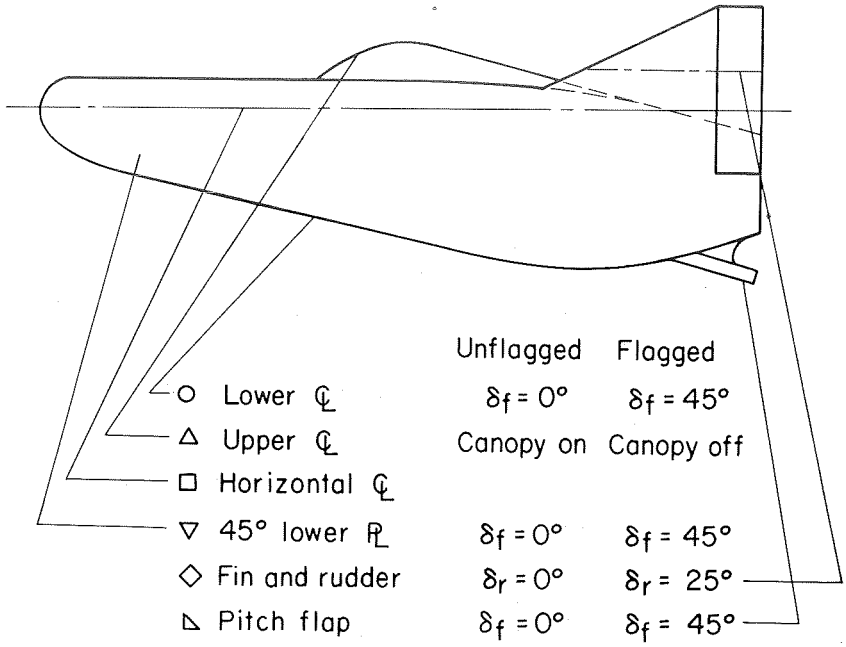

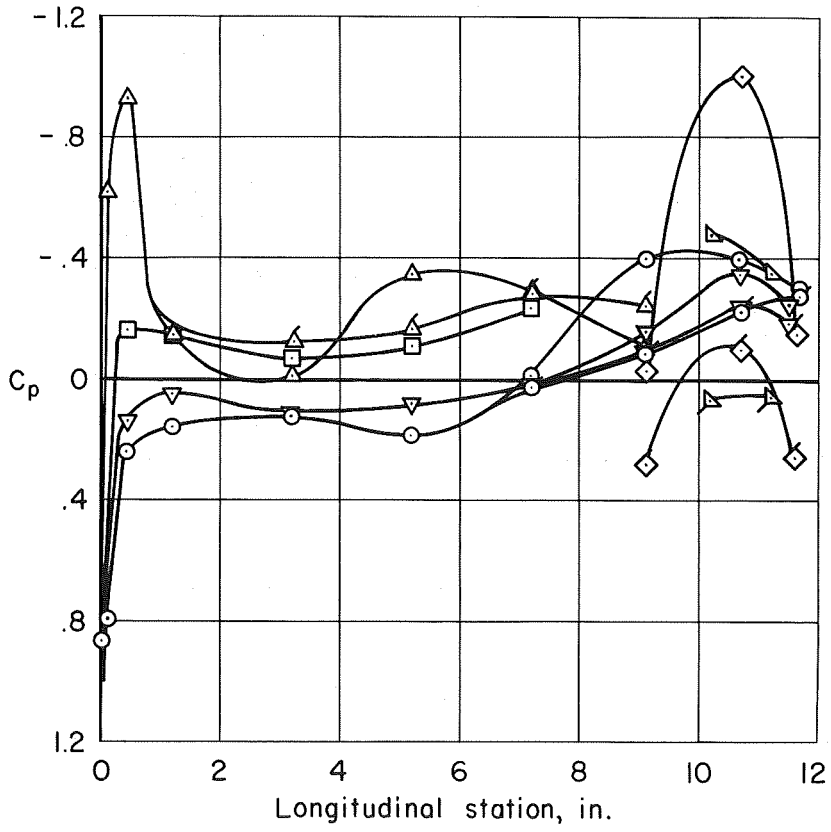

(b) $\alpha = 6^{\circ}$

Figure 5.- Continued.

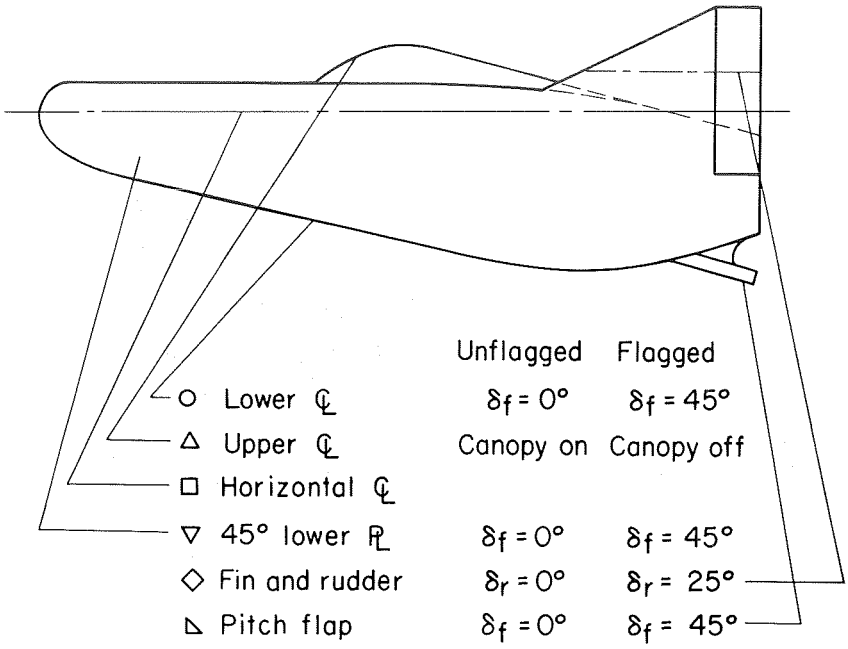

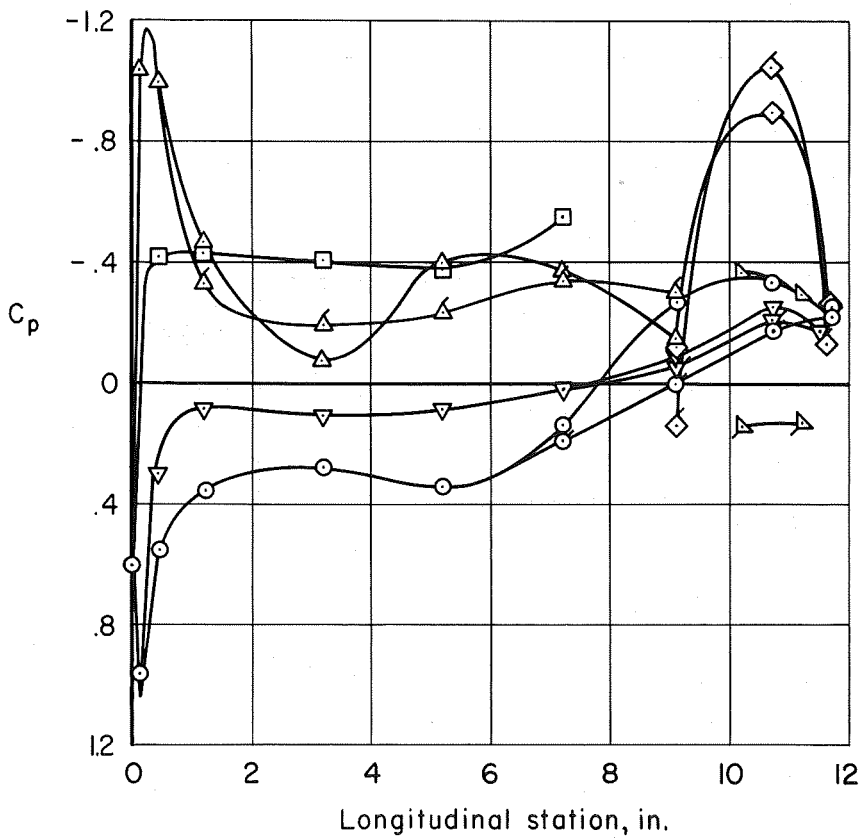

(c) $\alpha = 15^{\circ}$

Figure 5.- Continued.

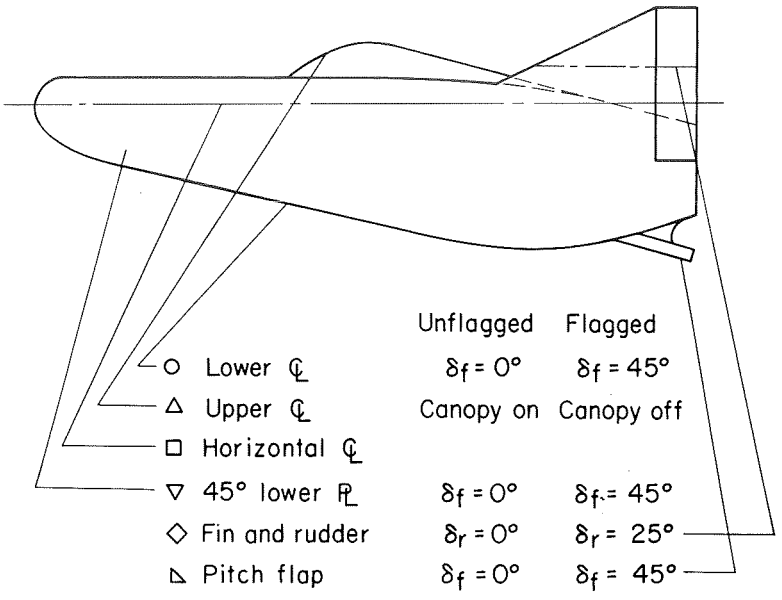

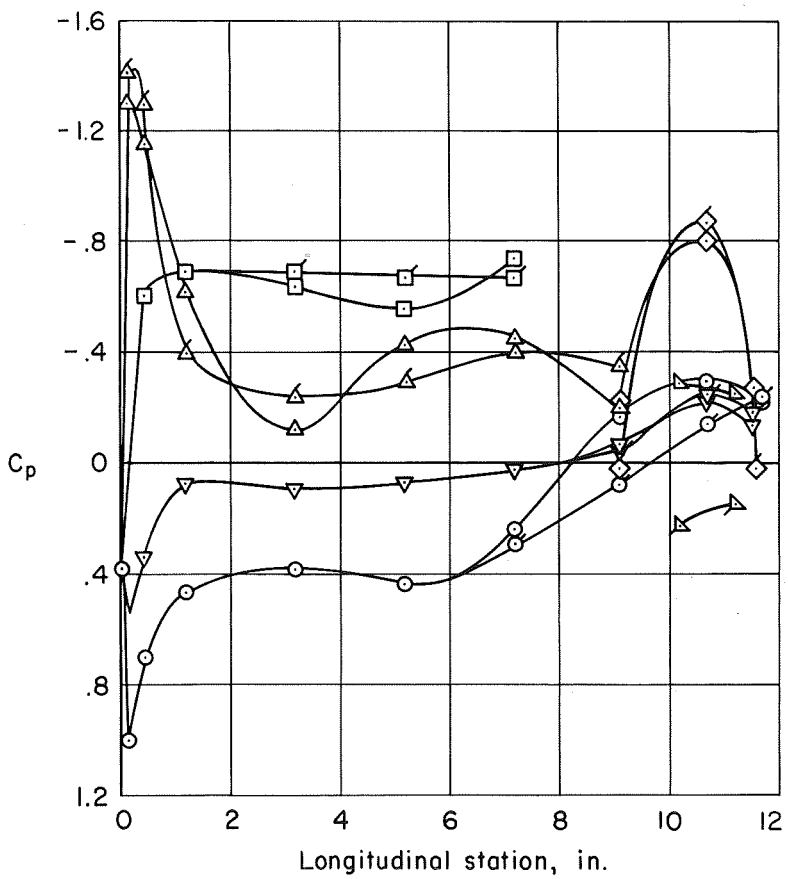

(d) $\alpha = 20^{\circ}$

Figure 5.- Continued.

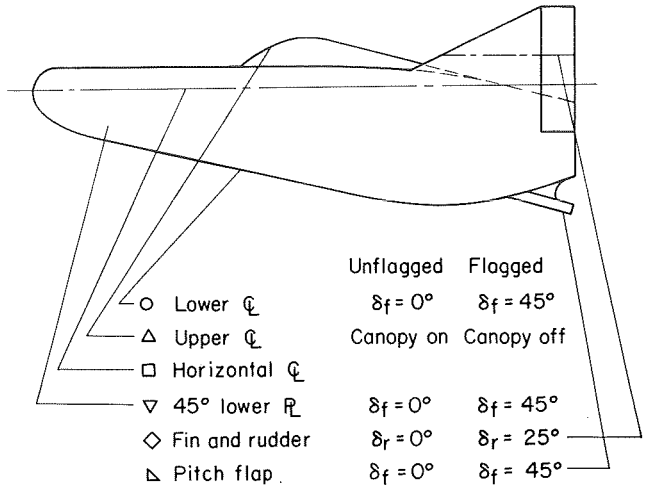

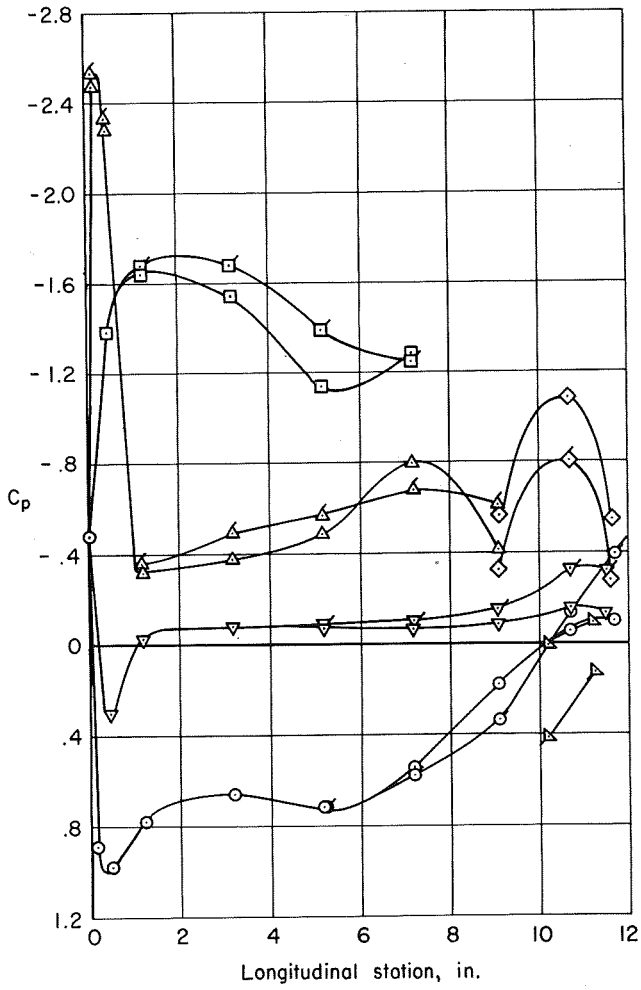

(e) $\alpha = 35^{\circ}$

Figure 5.- Concluded.

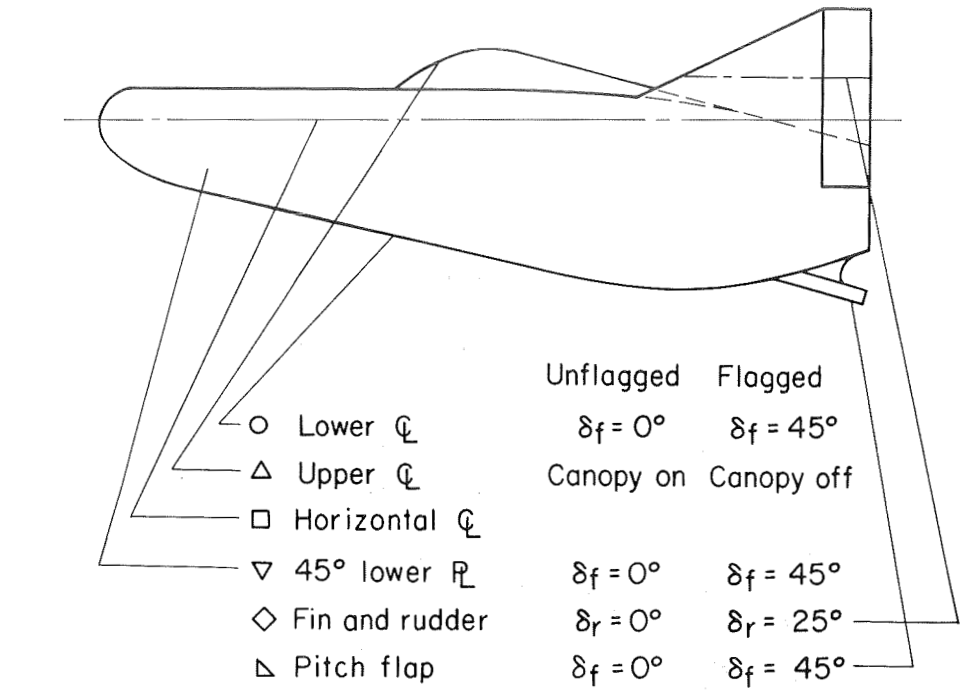

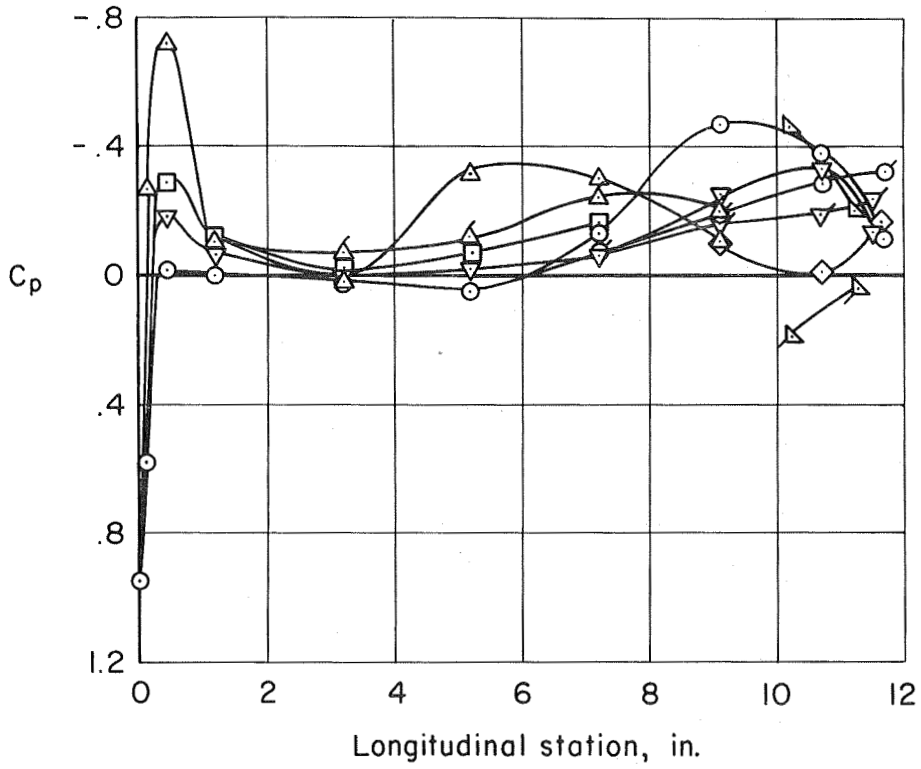

(a) $\beta = 6^{\circ}$

Figure 6.- Subsonic pressure distribution for the model in sideslip; M = 0.23; $\alpha = 0^{\circ}$.

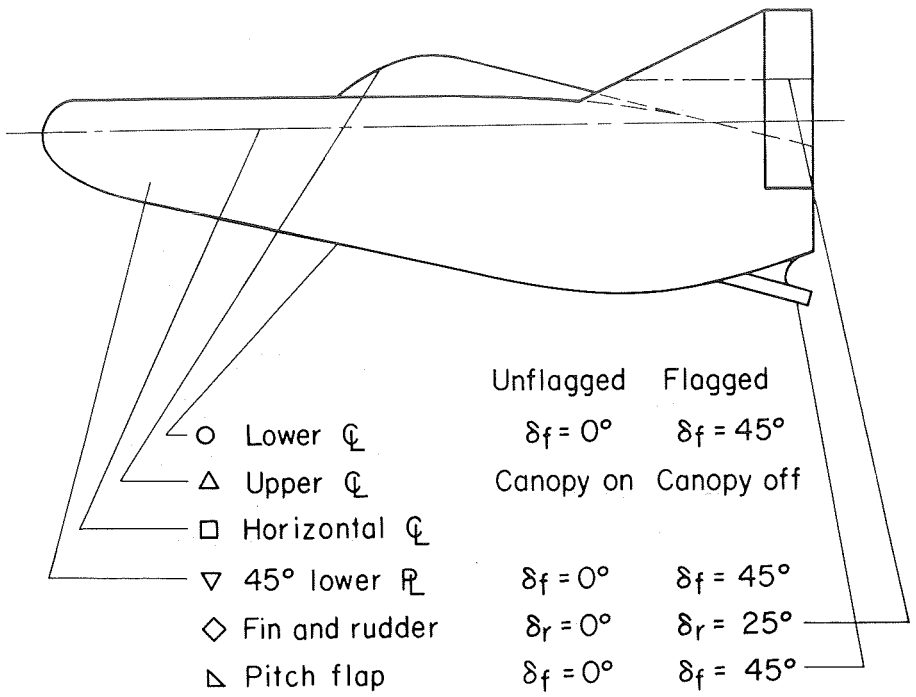

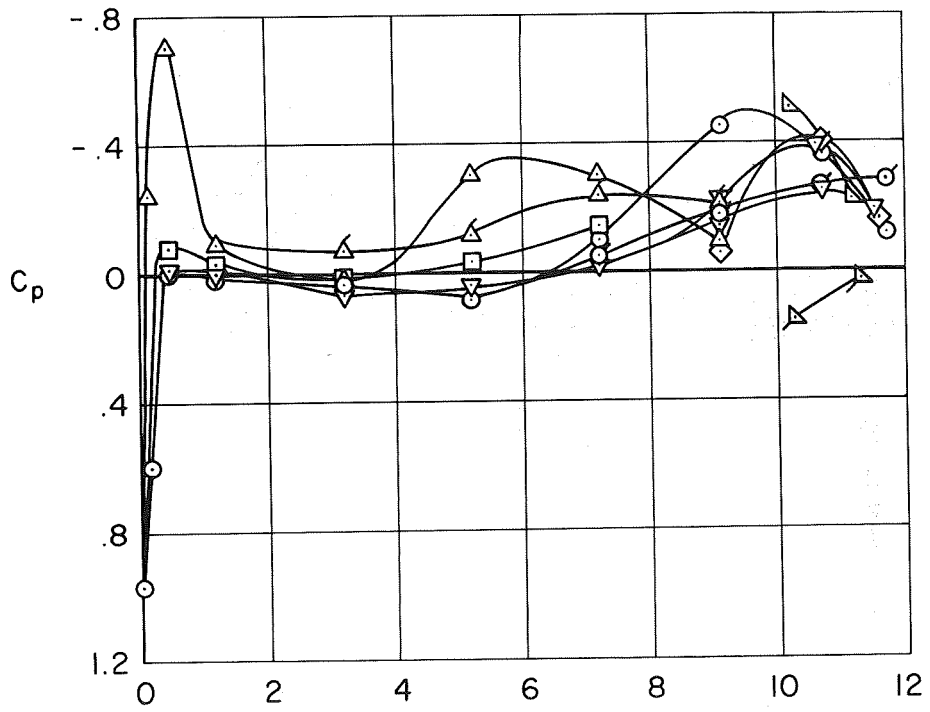

(b) $\beta = 0^{\circ}$

Figure 6.- Continued.

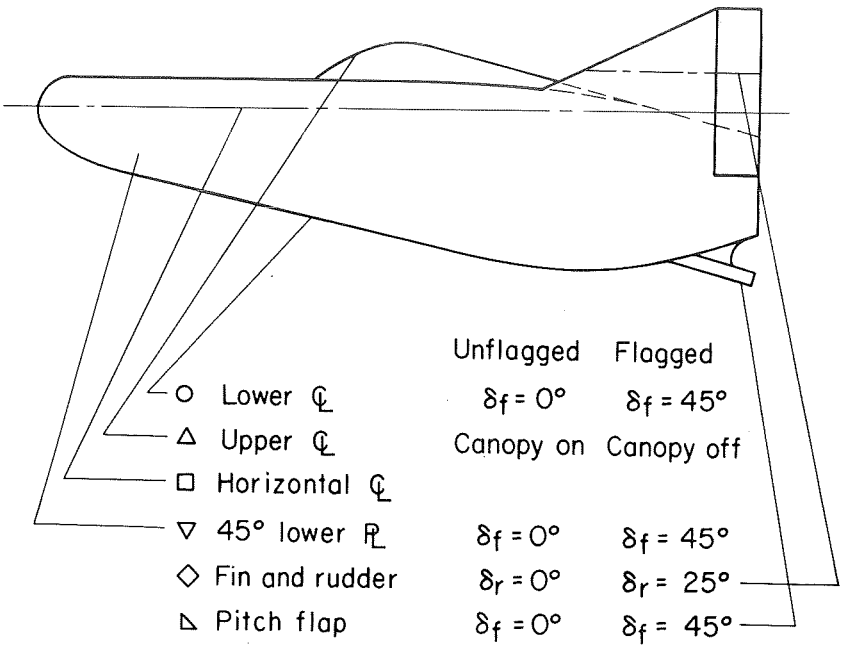

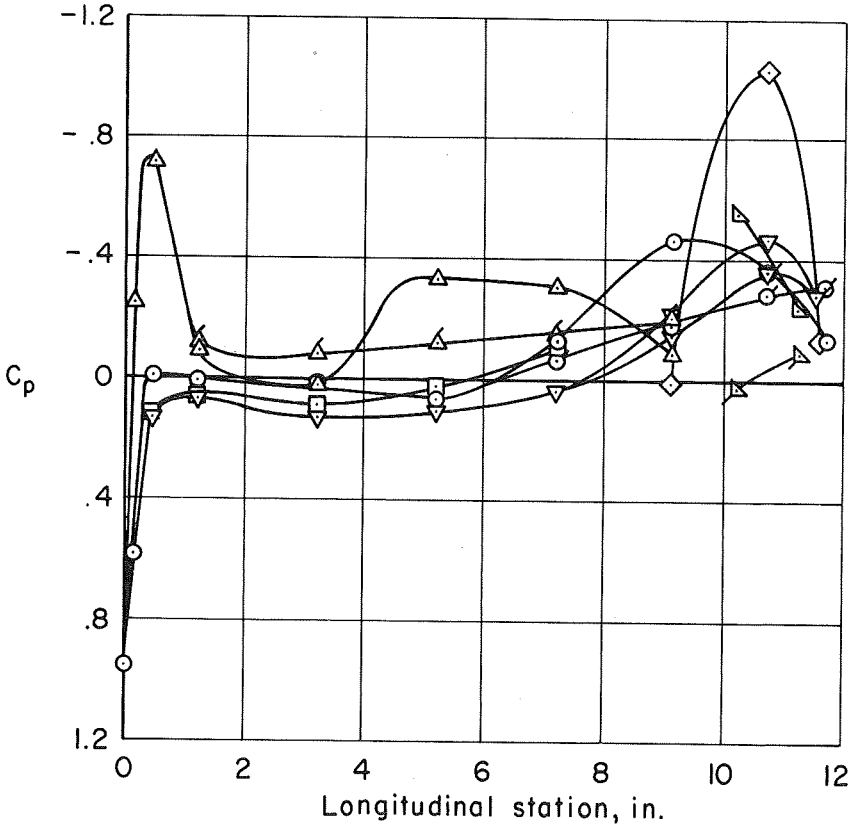

(c) $\beta = -6^{\circ}$

Figure 6.- Continued.

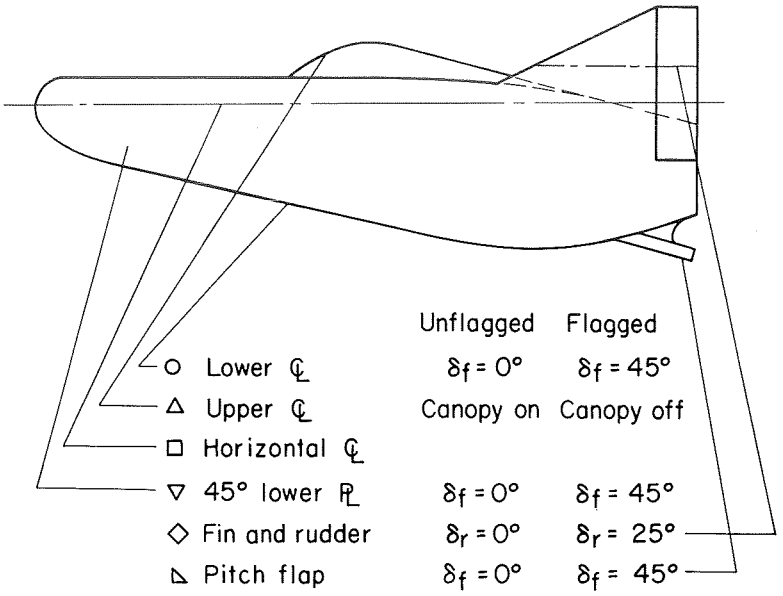

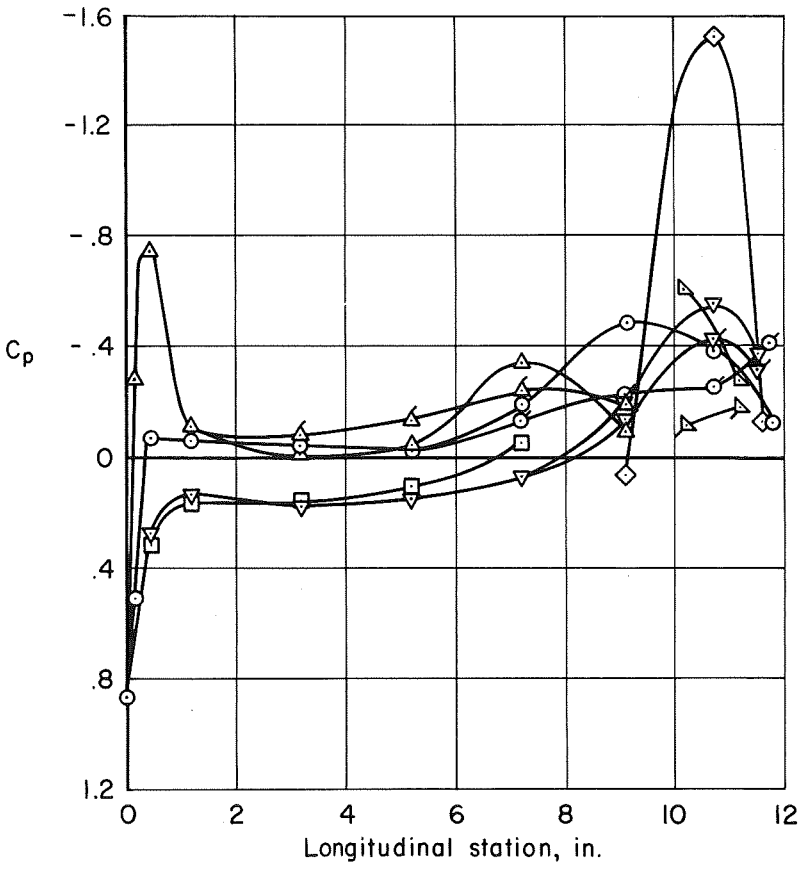

(d) $\beta = -12^{\circ}$

Figure 6.- Concluded.

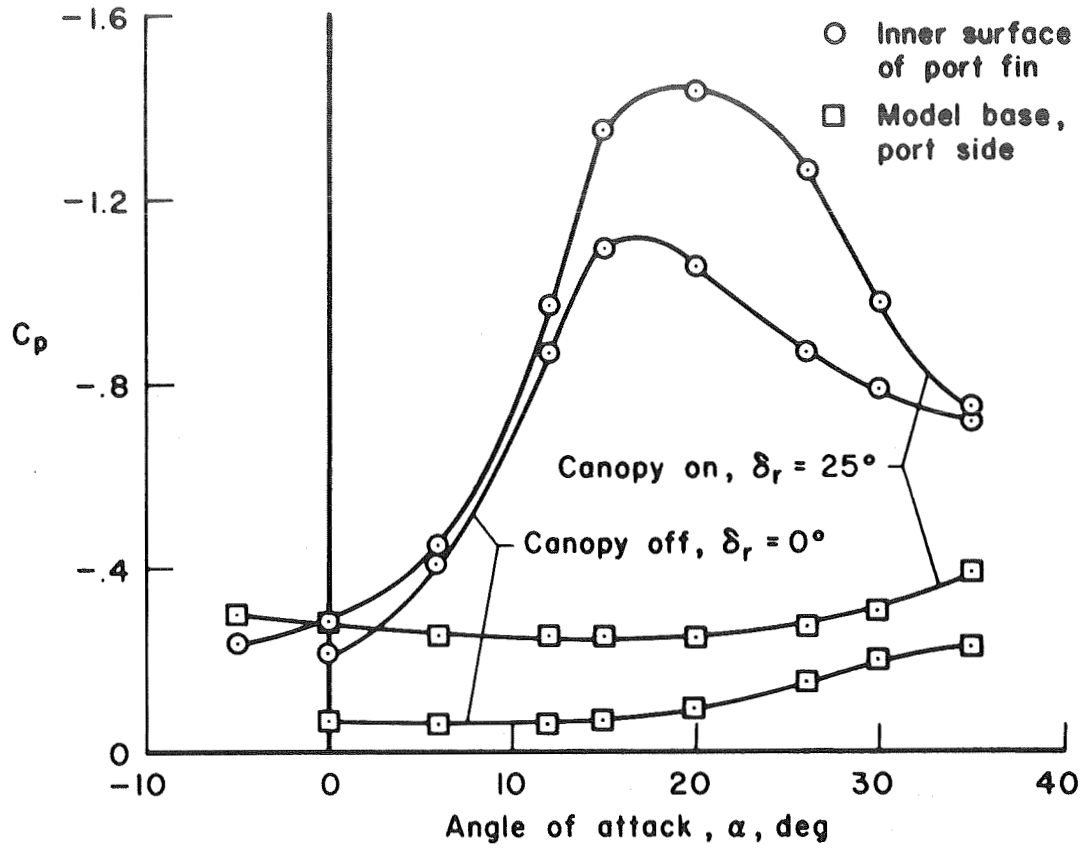

(a) Model in pitch.

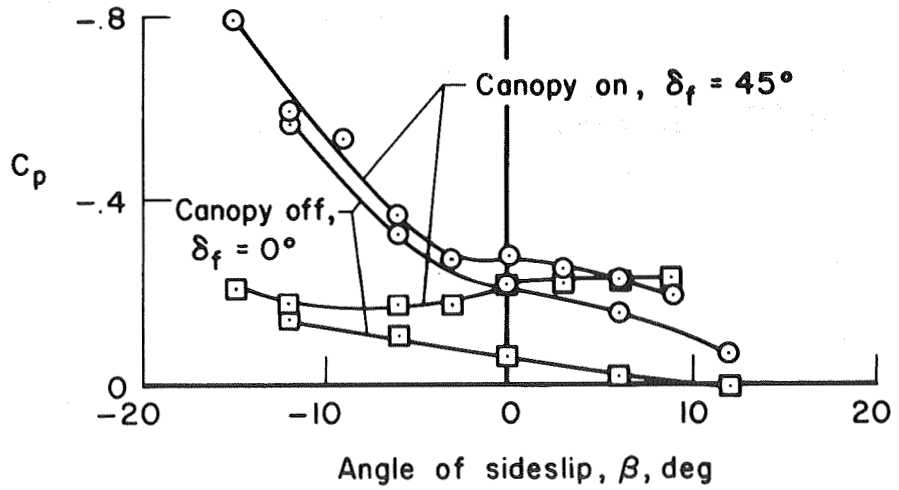

(b) Model in sideslip; $\delta_r = 0^\circ$, $\alpha = 0^\circ$.

Figure 7.- Subsonic pressure coefficients for the inboard surface of the fin and for the model base.

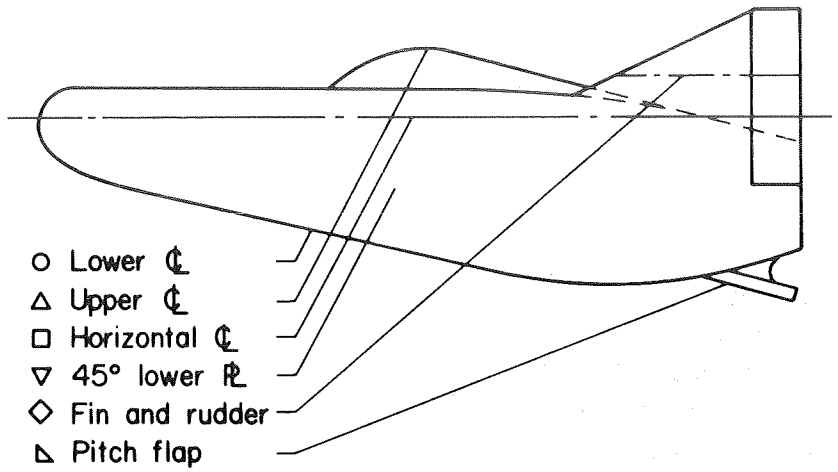

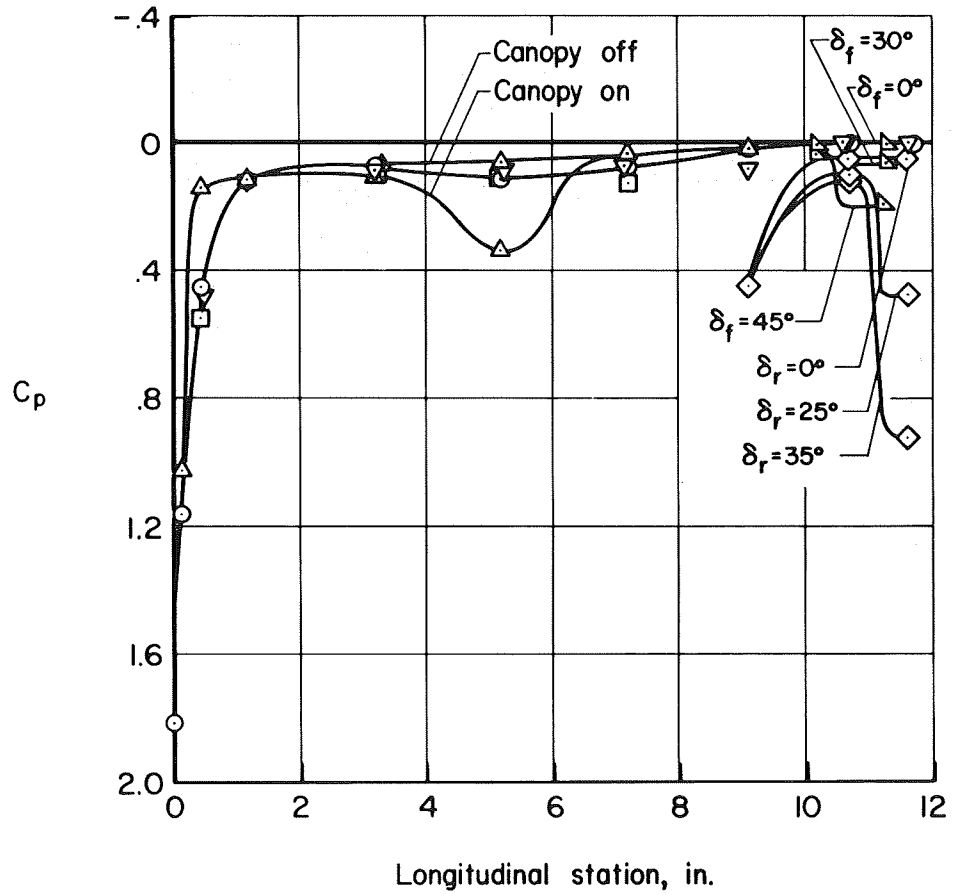

(a) $\alpha = -5.4^\circ$

Figure 8.- Distribution of pressure coefficients for the model with and without canopy and with several deflections of the pitch flaps and rudders; M = 5.2.

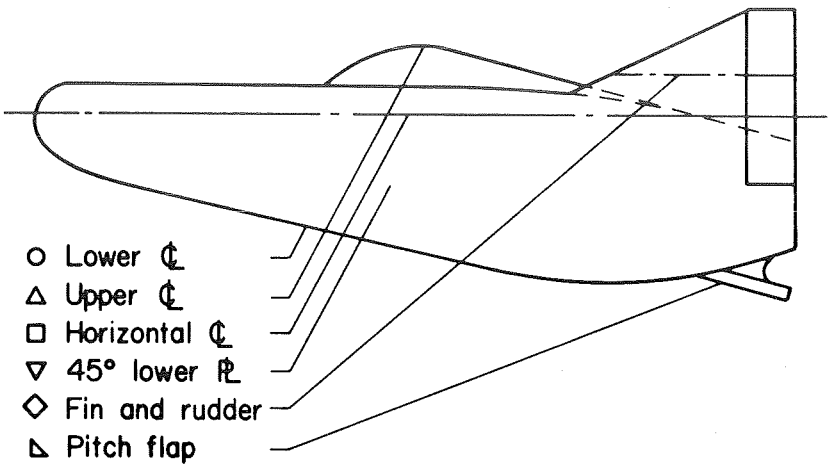

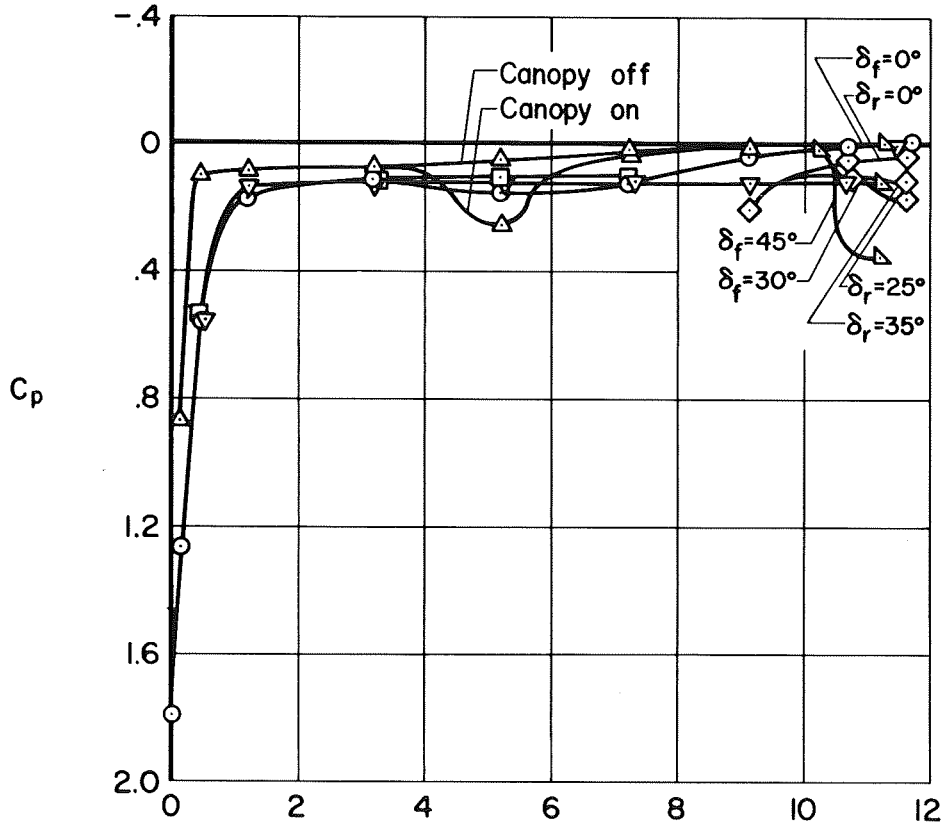

(b) $\alpha = -0.4^\circ$

Figure 8.- Continued.

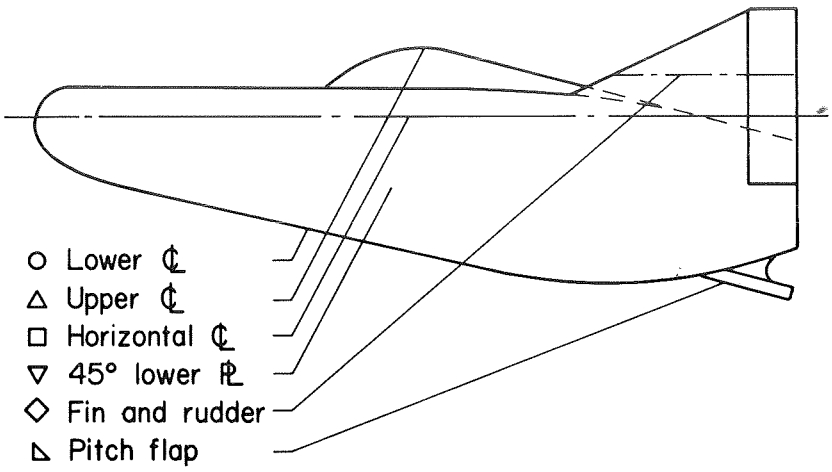

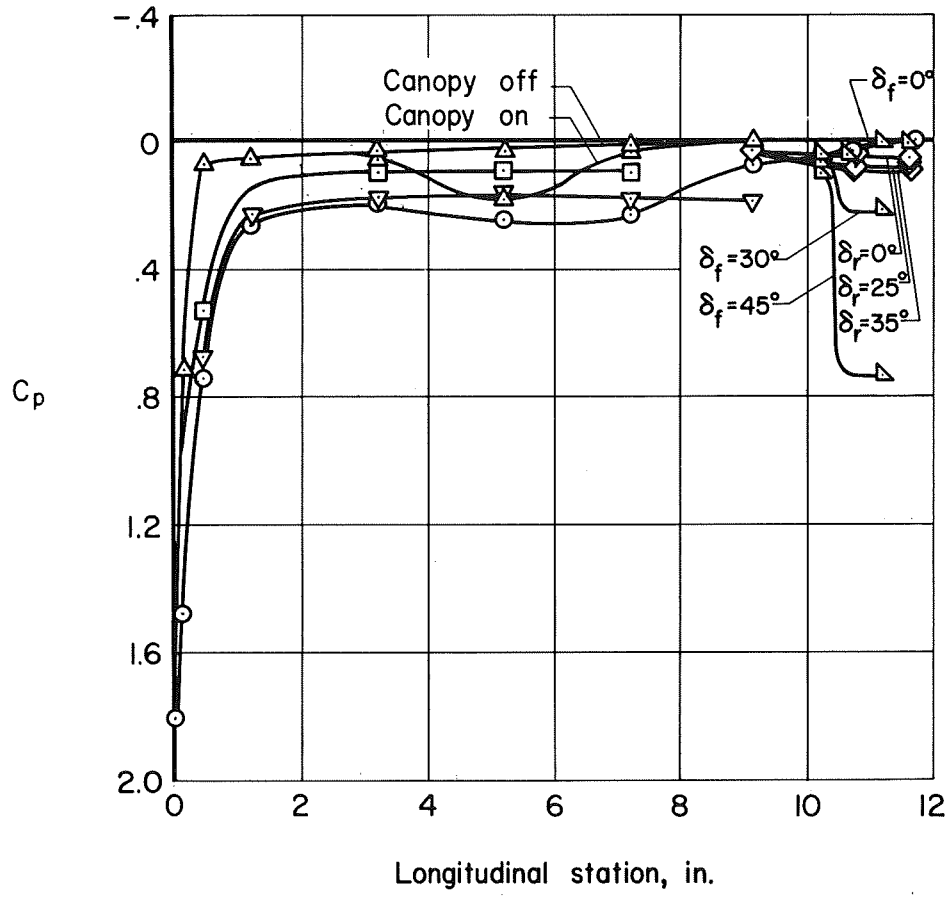

(c) $\alpha = 5.6^\circ$

Figure 8.- Continued.

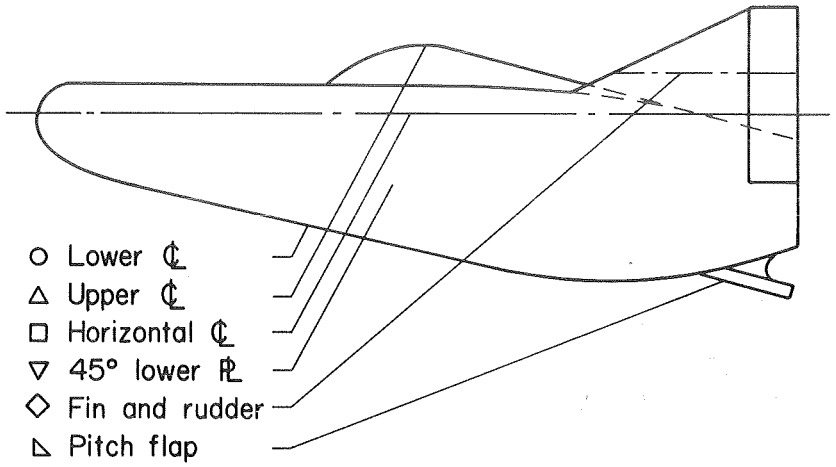

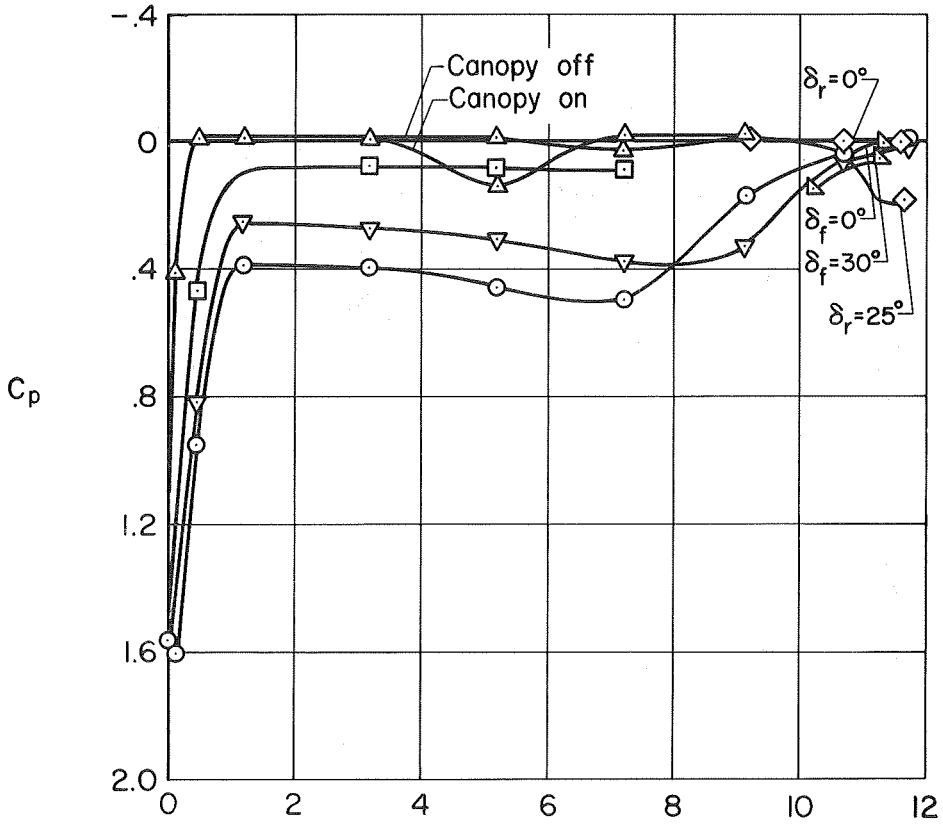

(d) $\alpha = 15.0^\circ$

Figure 8.- Continued.

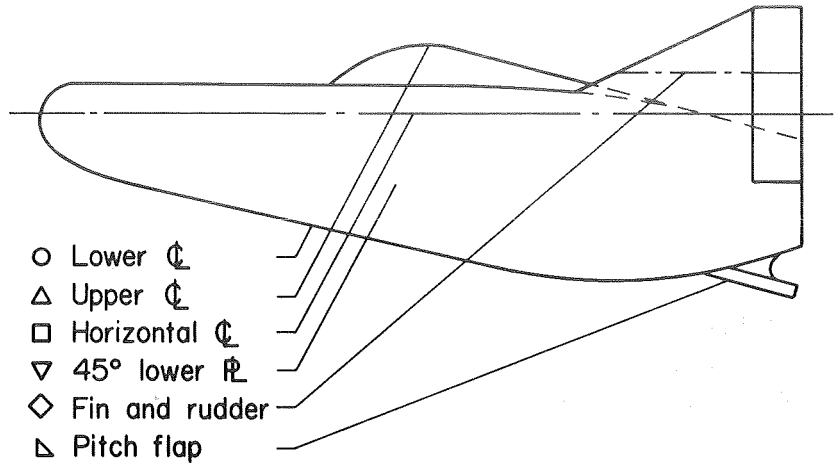

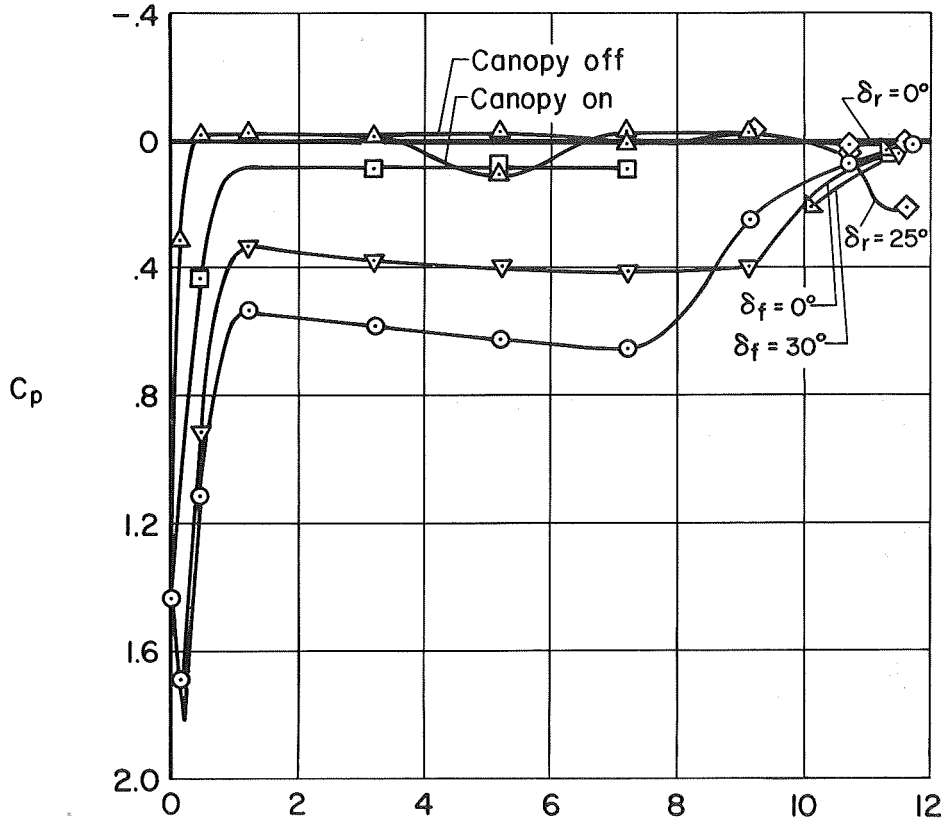

(e) $\alpha = 20.0°$

Figure 8.- Continued.

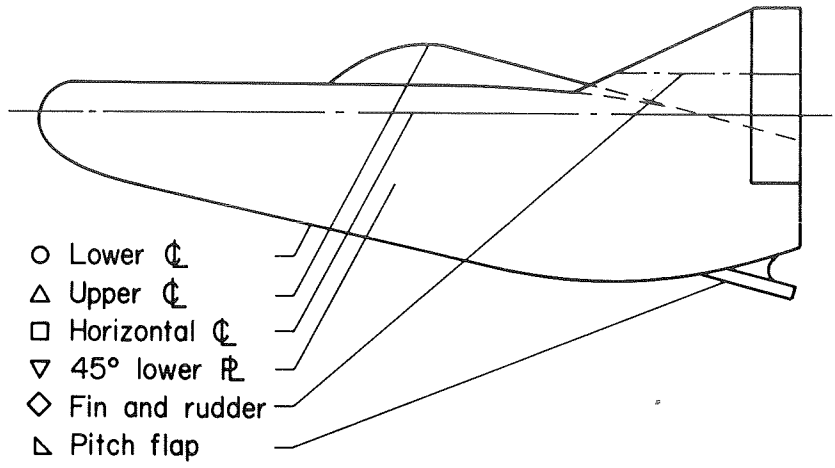

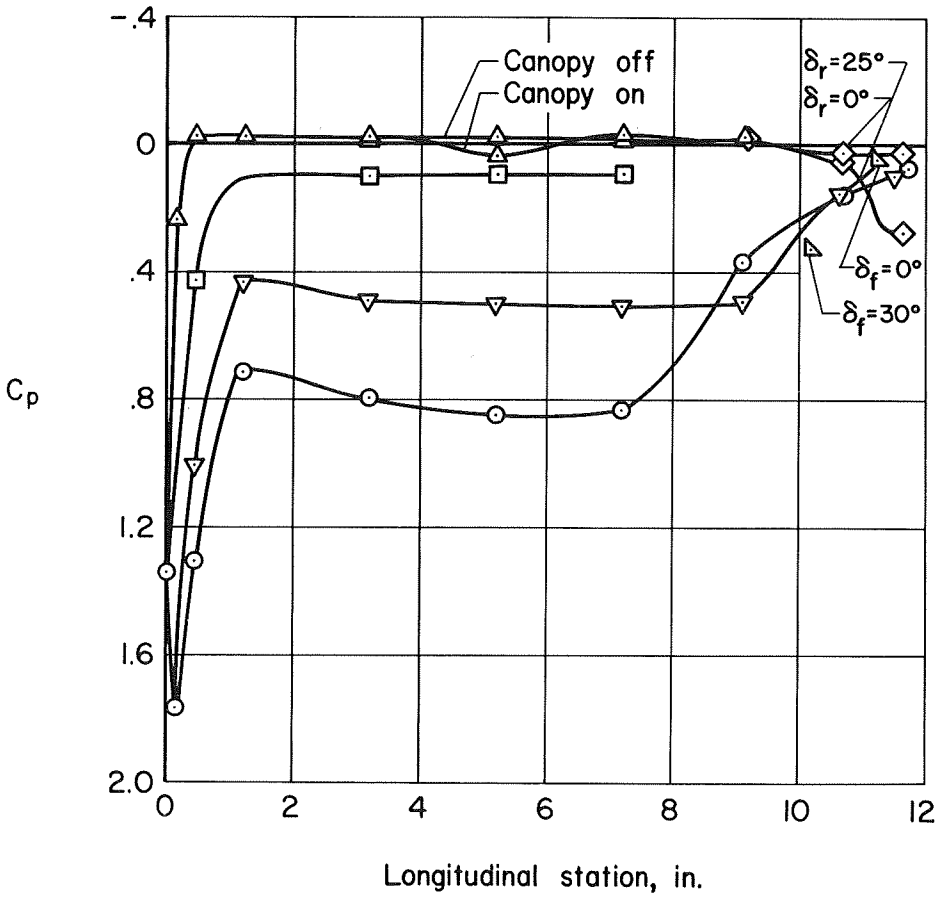

(f) $\alpha = 25.9^\circ$

Figure 8.- Continued.

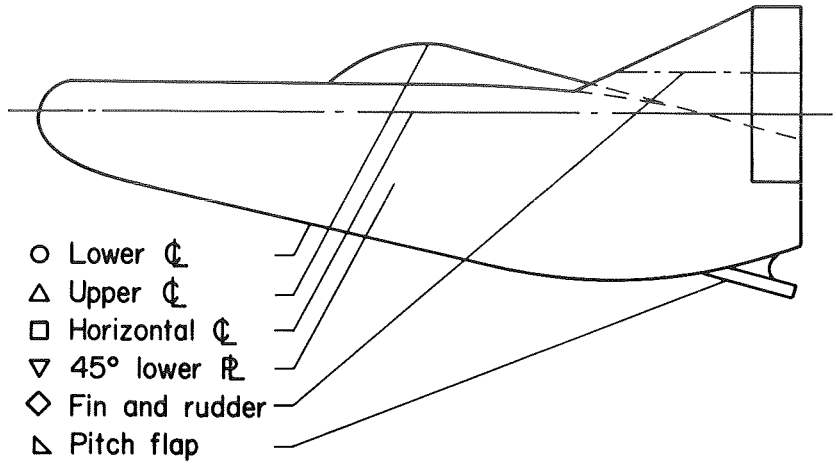

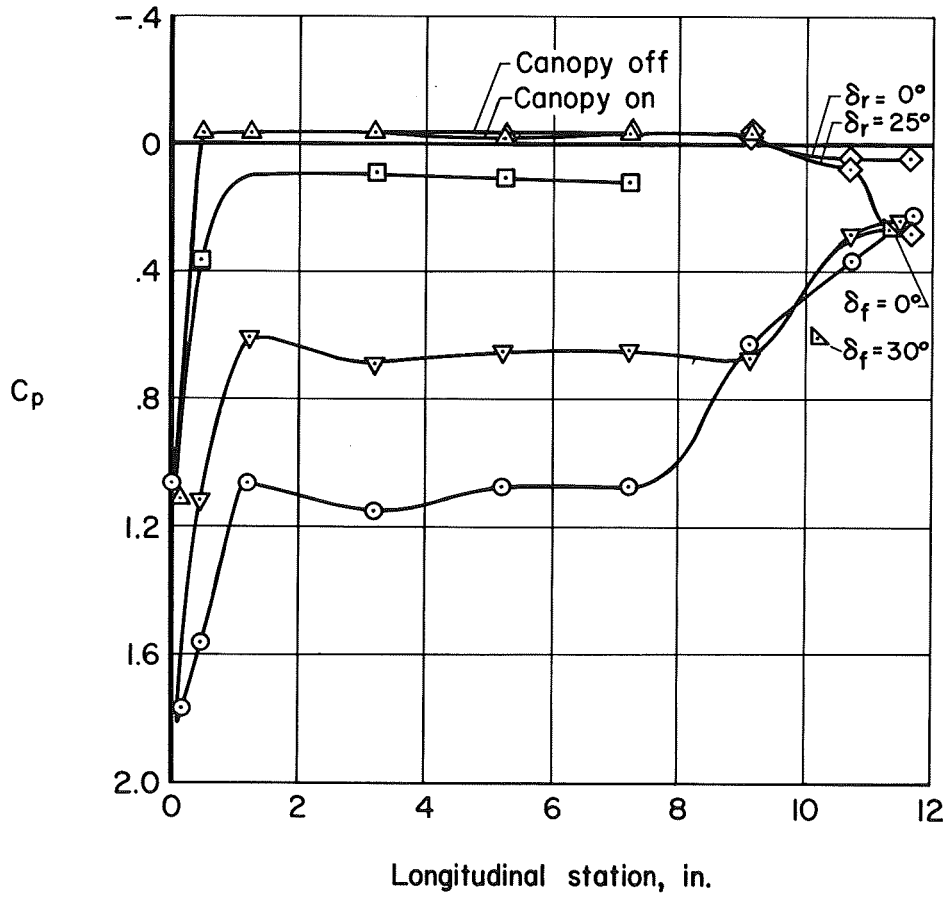

(g) $\alpha = 35.0^{\circ}$

Figure 8.- Continued.

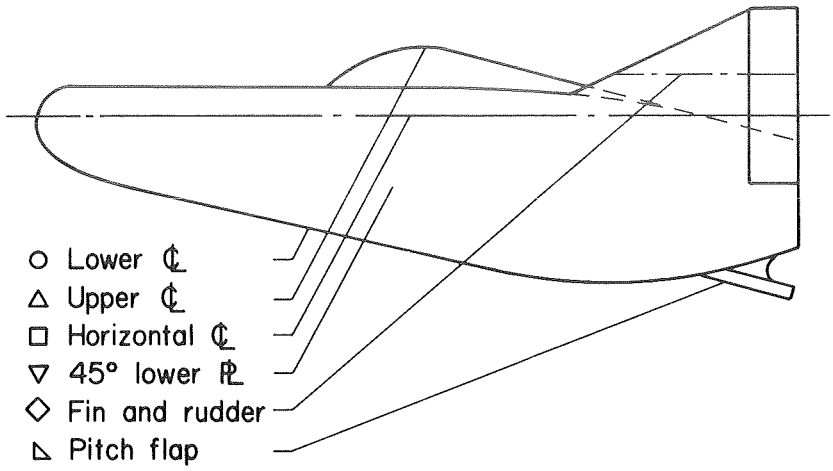

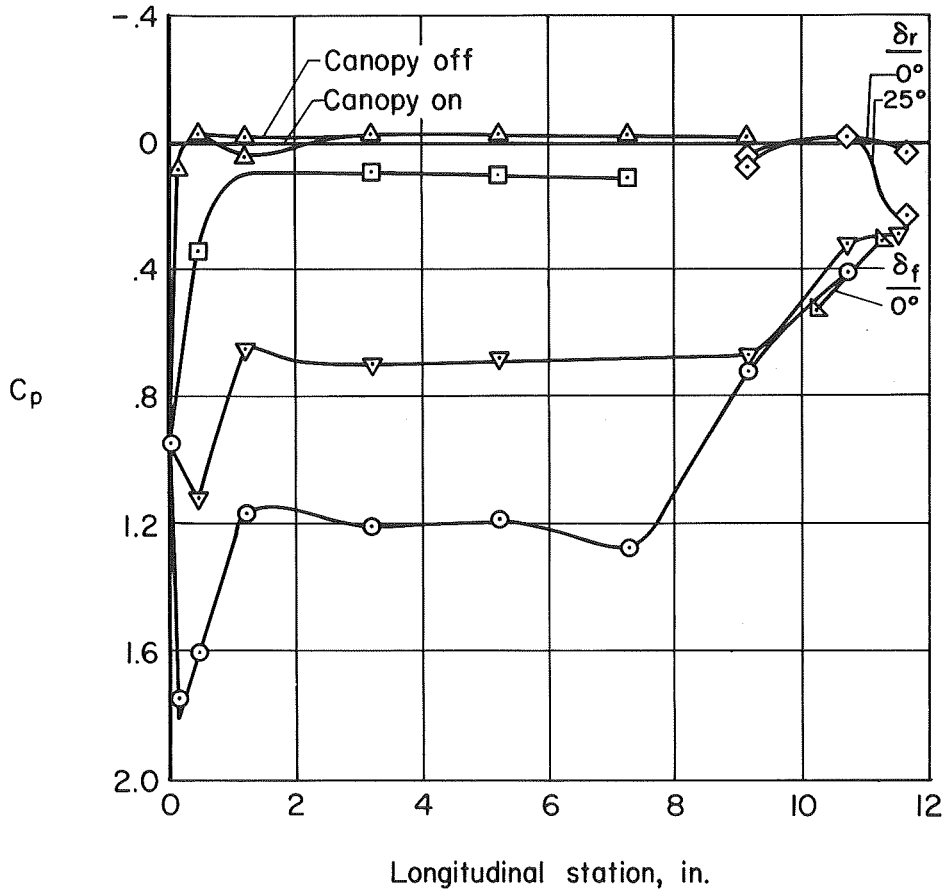

(h) $\alpha = 39.4^{\circ}$

Figure 8.- Continued.

CONFIDENTIAL

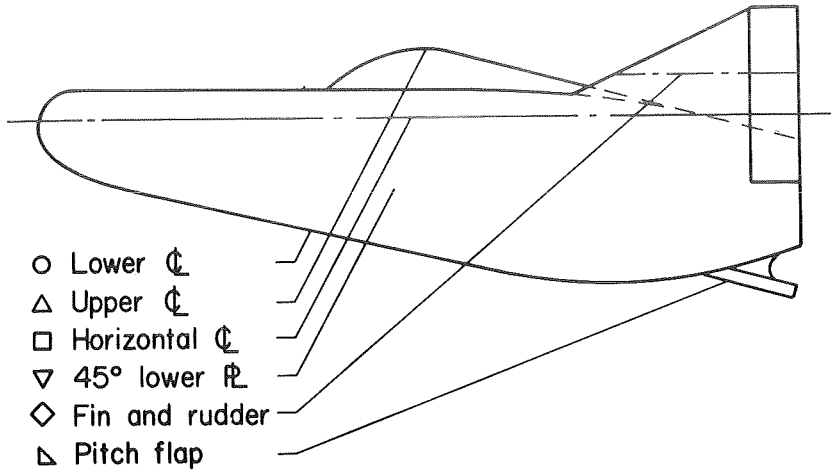

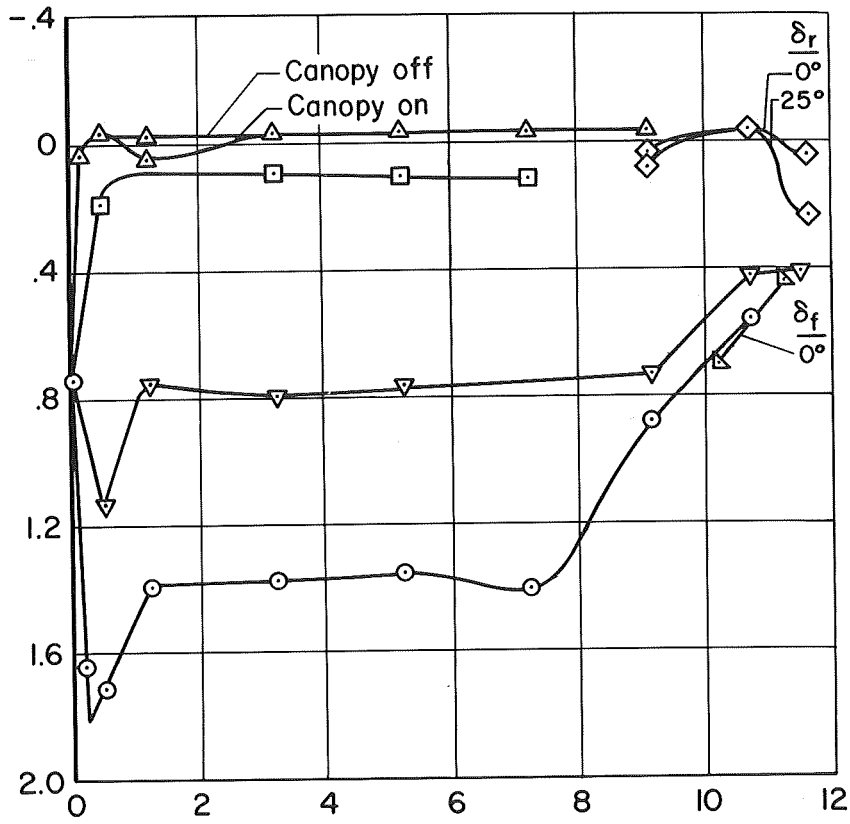

(i) $\alpha = 45.3^{\circ}$

Figure 8.- Continued.

CONFIDENTIAL

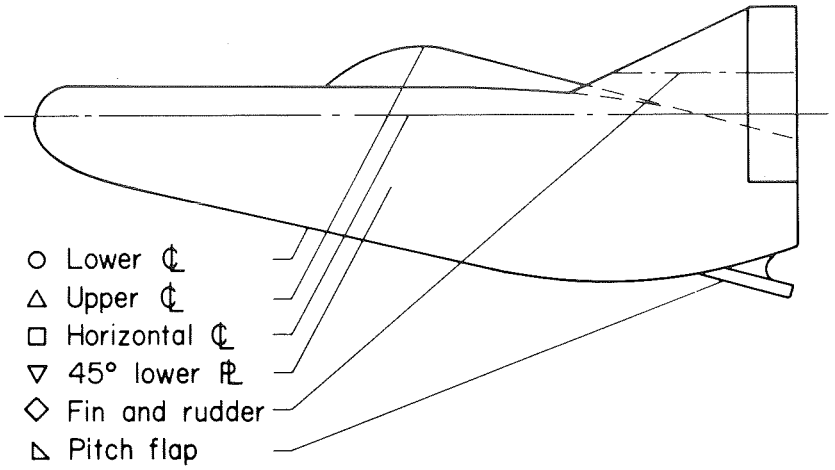

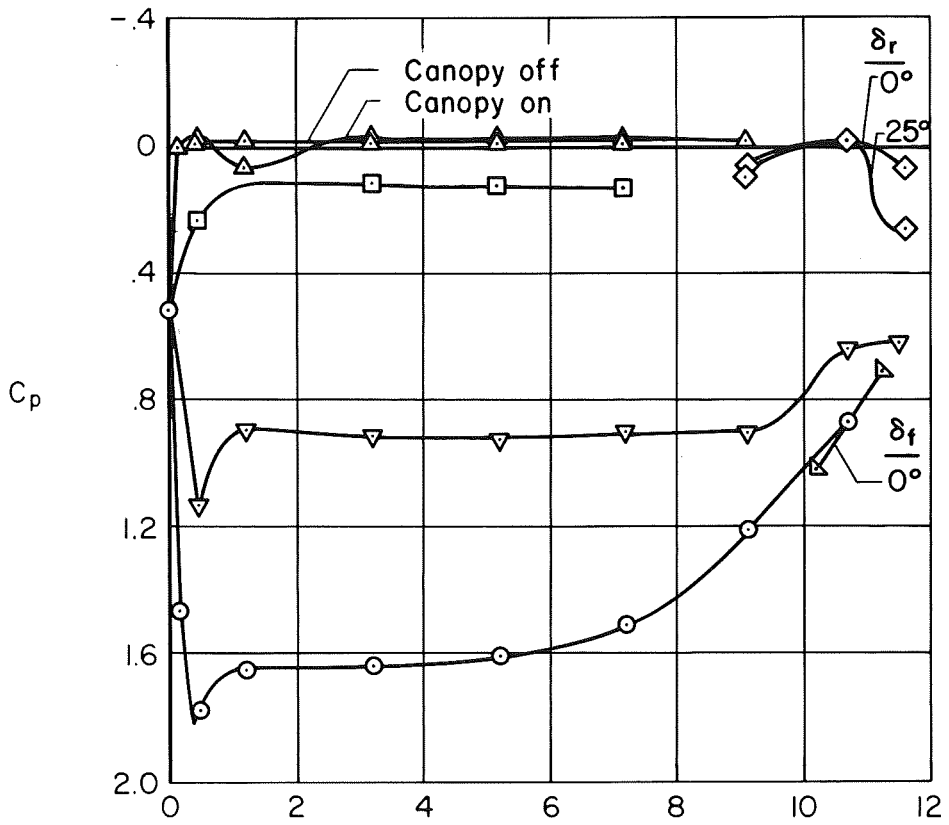

(j) $\alpha = 54.4^{\circ}$

Figure 8.- Concluded.

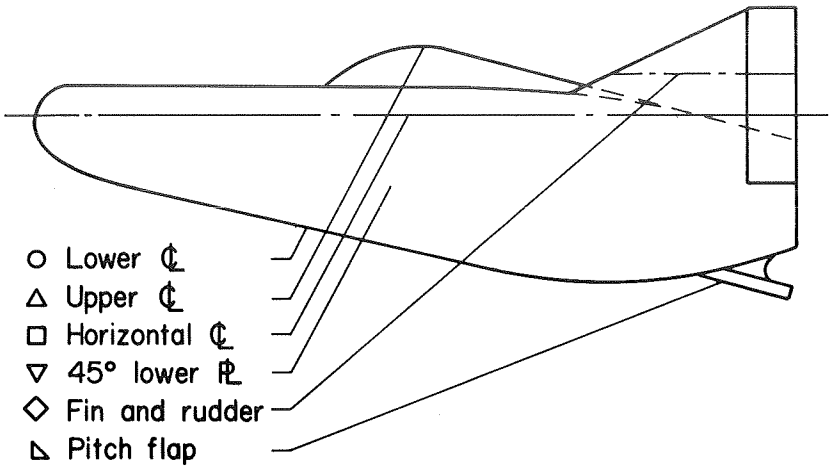

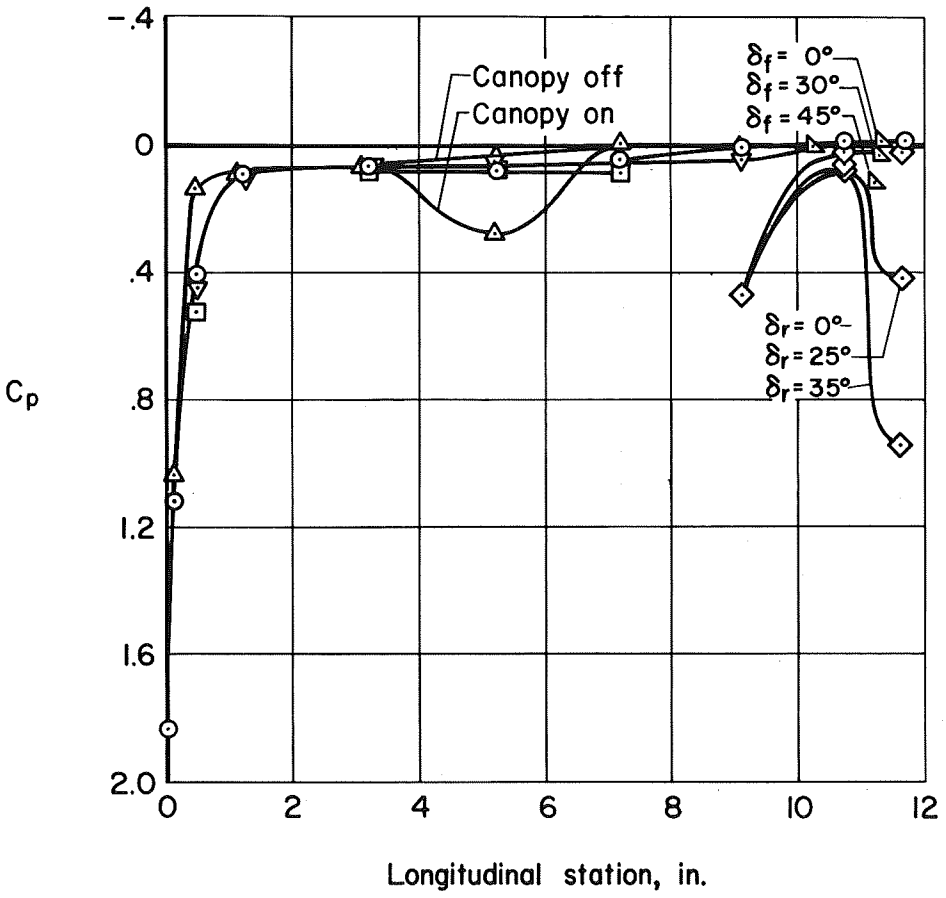

(a) $\alpha = -5.0^\circ$

Figure 9.- Distribution of pressure coefficients for the model with and without canopy and with several deflections of the pitch flaps and rudders; M = 7.4.

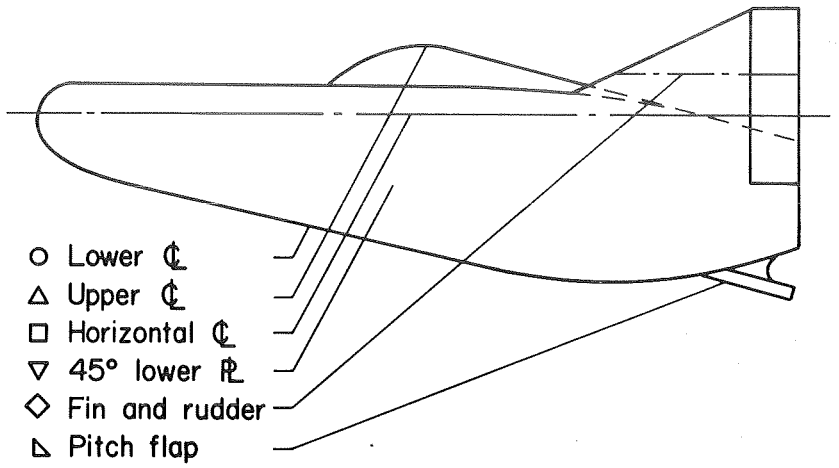

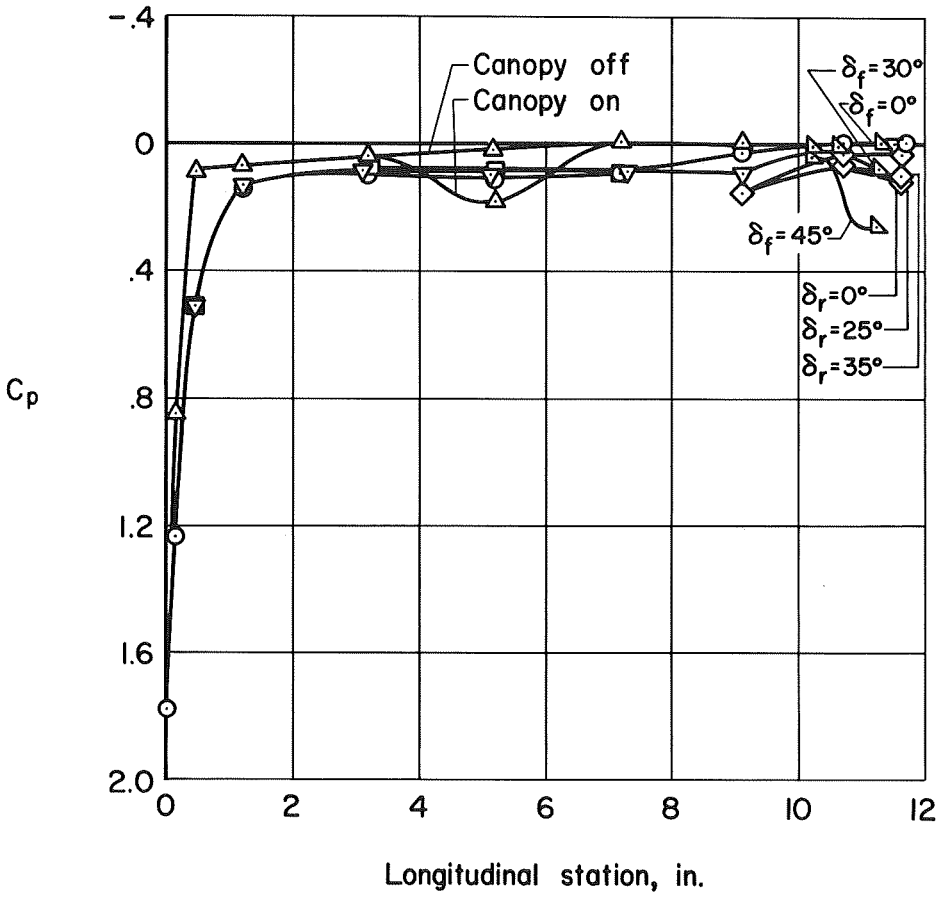

(b) $\alpha = 0^{\circ}$

Figure 9.- Continued.

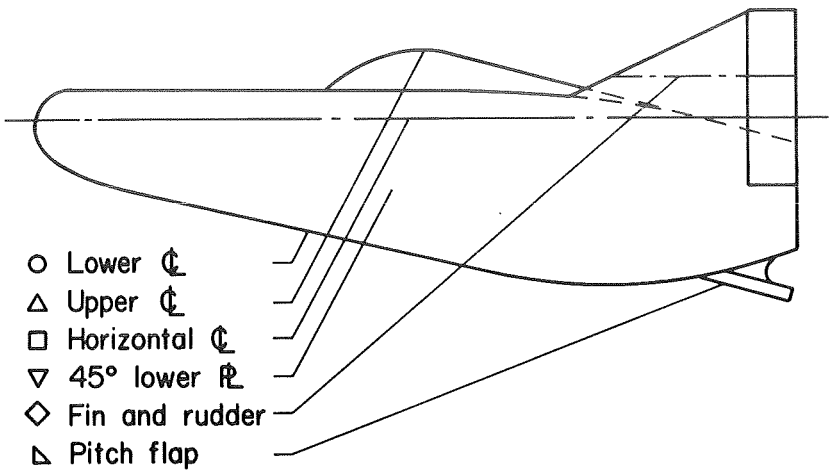

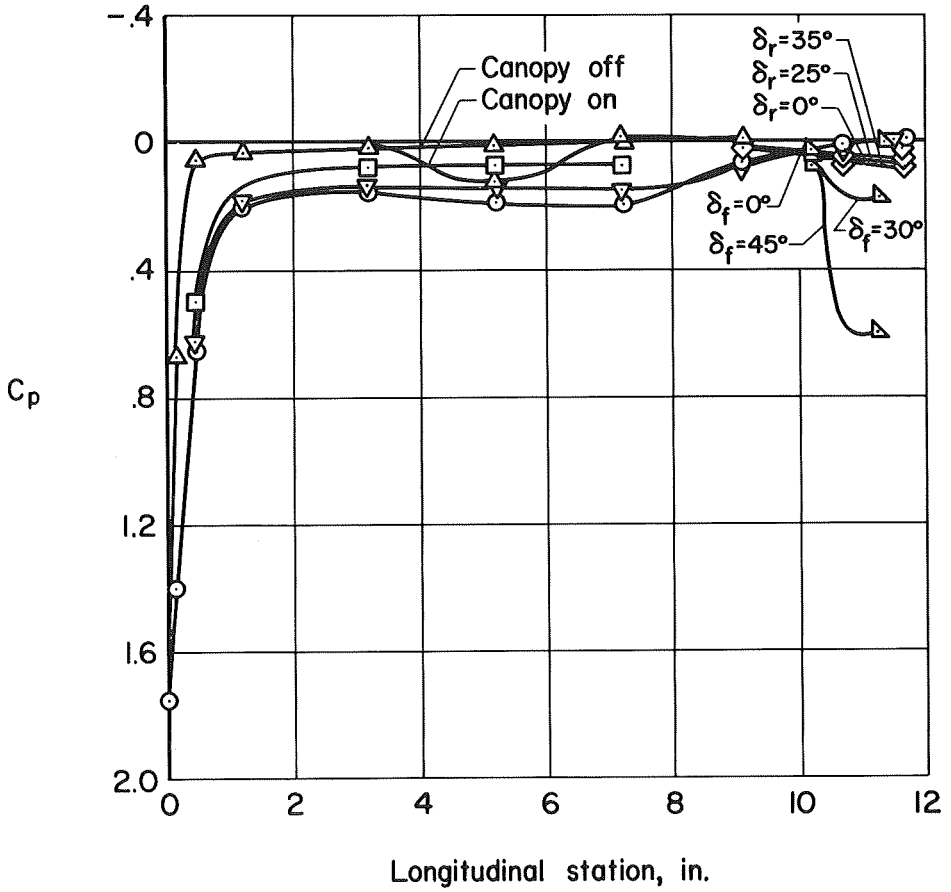

(c) $\alpha = 5.9^\circ$

Figure 9.- Continued.

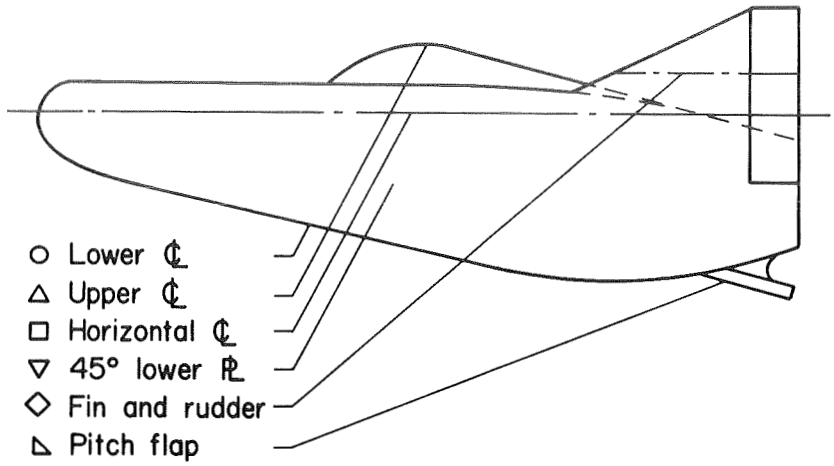

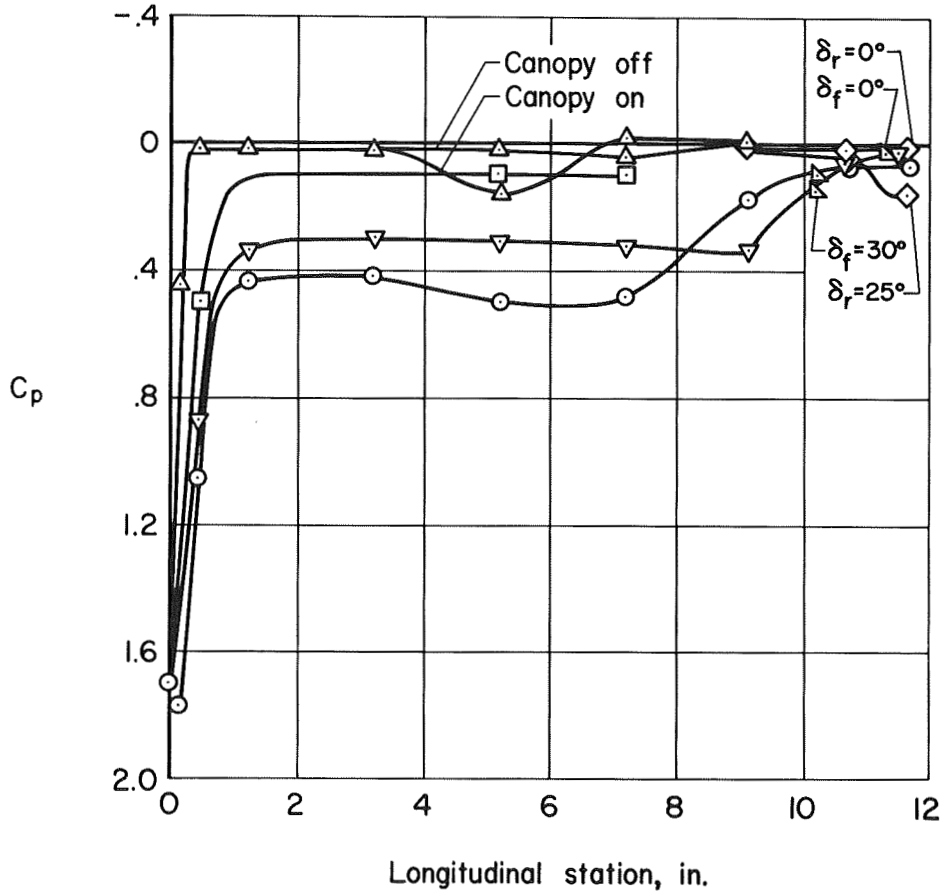

(d) $\alpha = 15.0^\circ$

Figure 9.- Continued.

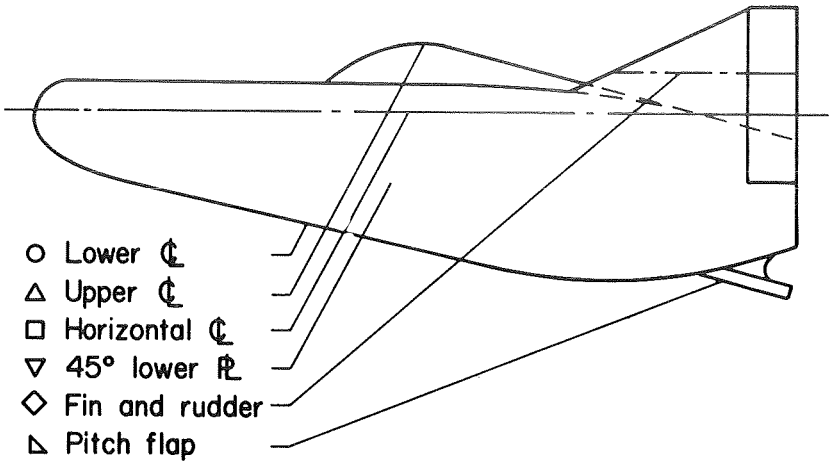

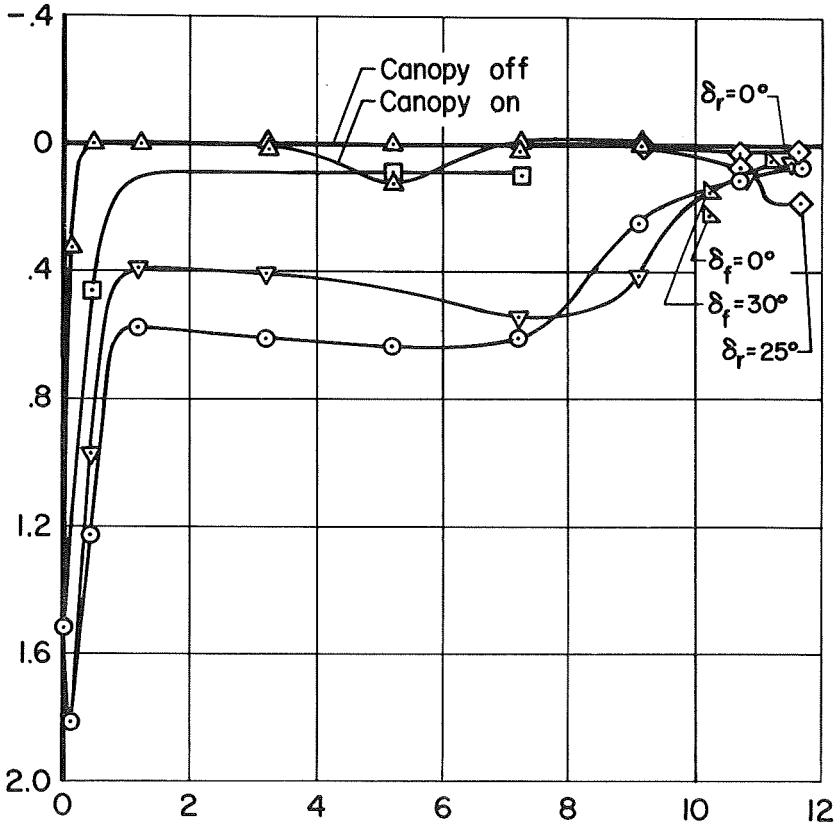

(e) $\alpha = 20.0^{\circ}$

Figure 9.- Continued.

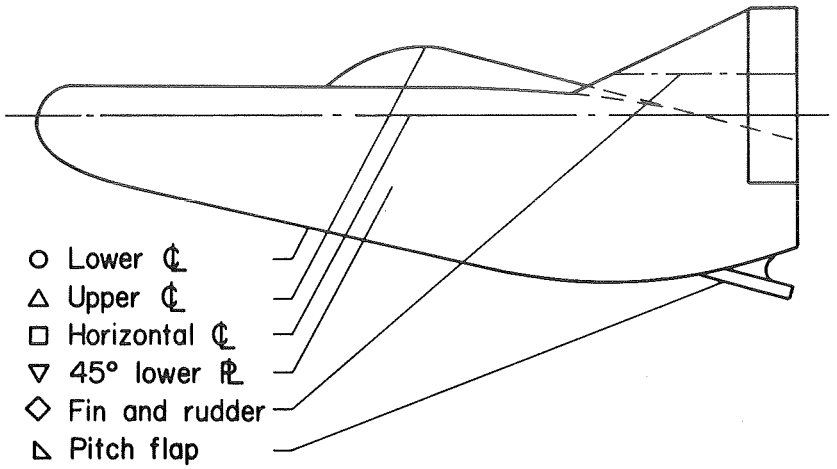

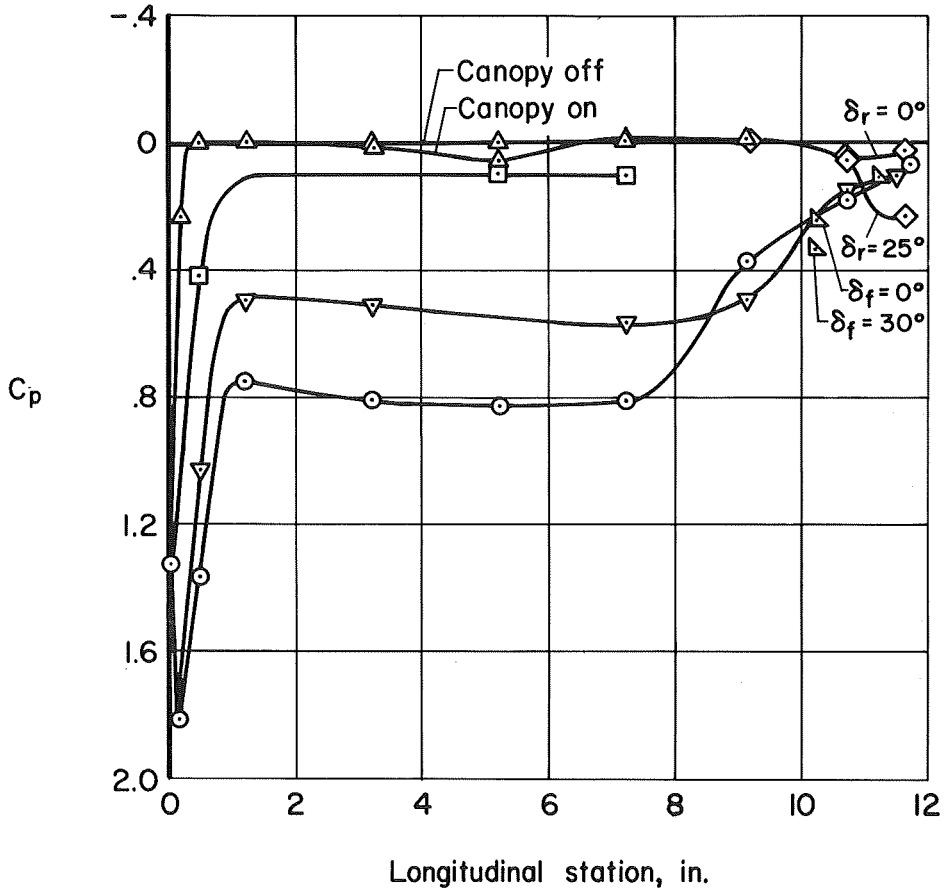

(f) $\alpha = 25.9^{\circ}$

Figure 9.- Continued.

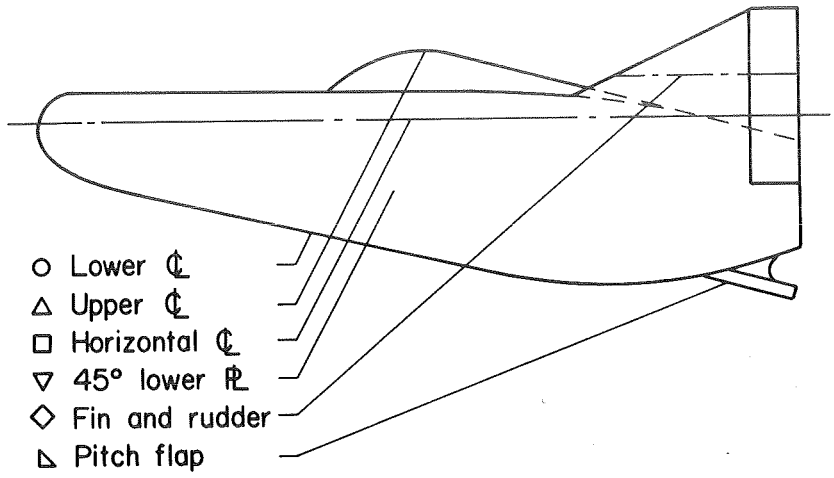

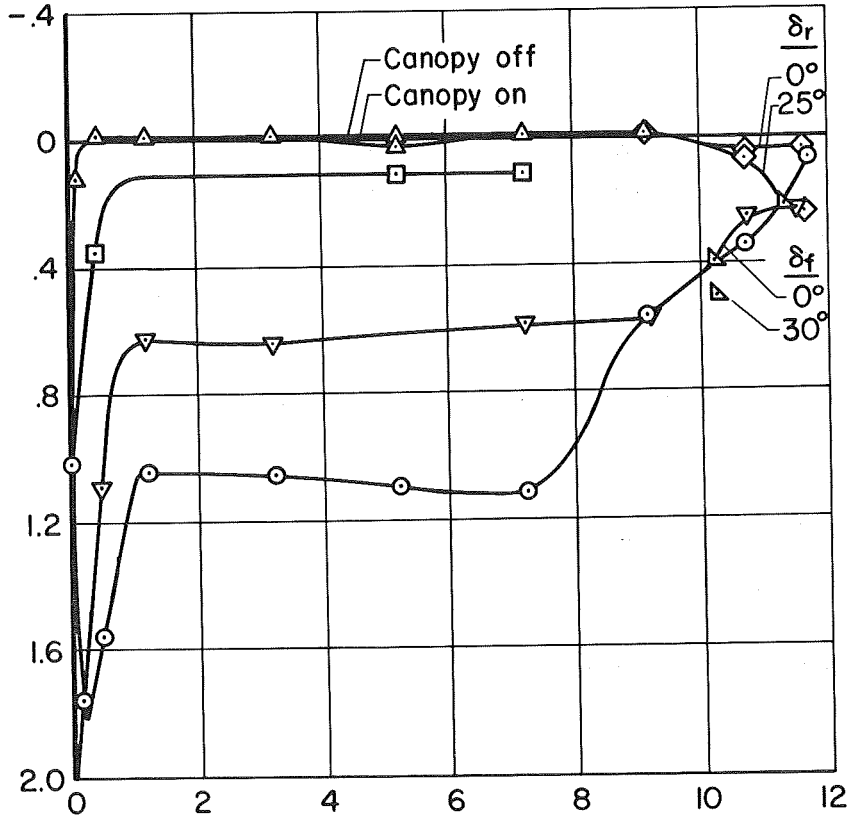

(g) $\alpha = 35.0^{\circ}$

Figure 9.- Continued.

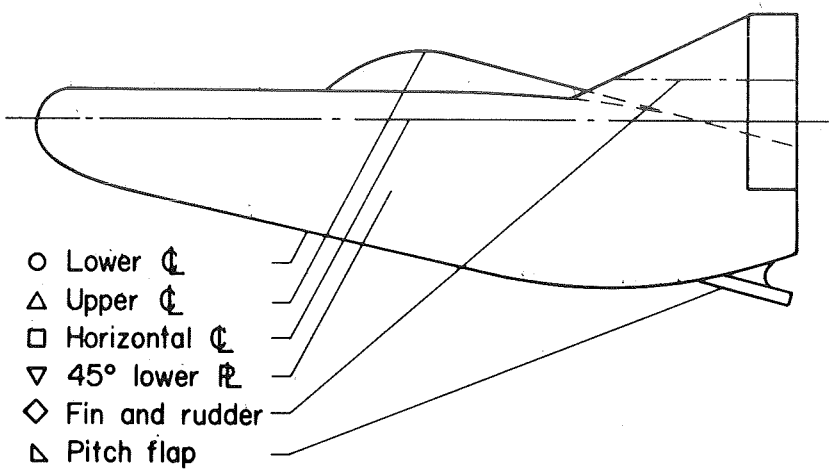

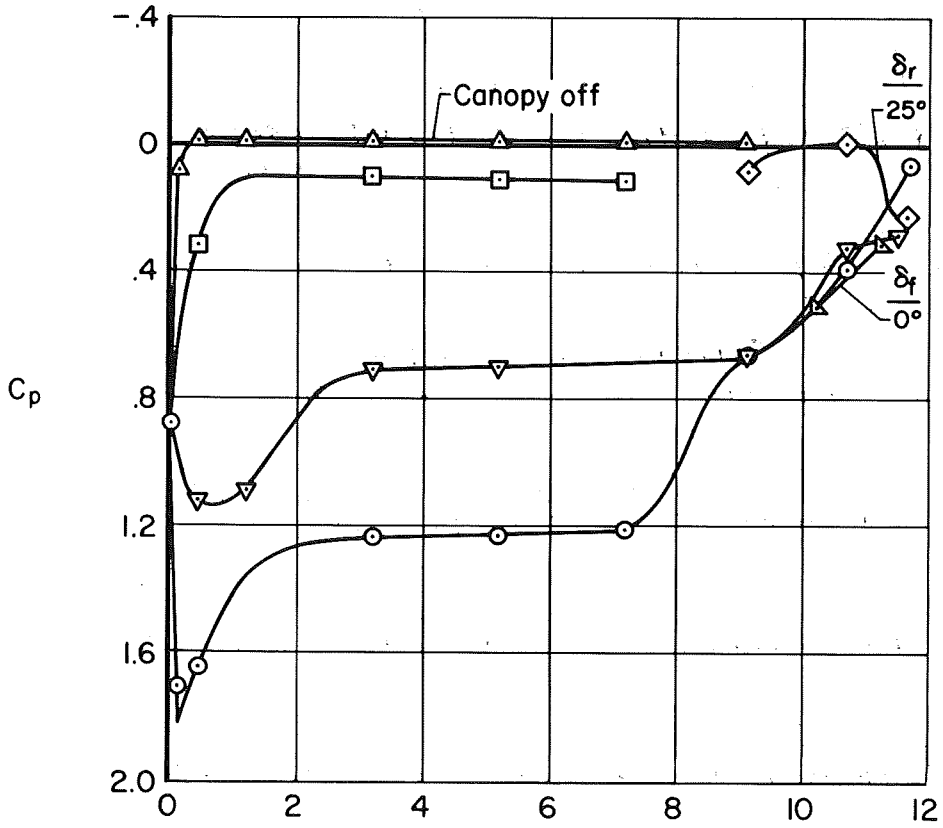

(h) $\alpha = 39.3^{\circ}$

Figure 9.- Continued.

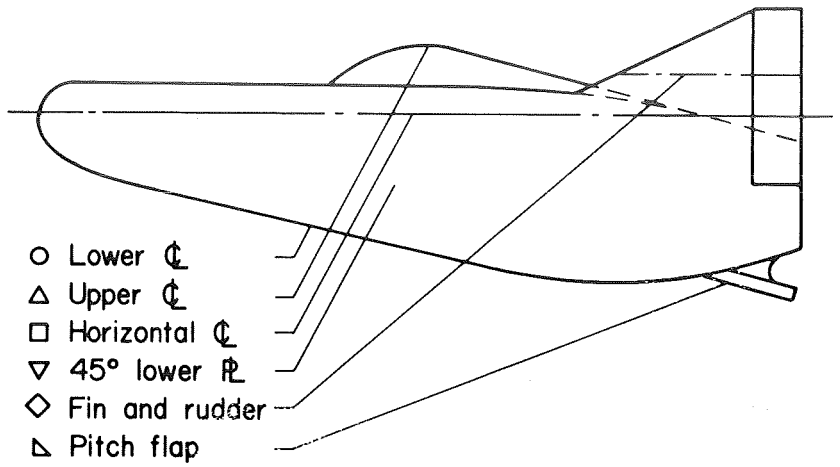

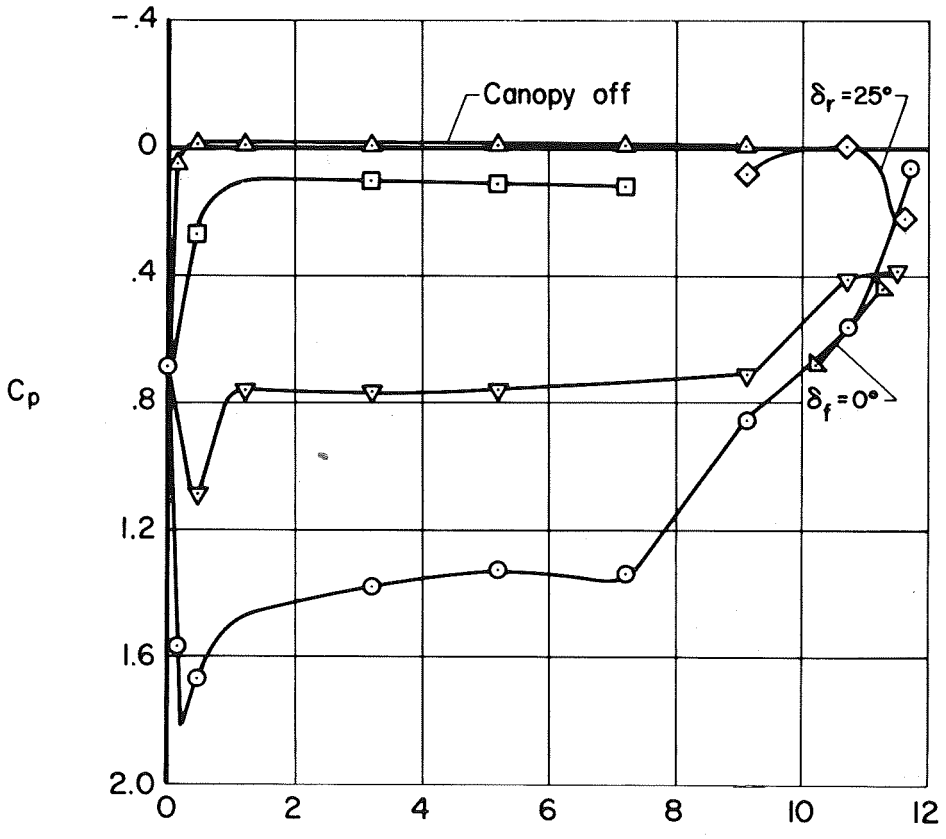

(i) $\alpha = 45.2^{\circ}$

Figure 9.- Continued.

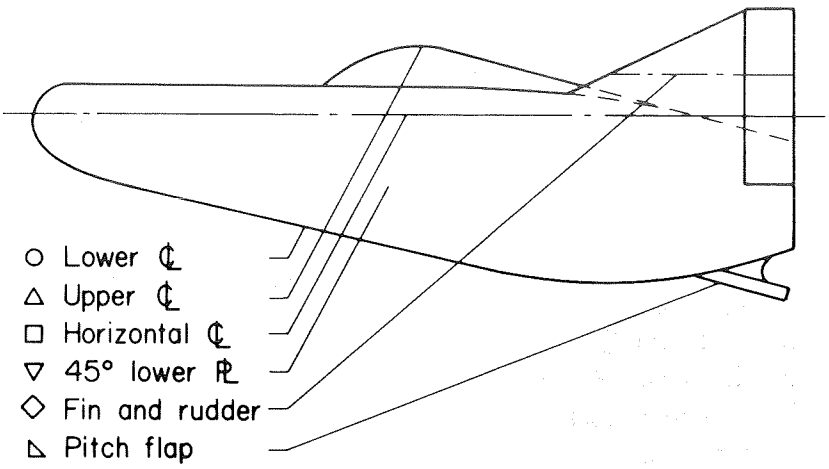

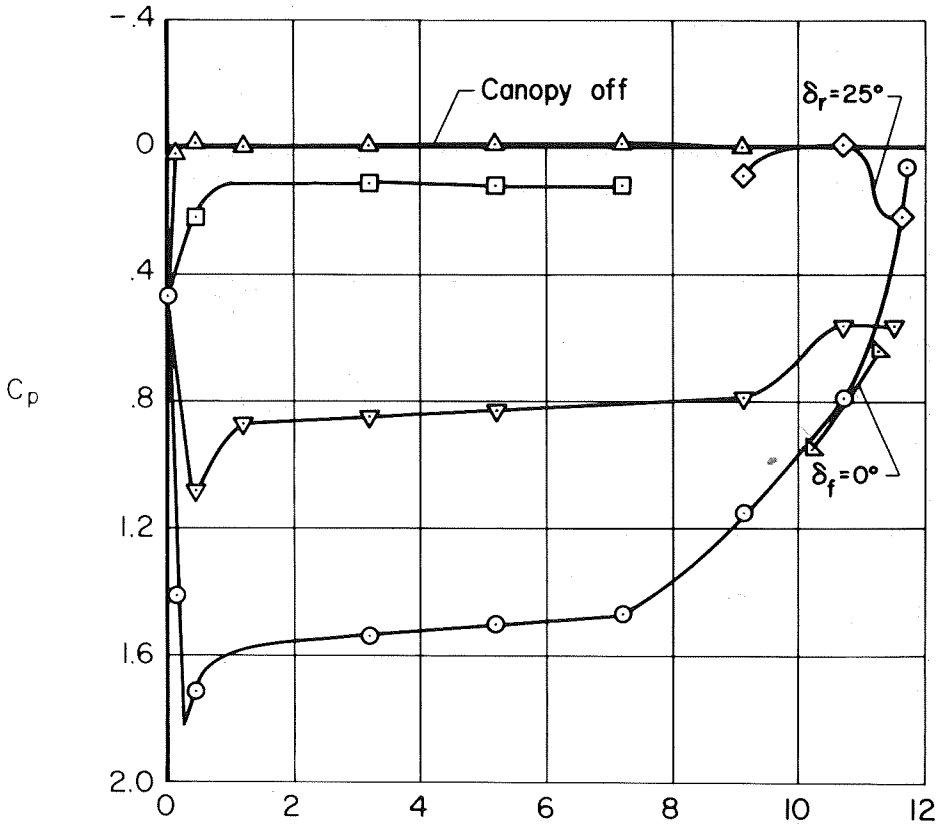

(j) $\alpha = 54.3^{\circ}$

Figure 9.- Concluded.

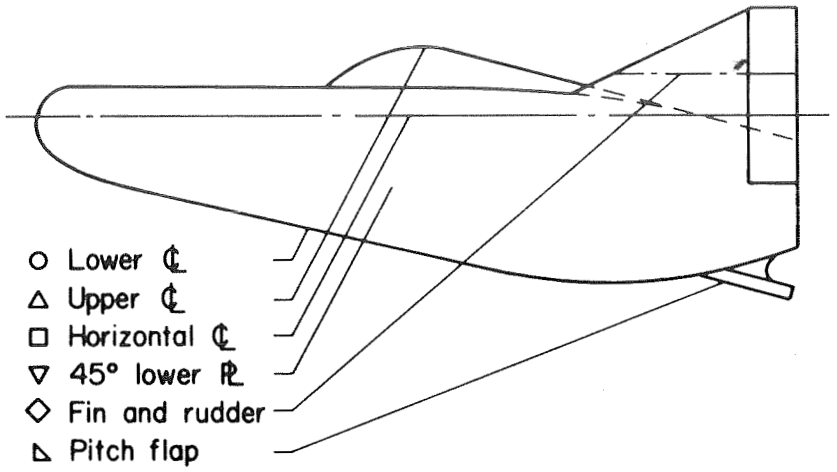

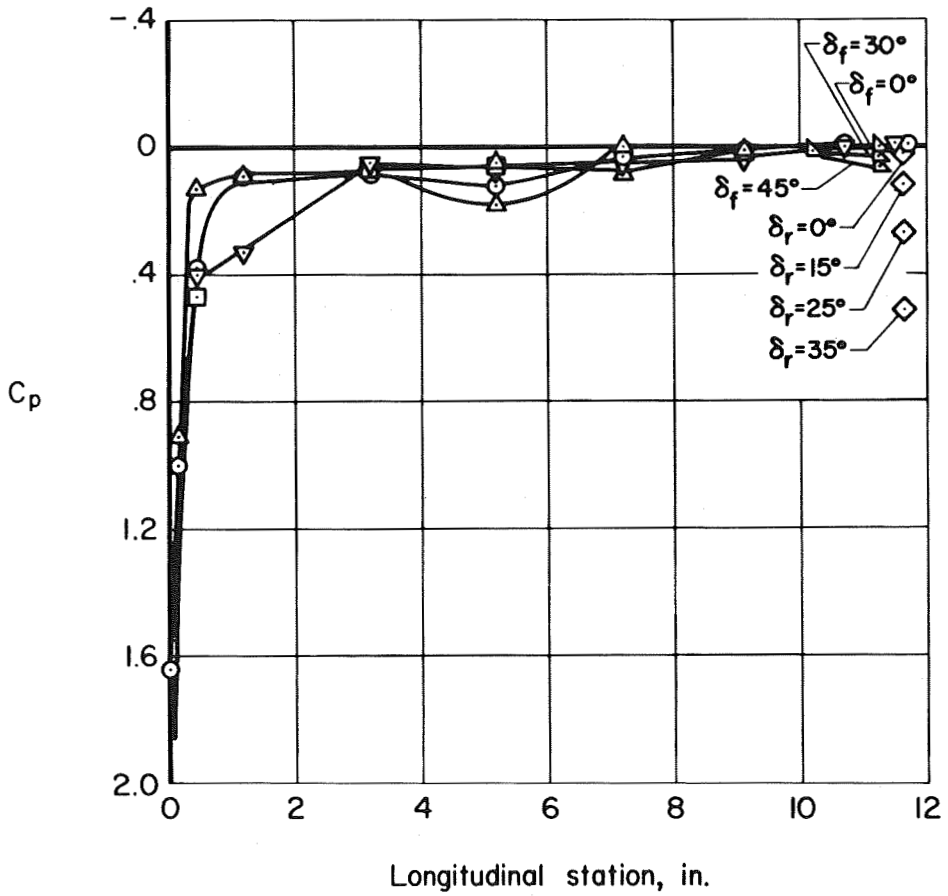

(a) $\alpha = -5.3^{\circ}$

Figure 10.- Distribution of pressure coefficients for the model with and without canopy and with several deflections of the pitch flaps and rudders; M = 10.4.

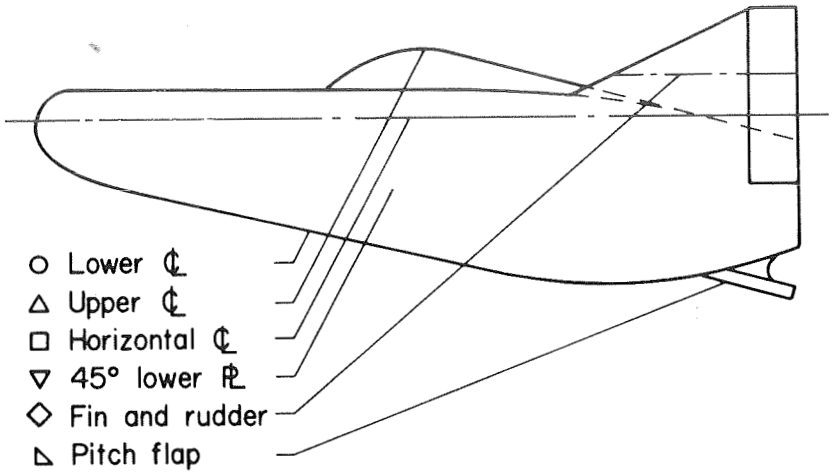

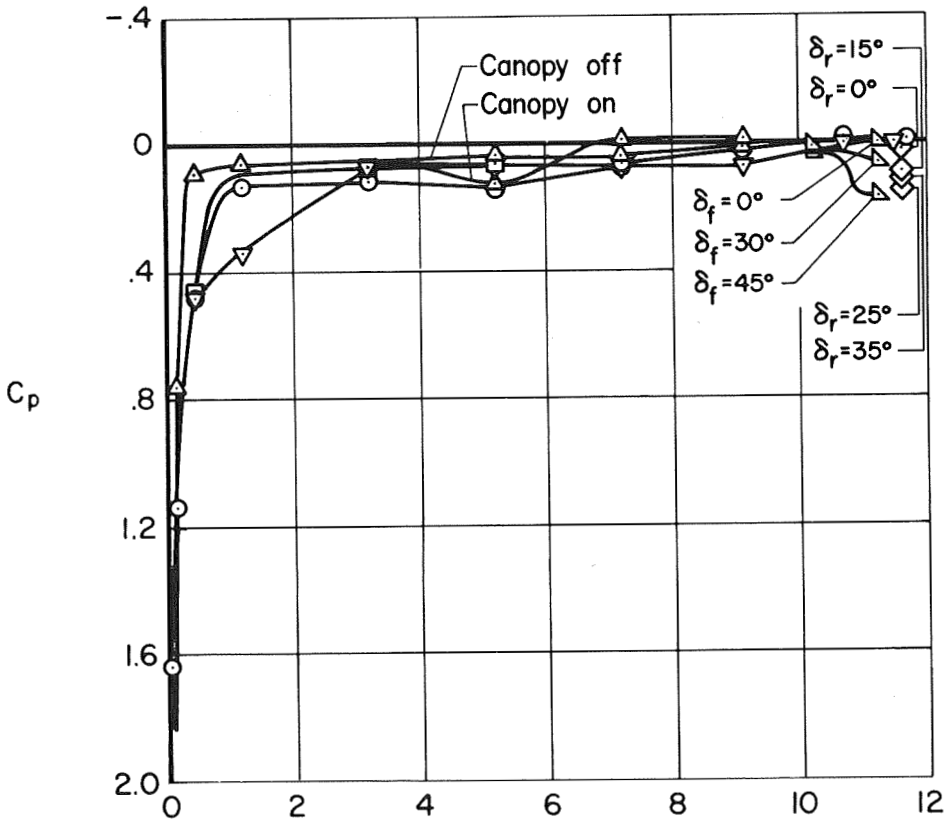

(b) $\alpha = -0.3^{\circ}$

Figure 10.- Continued.

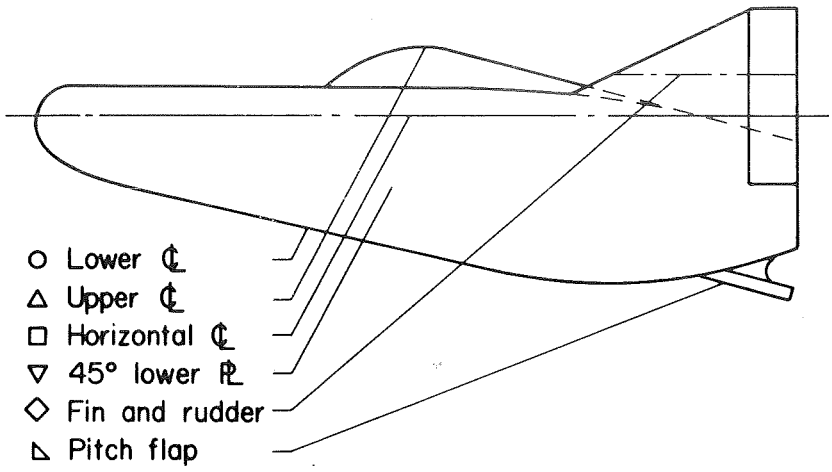

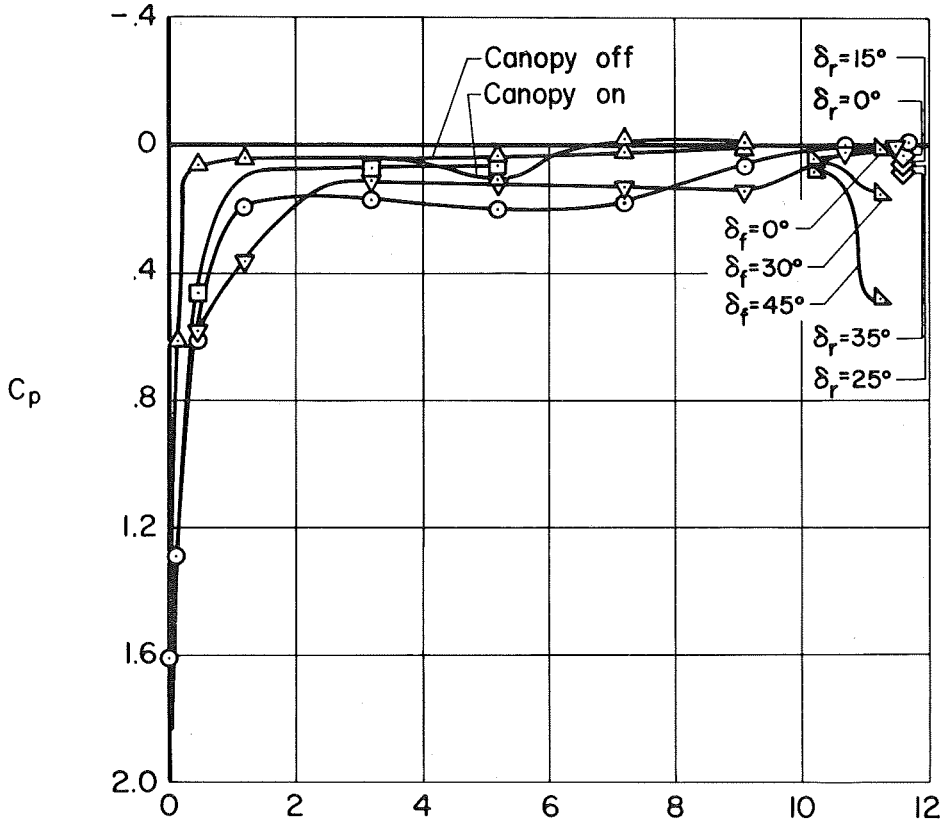

(c) $\alpha = 5.6°$

Figure 10.- Continued.

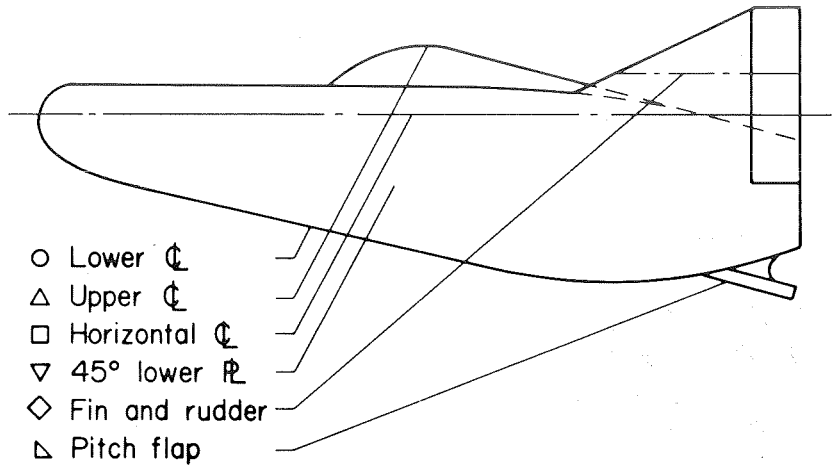

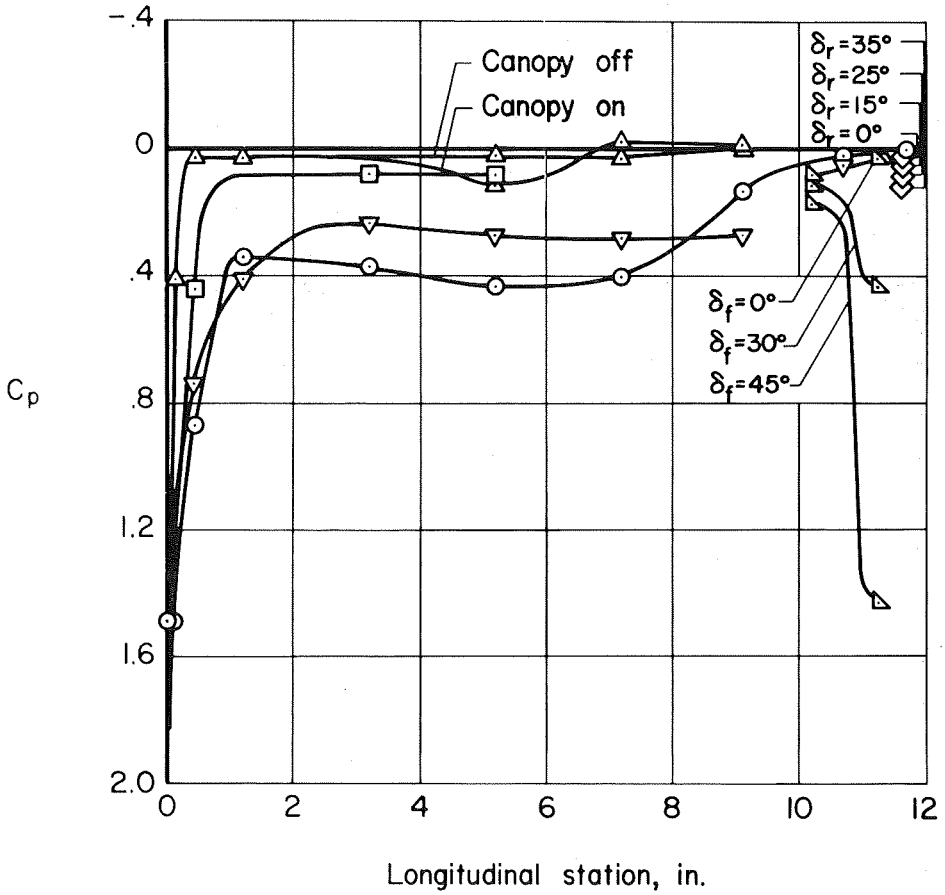

(d) $\alpha = 14.6^\circ$

Figure 10.- Continued.

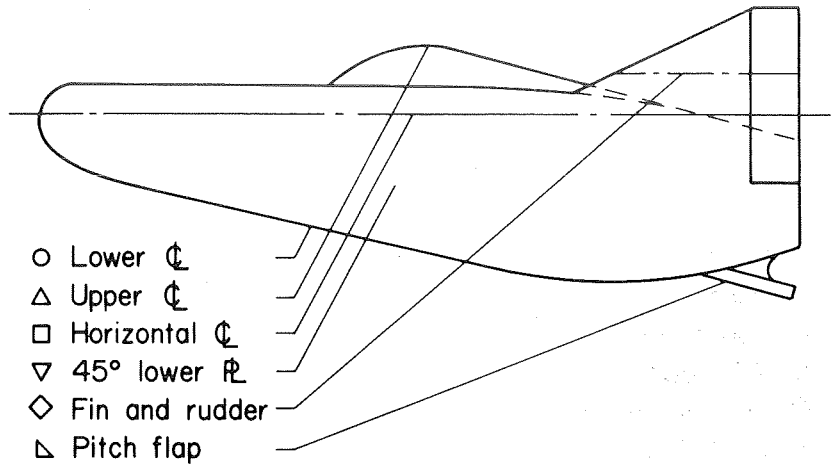

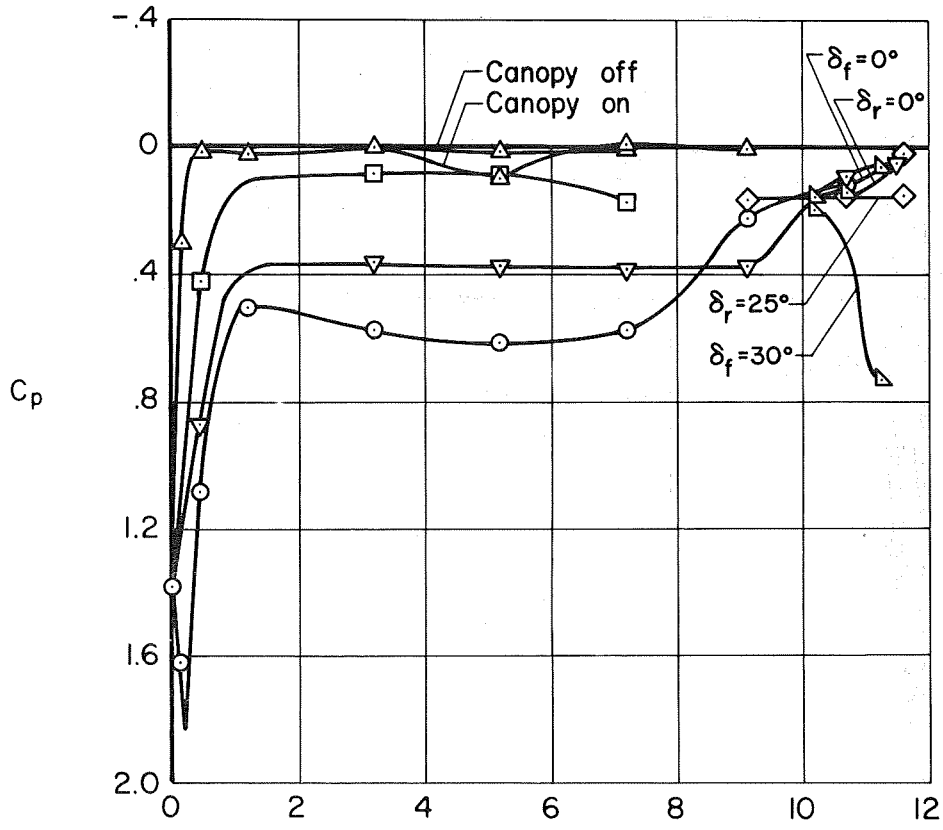

(e) $\alpha = 20.0^{\circ}$

Figure 10.- Continued.

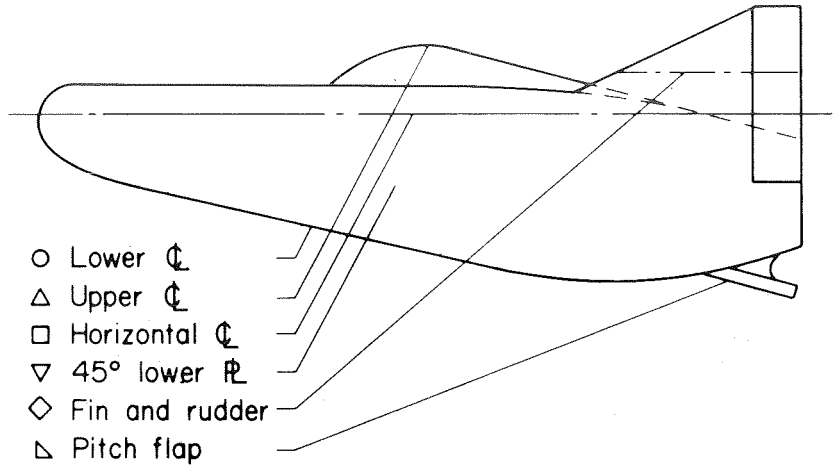

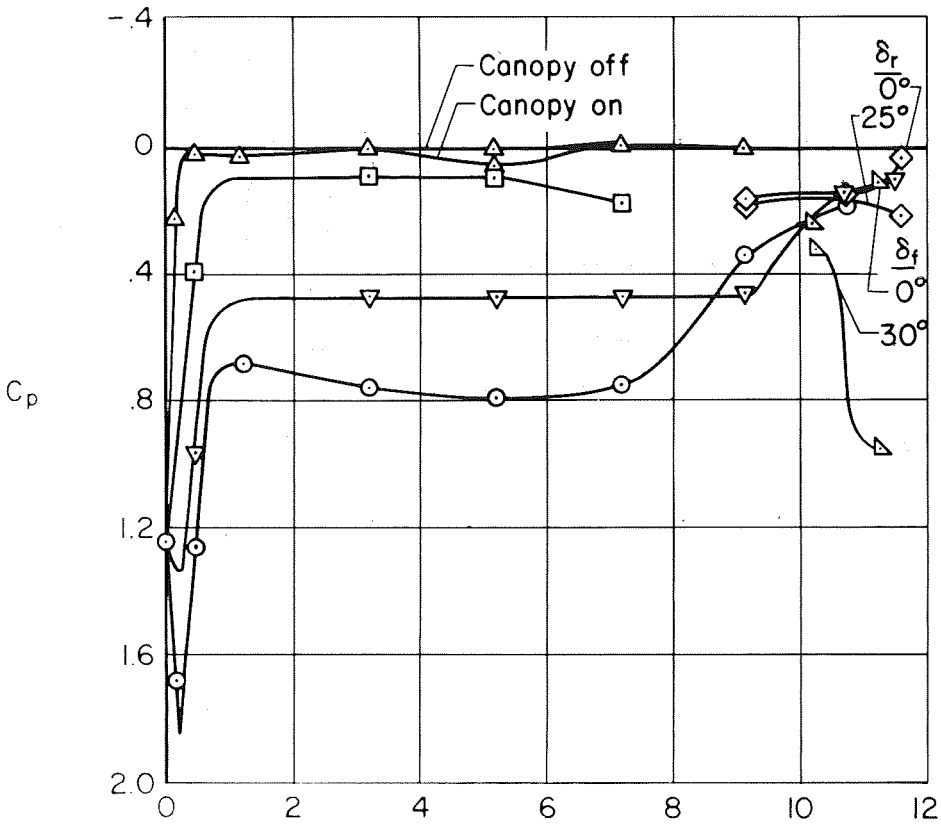

(f) $\alpha = 26^{\circ}$

Figure 10.- Continued.

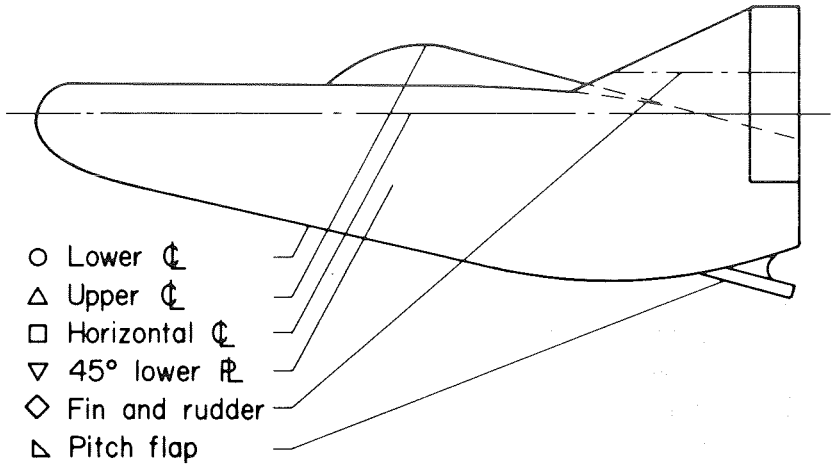

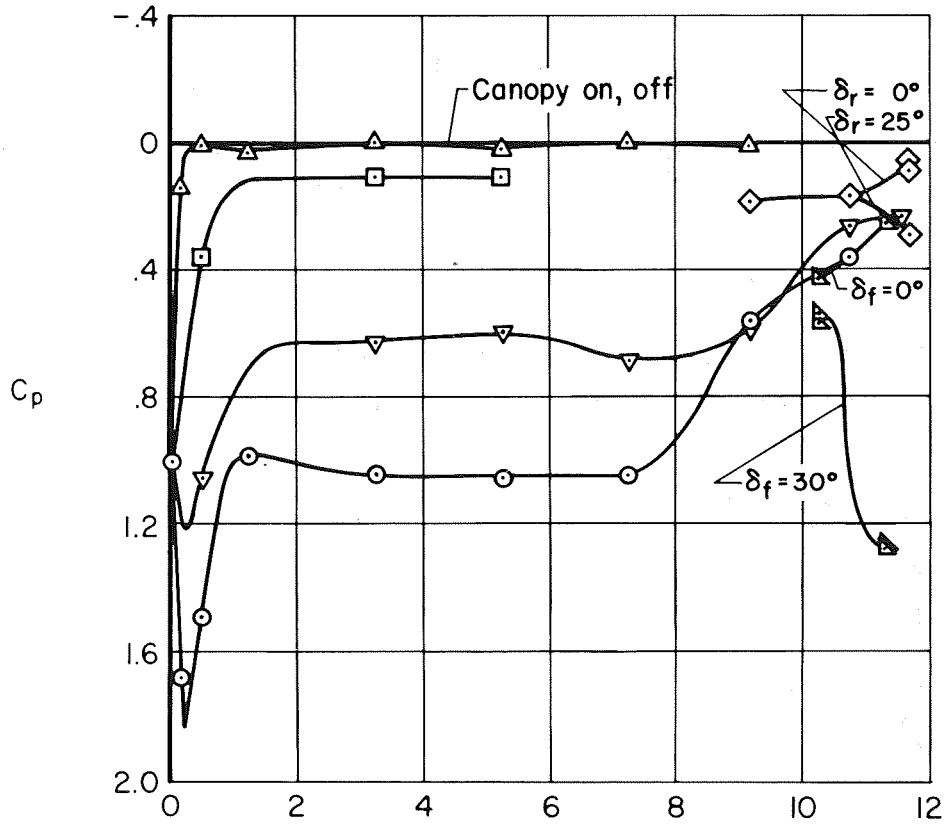

(g) $\alpha = 35.0^{\circ}$

Figure 10.- Continued.

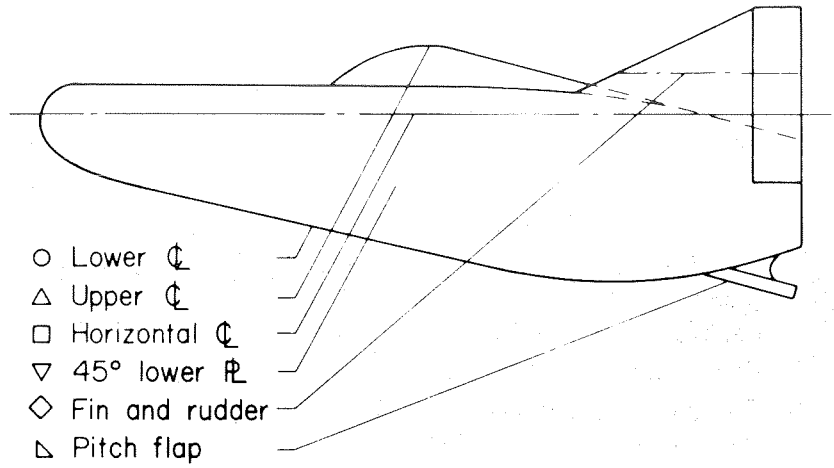

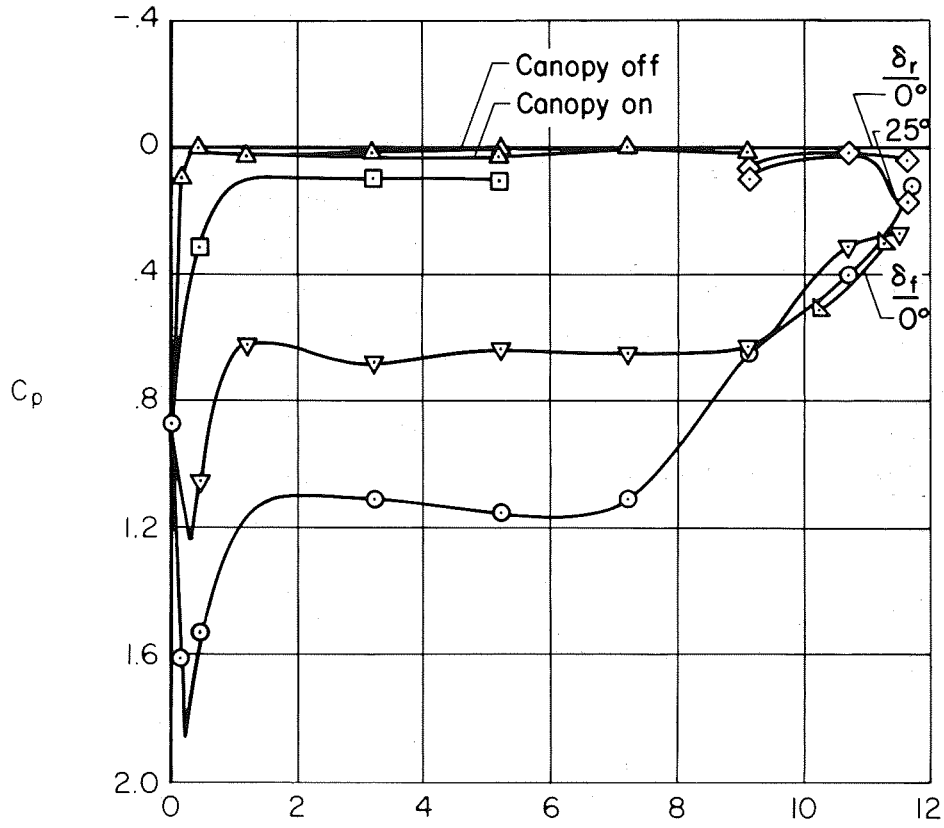

(h) $\alpha = 39.7^{\circ}$

Figure 10.- Continued.

CONFIDENTIAL

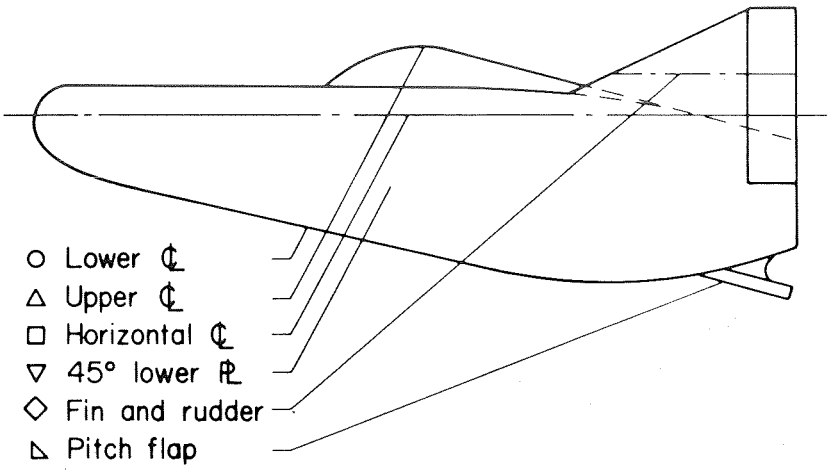

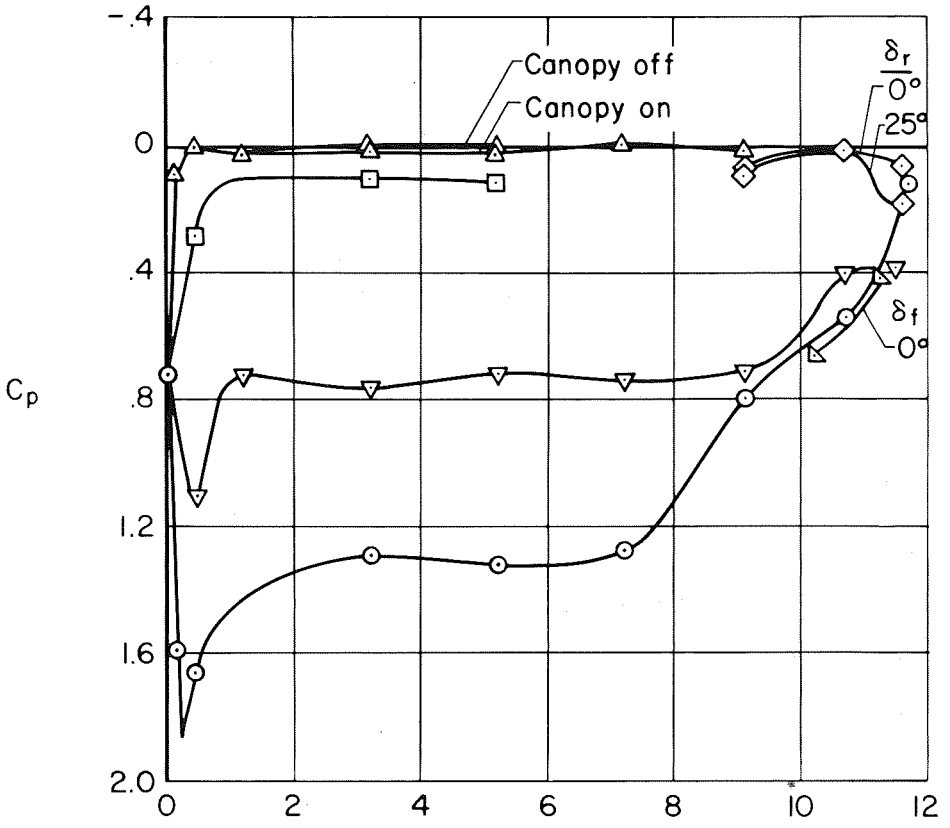

(i) $\alpha = 45.6^{\circ}$

Figure 10.- Continued.

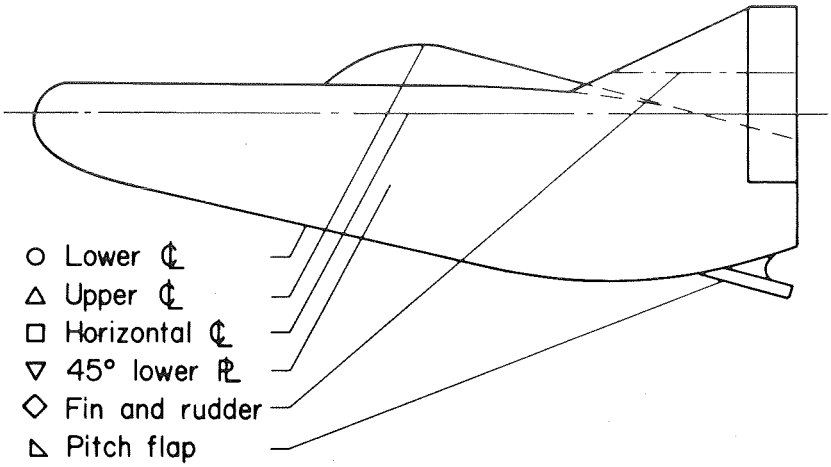

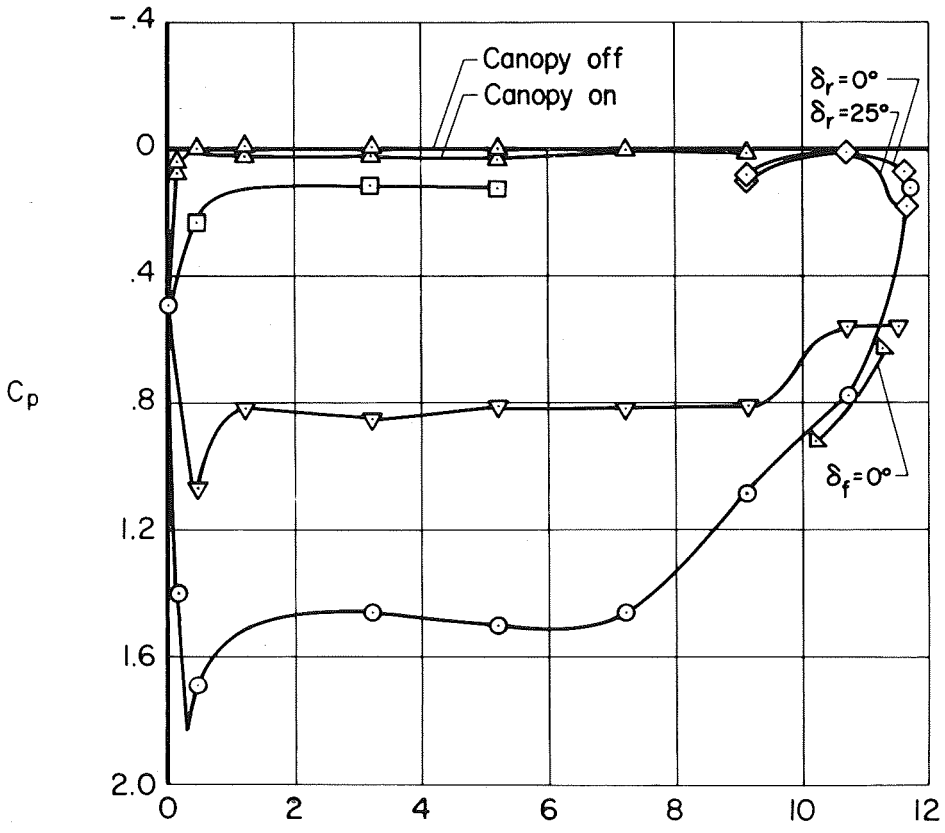

(j) $\alpha = 54.6^{\circ}$

Figure 10.- Concluded.

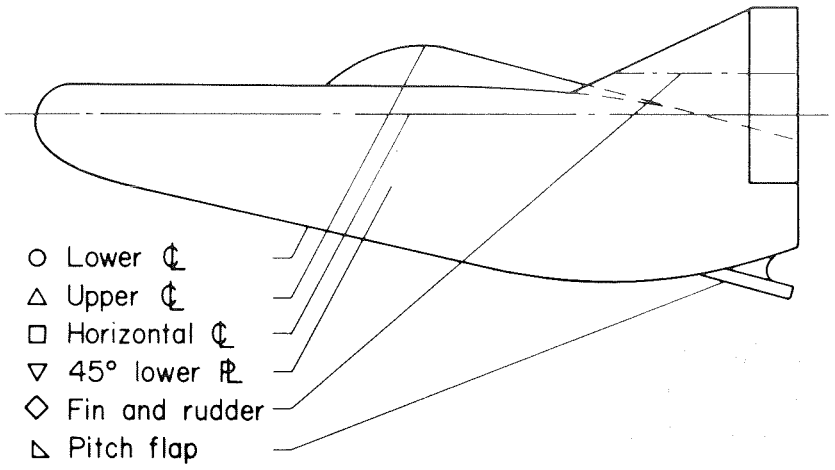

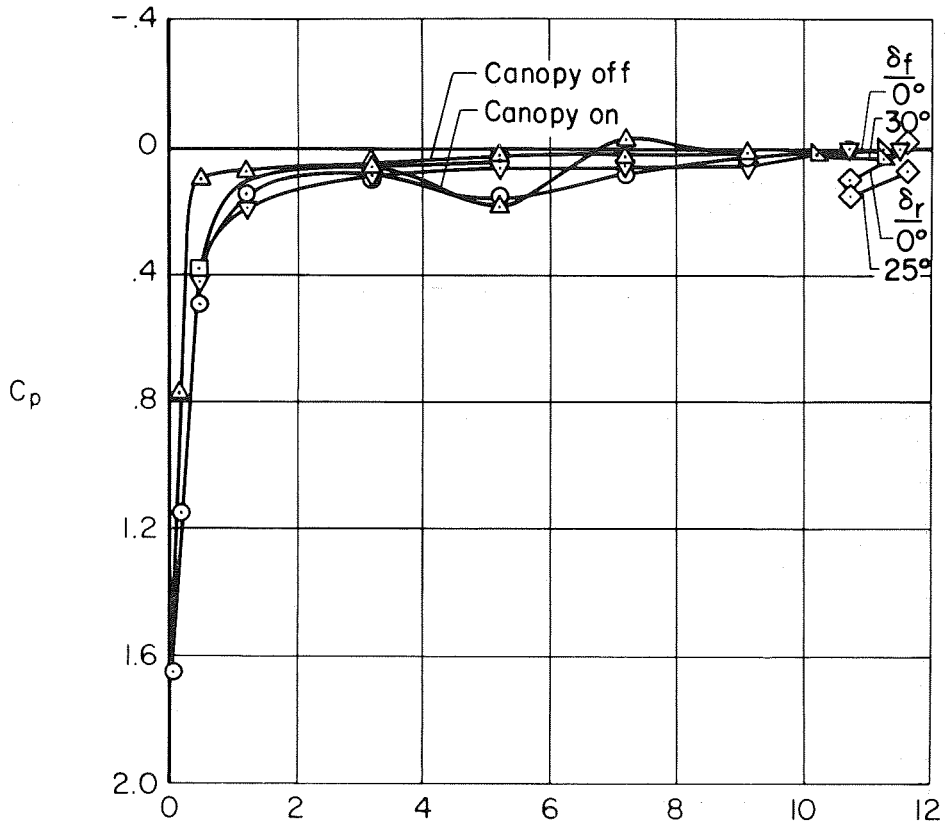

(a) $\beta = 5.3^\circ$

Figure 11.- Distribution of pressure coefficients for the model in sideslip; $M = 10.4$, $\alpha = 0^\circ$.

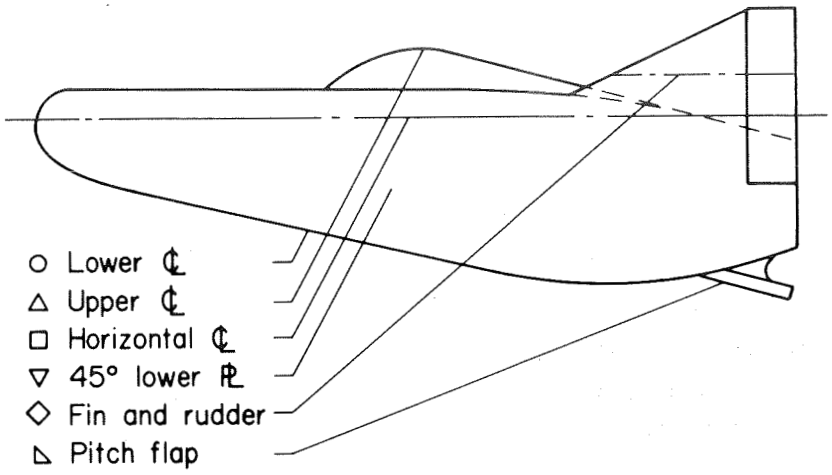

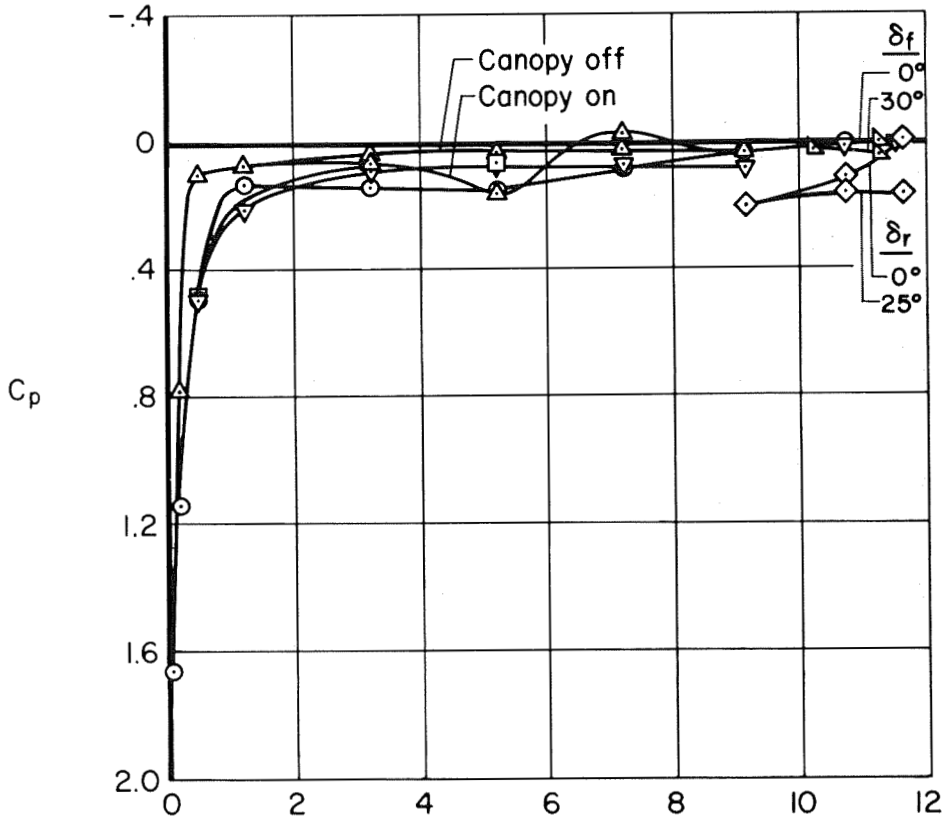

(b) $\beta = -0.3^\circ$

Figure 11.- Continued.

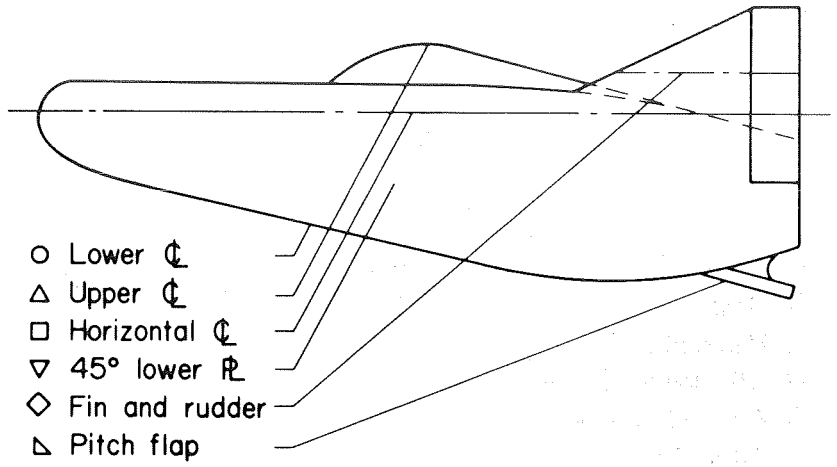

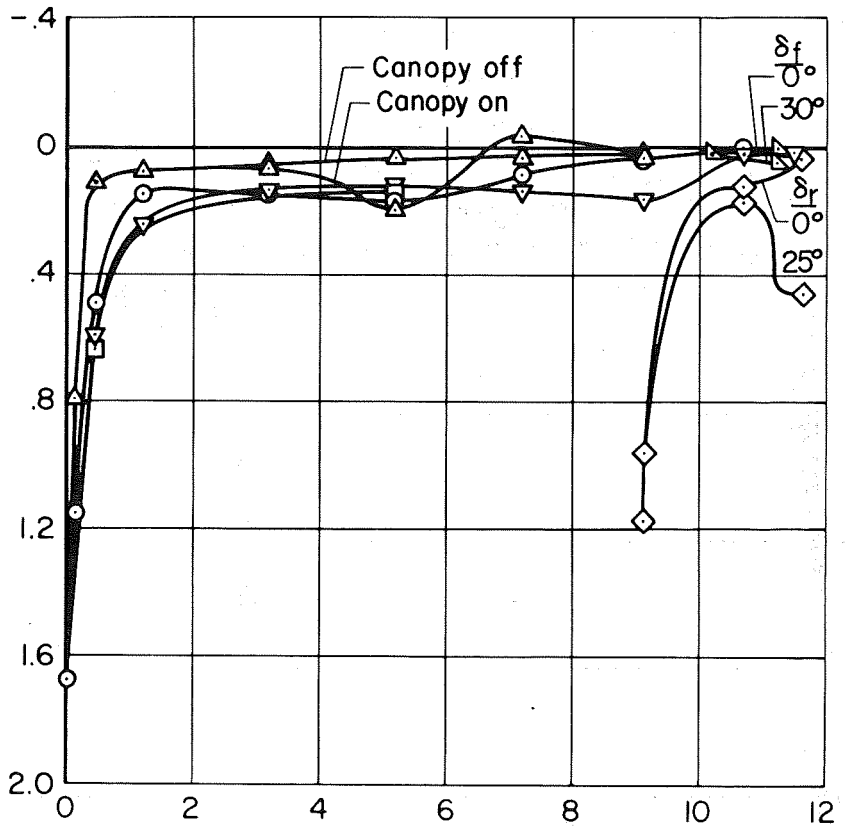

(c) $\beta = -5.6^{\circ}$

Figure 11.- Continued.

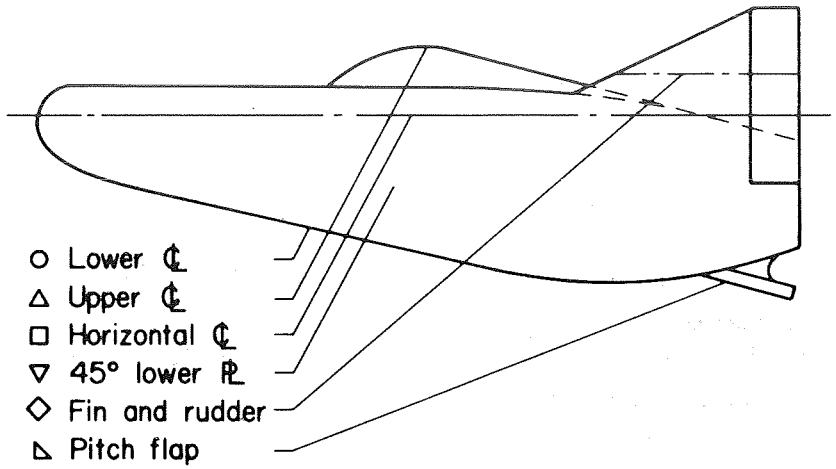

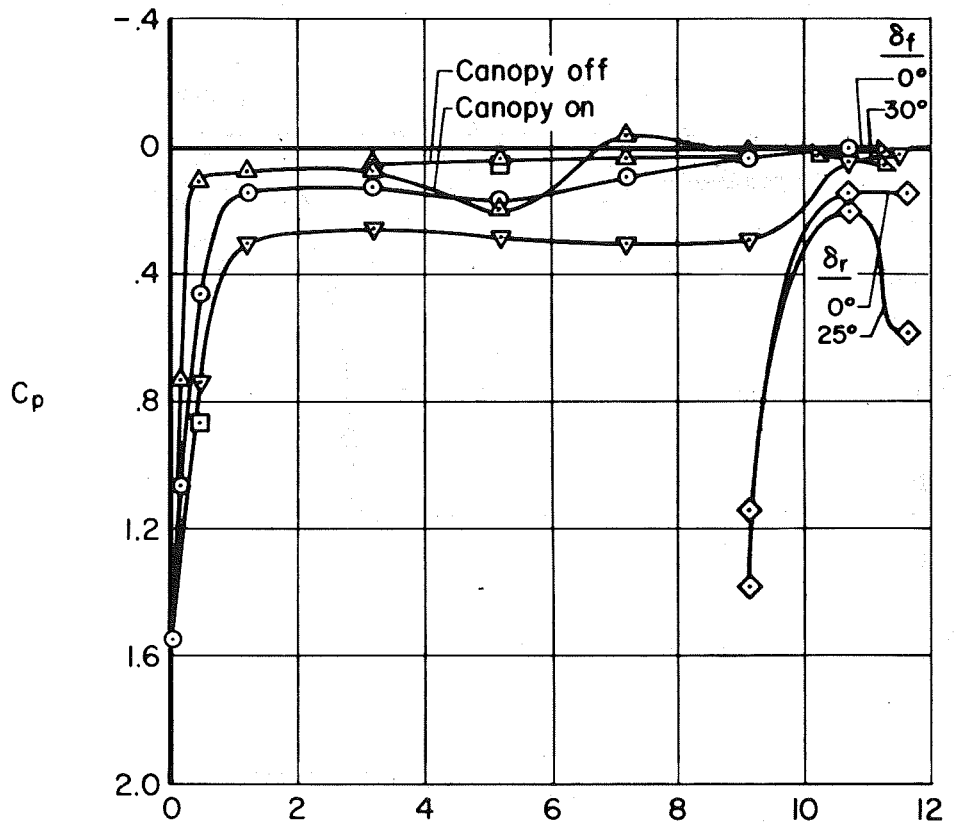

(d) $\beta = -14.6^\circ$

Figure 11.- Concluded.

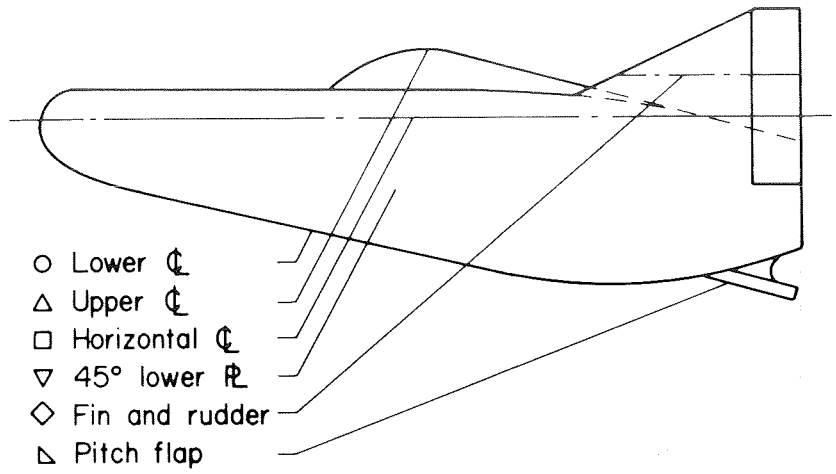

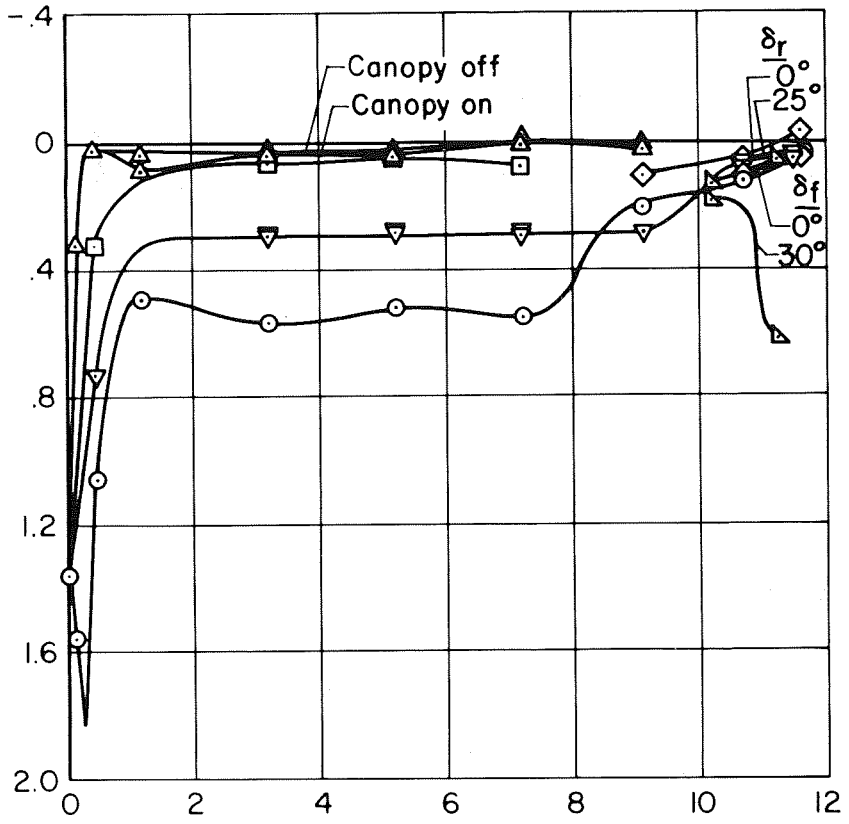

(a) $\beta = 5.25^{\circ}$

Figure 12.- Distribution of pressure for the model in sideslip; M = 10.4, $\alpha = 20^{\circ}$.

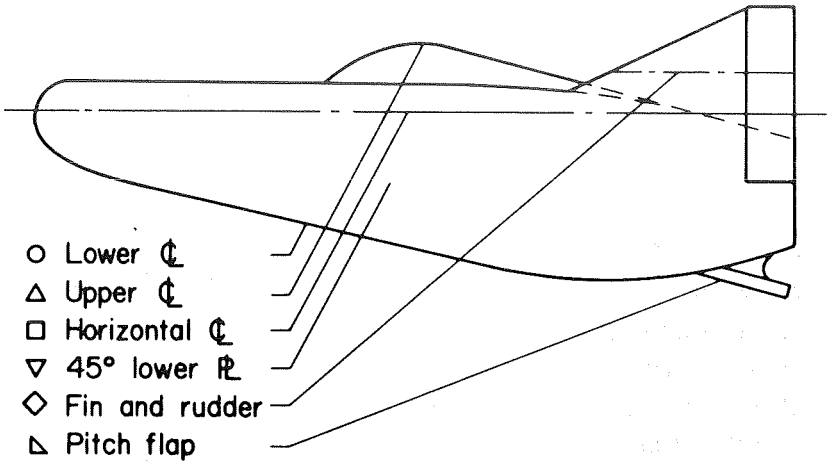

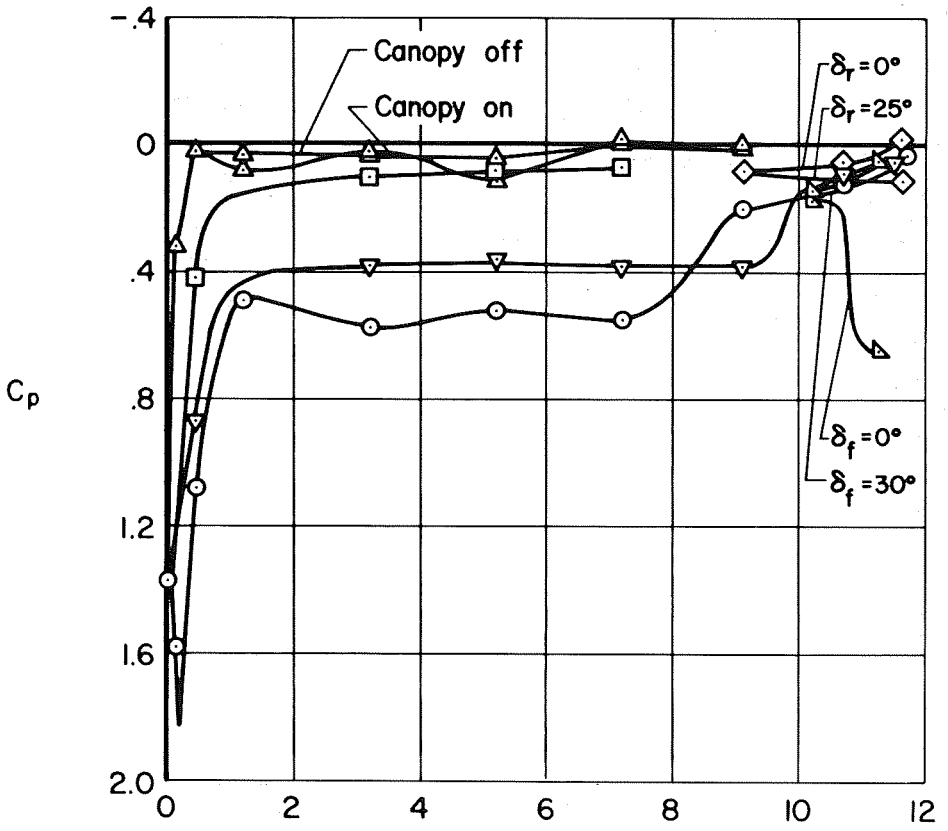

(b) $\beta = 0.2^{\circ}$

Figure 12.- Continued.

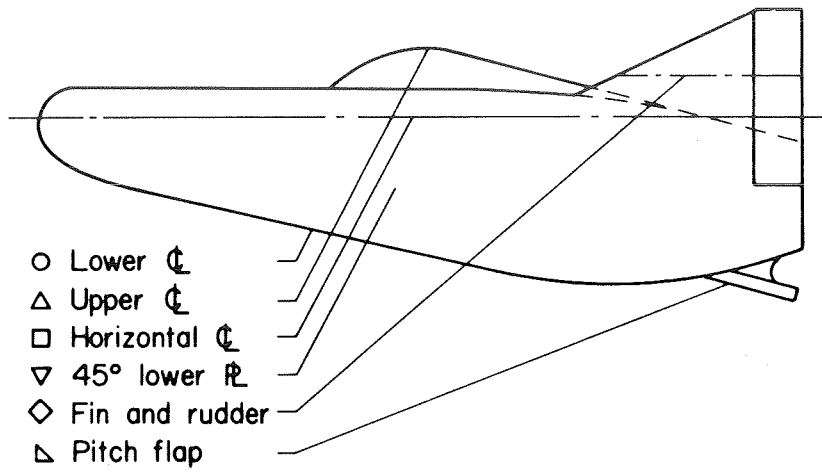

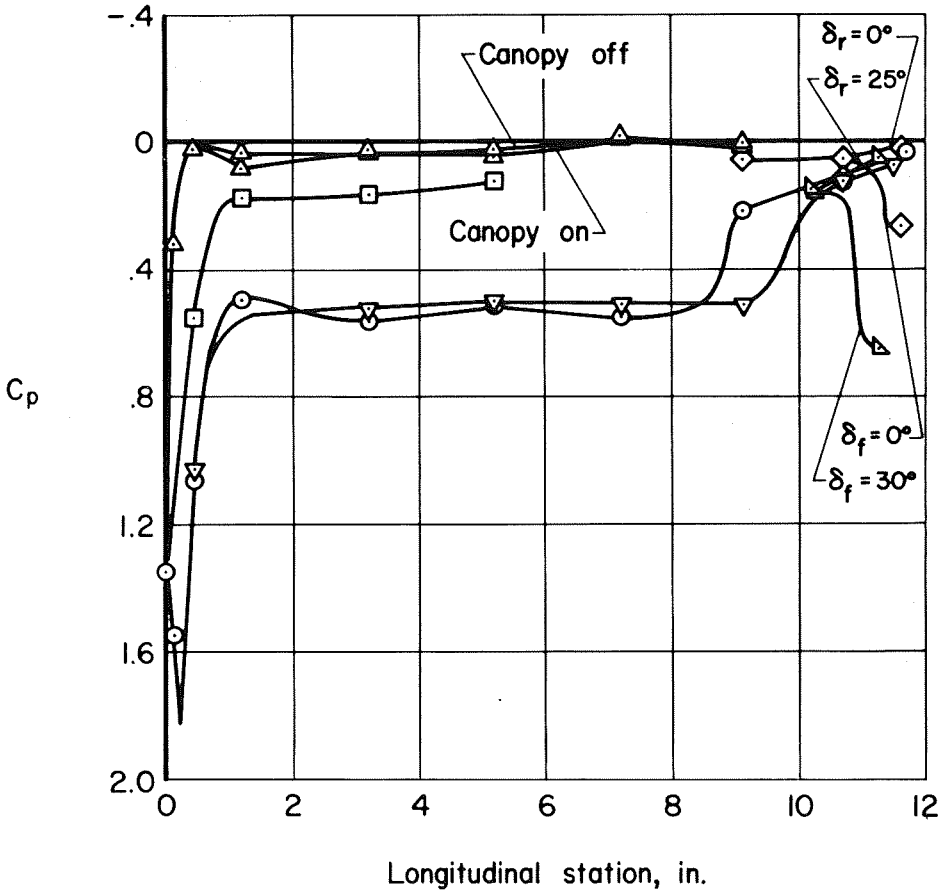

(c) $\beta = -5.9^{\circ}$

Figure 12.- Continued.

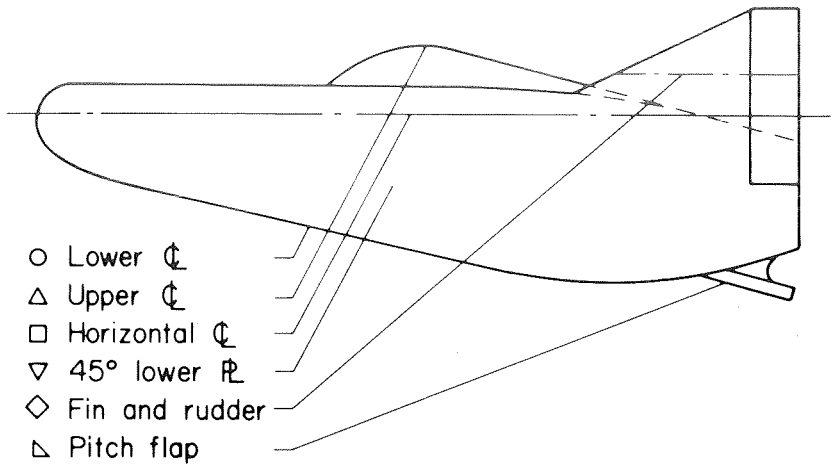

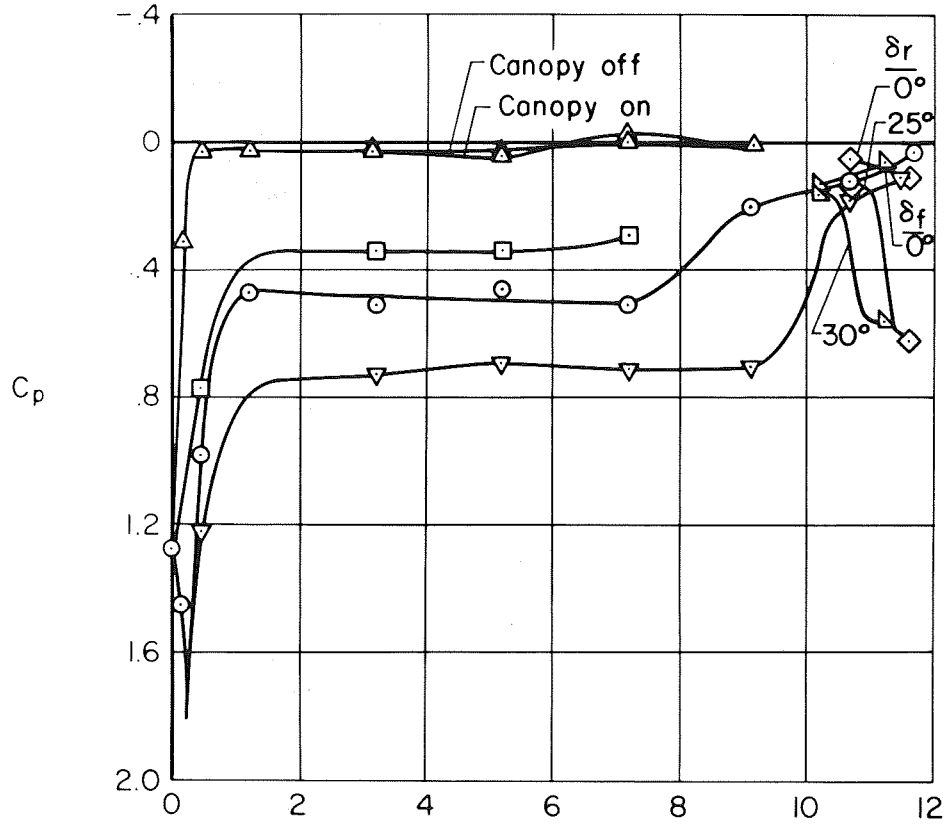

(d) $\beta = -14.7^{\circ}$

Figure 12.- Concluded.

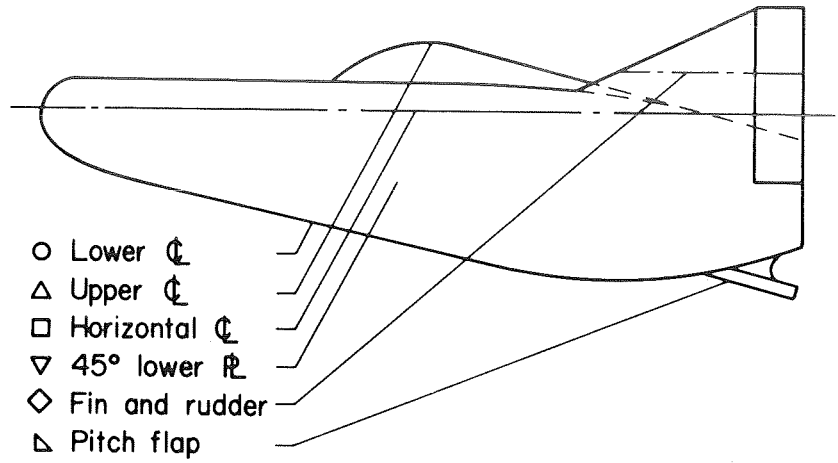

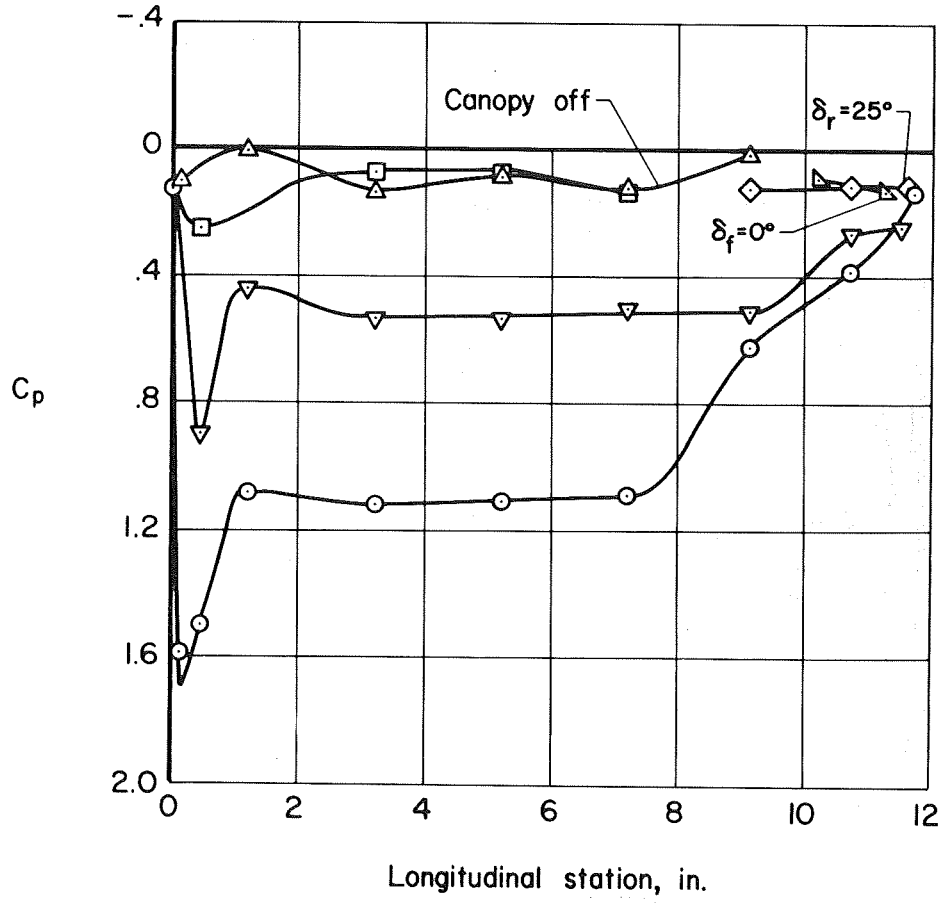

(a) $\beta = 5.3^\circ$

Figure 13.- Distribution of pressure coefficients for the model in sideslip; M = 10.4, $\alpha = 40^\circ$.

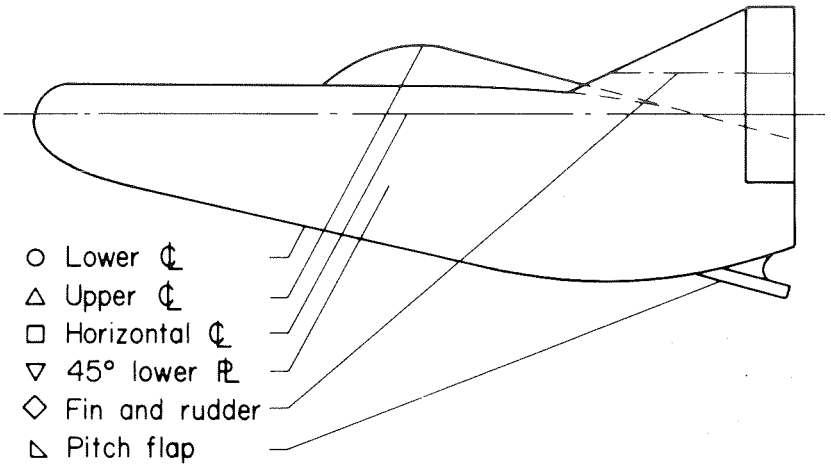

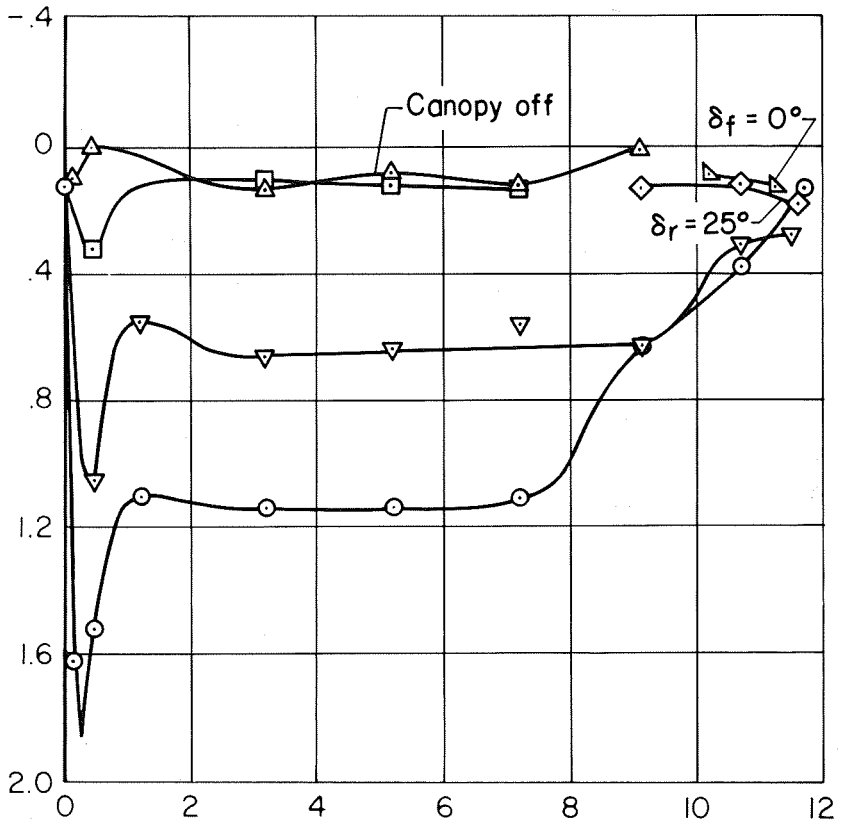

(b) $\beta = 0.2°$

Figure 13.- Continued.

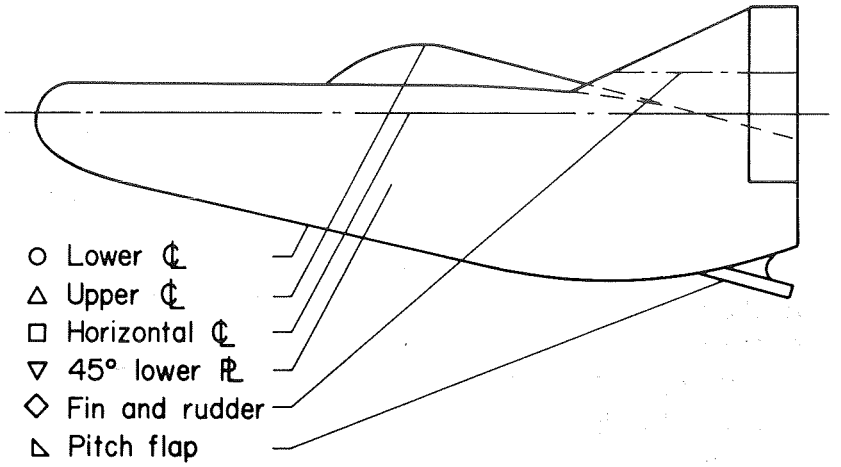

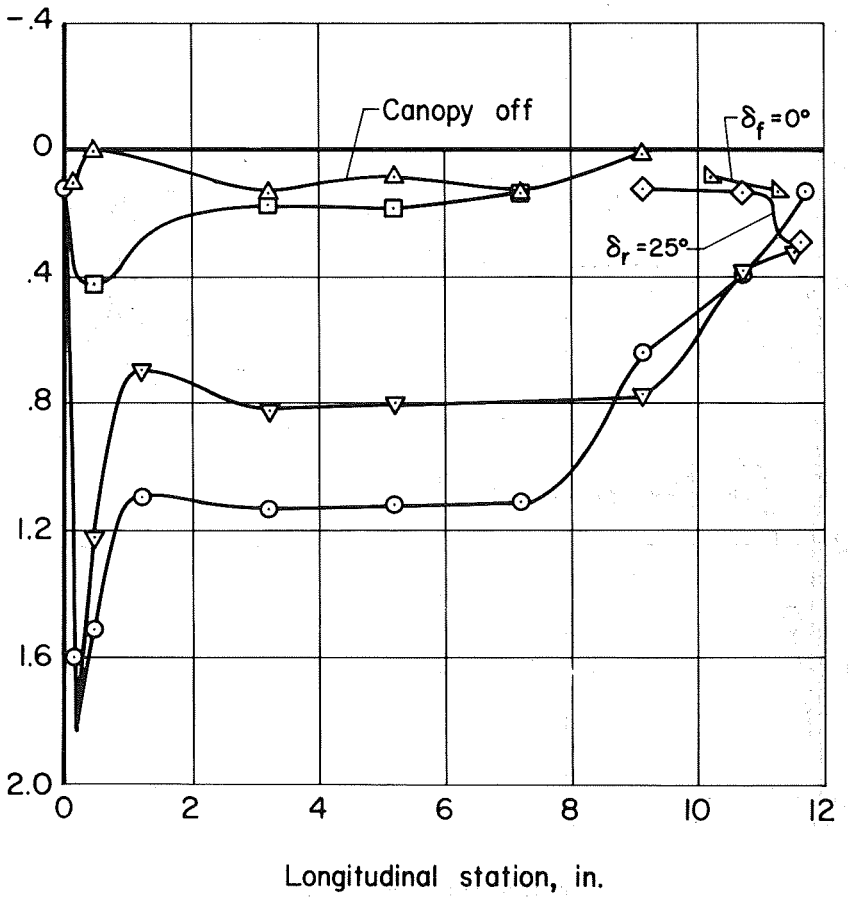

(c) $\beta = -5.7^{\circ}$

Figure 13.- Continued.

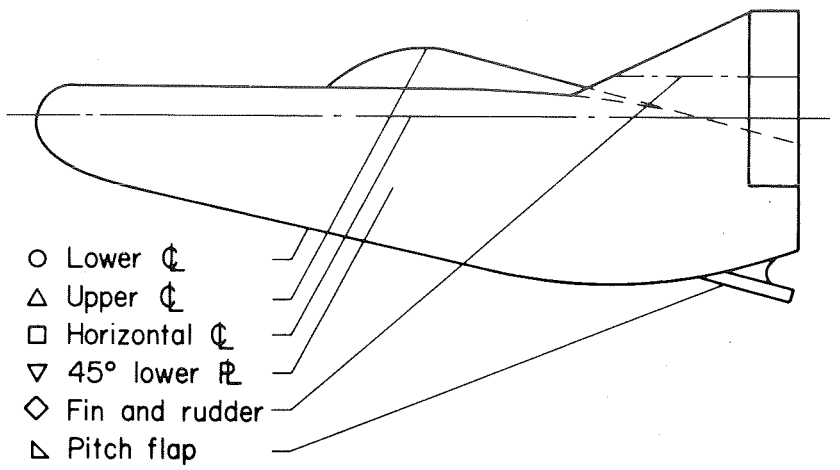

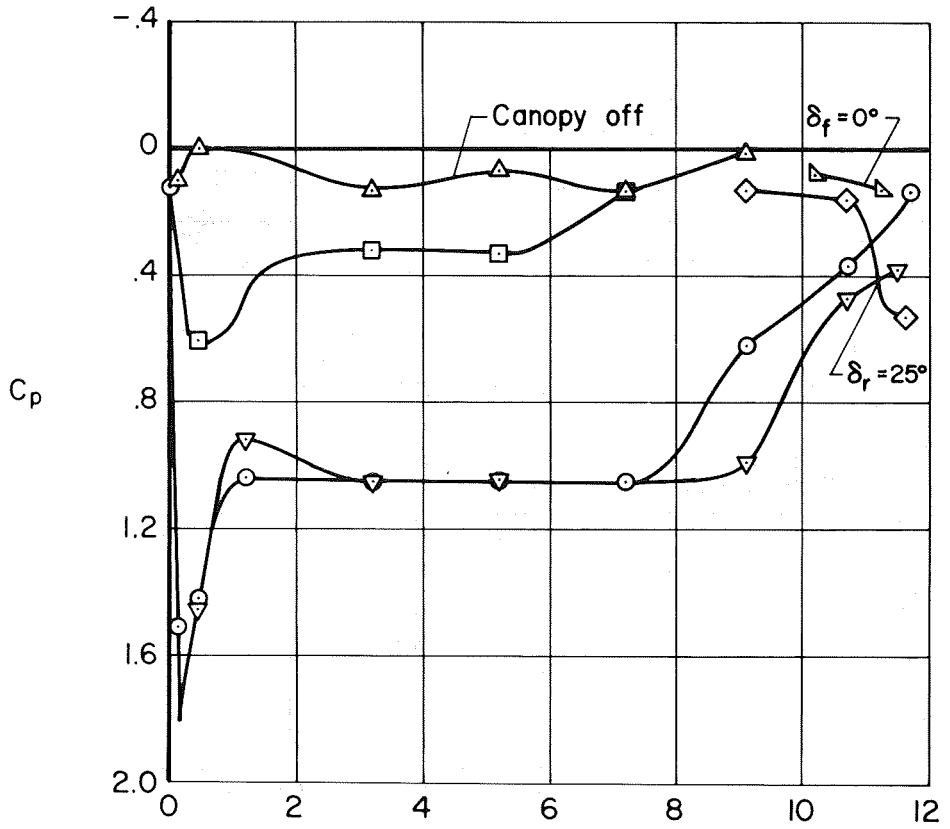

(d) $\beta = -14.7^\circ$

Figure 13.- Concluded.

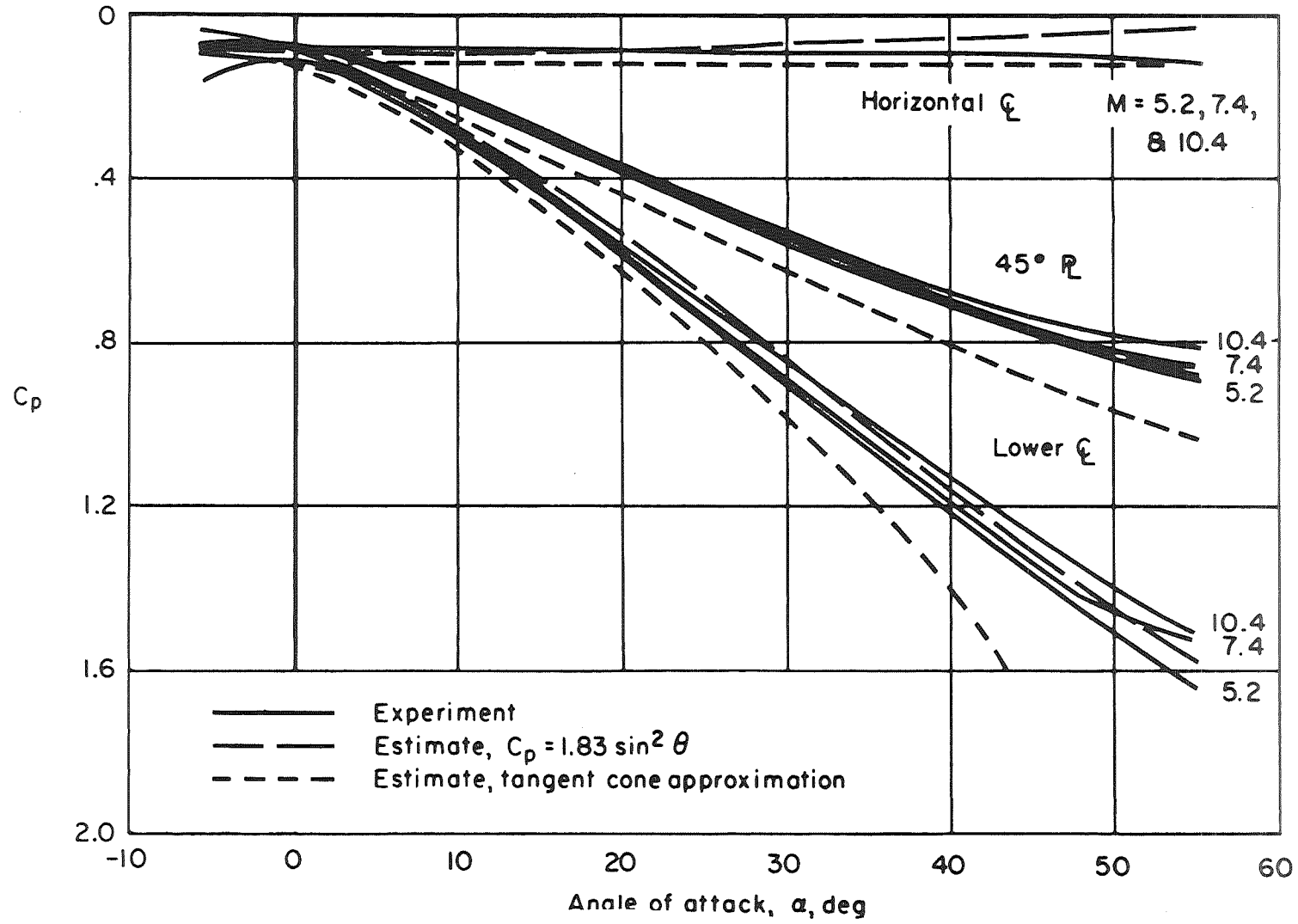

Figure 14.- Summary of averaged pressure coefficients on the conical portion of the body; $\beta = 0^{\circ}$.

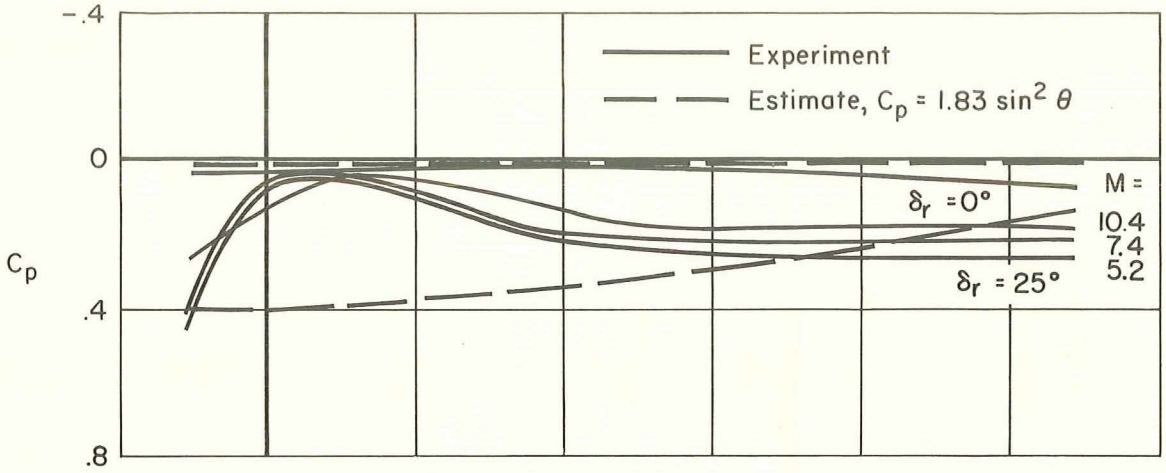

(a) Rudder.

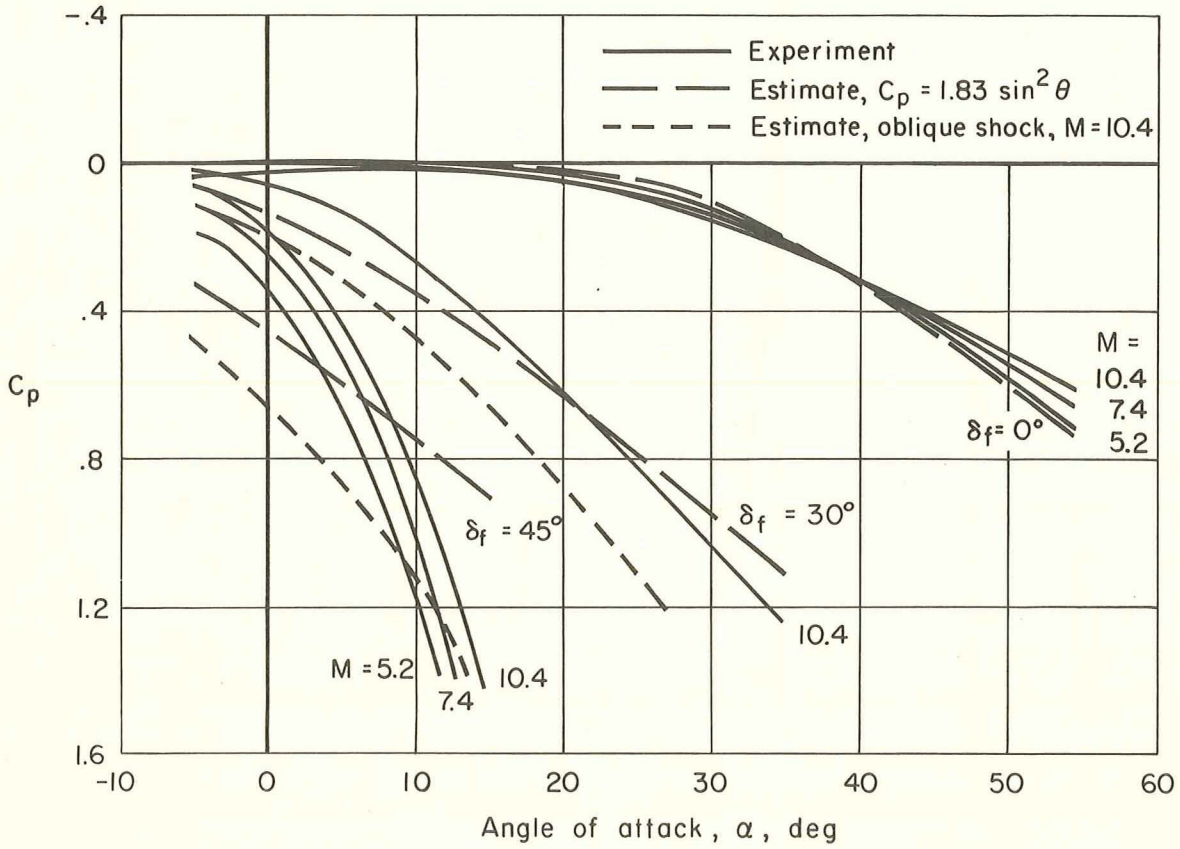

(b) Pitch flap.

Figure 15.- Summary of the pressure coefficients for the pitch flap and rudder; $\beta = 0^\circ$.

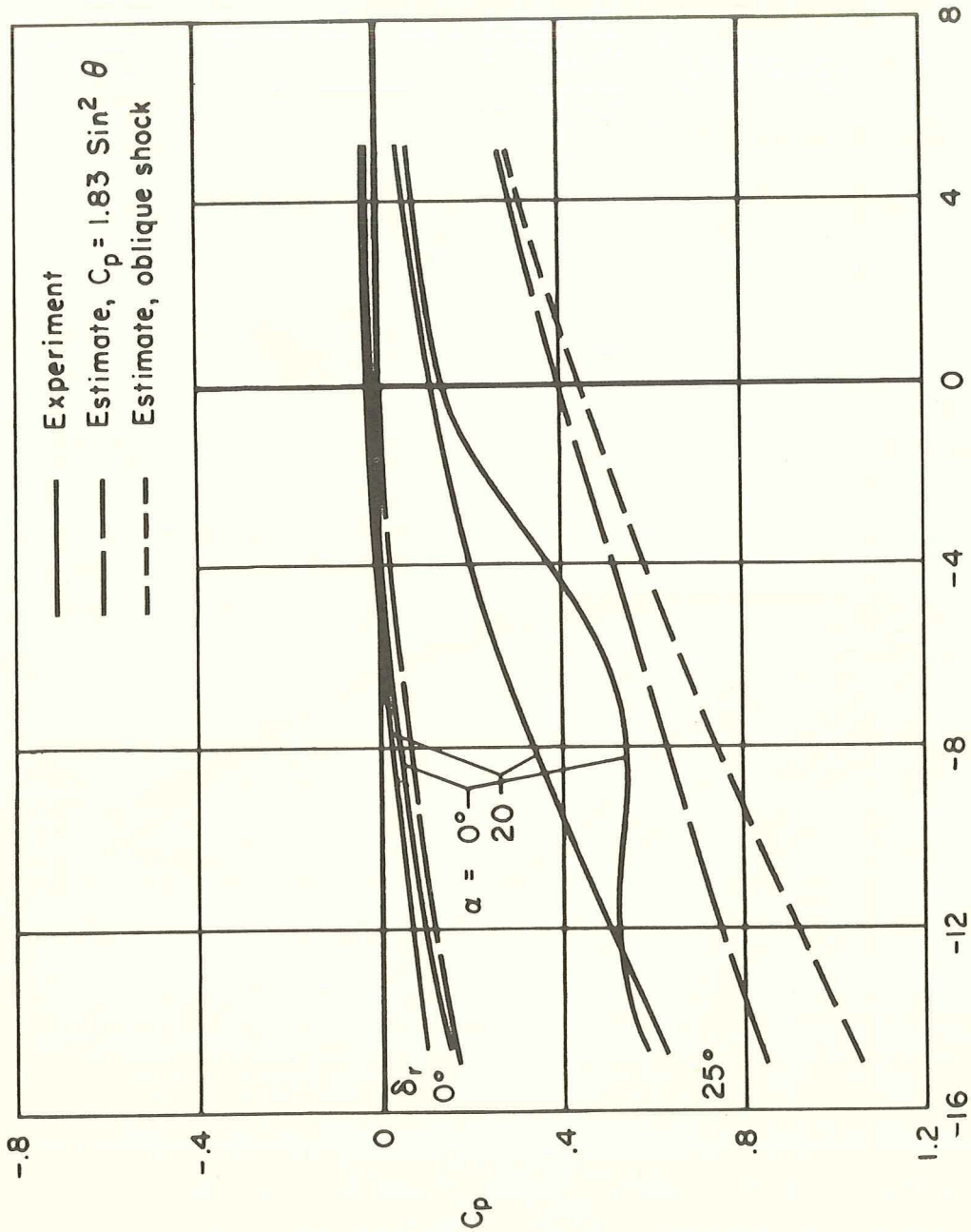

Figure 16.- Summary of the pressure coefficients during sideslip for the rudder outboard surface for model angles of attack of 0° and 20°; M = 10.40.

CONFIDENTIAL

"The aeronautical and space activities of the United States shall be conducted so as to contribute . . . to the expansion of human knowledge of phenomena in the atmosphere and space. The Administration shall provide for the widest practicable and appropriate dissemination of information concerning its activities and the results thereof."

—NATIONAL AERONAUTICS AND SPACE ACT OF 1958

NASA SCIENTIFIC AND TECHNICAL PUBLICATIONS

TECHNICAL REPORTS: Scientific and technical information considered important, complete, and a lasting contribution to existing knowledge.

TECHNICAL NOTES: Information less broad in scope but nevertheless of importance as a contribution to existing knowledge.

TECHNICAL MEMORANDUMS: Information receiving limited distribution because of preliminary data, security classification, or other reasons.

CONTRACTOR REPORTS: Technical information generated in connection with a NASA contract or grant and released under NASA auspices.

TECHNICAL TRANSLATIONS: Information published in a foreign language considered to merit NASA distribution in English.

TECHNICAL REPRINTS: Information derived from NASA activities and initially published in the form of journal articles.

SPECIAL PUBLICATIONS: Information derived from or of value to NASA activities but not necessarily reporting the results of individual NASA-programmed scientific efforts. Publications include conference proceedings, monographs, data compilations, handbooks, sourcebooks, and special bibliographies.

Details on the availability of these publications may be obtained from:

SCIENTIFIC AND TECHNICAL INFORMATION DIVISION

NATIONAL AERONAUTICS AND SPACE ADMINISTRATION

Washington, D.C. 20546

CONFIDENTIAL